SISSA - SCUOLA
INTERNAZIONALE
SUPERIORE
DI STUDI AVANZATI
TRIESTE
Strada Costiera 11

ISAS - INTERNATIONAL SCHOOL FOR ADVANCED STUDIES

THE STABILITY OF THICK ACCRETION DISKS

Thesis submitted for the degree of

"Doctor Philosophiae"

CANDIDATE

O.M. Blaes

SUPERVISOR

M.A. Abramowicz

September 1986

TRIESTE

THE STABILITY OF THICK ACCRETION DISKS

Thesis submitted for the degree of

"Doctor Philosophiae"

CANDIDATE

O.M. Blaes

SUPERVISOR

M.A. Abramowicz

September 1986

Chi arriva a Tecla, poco vede della cittá, dietro gli steccati di tavole, i ripari di tela di sacco, le impalcature, le armature metalliche, i ponti di legno sospesi a funi o sostenuti da cavalletti, le scale a pioli, i tralicci. Alla domanda : - Perché la costruzione di Tecla continua cosí a lungo? - gli abitanti senza smettere d'issare secchi, di calare fili a piombo, di muovere in su e in giú lunghi pennelli. - Perché non cominci la distruzione, - rispondono. E richiesti se temono che appena tolte le impalcature la cittá cominci a sgretolarsi e a andare in pezzi, soggiungono in fretta, sottovoce : - Non soltanto la cittá.

Se, insoddisfatto delle risposte, qualcuno applica l'occhio alla fessura d'una staccionata, vede gru che tirano su altre gru, incastellature che rivestono altre incastellature, travi che puntellano altre travi. - Che senso ha il vostro costruire? - domanda. - Qual é il fine d'una cittá in costruzione se non una cittá? Dov'é il piano che seguite, il progetto?

- Te lo mostreremo appena termina la giornata; ora non possiamo interrompere, - rispondono.

Il lavoro cessa al tramonto. Scende la notte sul cantiere. É una notte stellata. - Ecco il progetto, - dicono.

Italo Calvino - Le cittá invisibili

ACKNOWLEDGEMENTS

I have benefitted enormously from discussions with Juhan Frank, who informed me of his numerical work long before it was completed, and Bernard Schutz, who enlightened me on mathematical aspects of stability theory. The work on incompressible annuli (chapter V) was done in collaboration with Wolfgang Glatzel while the formulation of the pseudobarotropic perturbation equation (section III.4(b)) was suggested to me by John Papaloizou. I am also grateful to them for many long and useful conversations (and to W.G. in particular for his warm hospitality in Cambridge and Munich).

The numerical work on secular evolution of tori (section I.4) was done with Marek Abramowicz and Roberto Turolla. M.A., as my thesis supervisor, also deserves my thanks for giving me such a "hot" problem and advising me on how to proceed with it.

Finally I would like to thank Peter Goldreich, Jeremy Goodman and Ramesh Narayan for sending me a preprint of their work in advance of publication.

This work was financed by a UK Science and Engineering Research Council overseas studentship. The International School for Advanced Studies, Trieste, also provided travel and subsistence expenses for a number of scientific journeys.

ABSTRACT

The theory of geometrically thick accretion disks in its current form is reviewed and preliminary calculations concerning their possible secular evolution are presented. These disks are now known, however, to be subject to global dynamical instabilities discovered by Papaloizou and Pringle. How far the theory has to be modified to account for this, and indeed the very existence of thick disks themselves, are as yet unanswered questions.

All work done on exploring the consequences of the instabilities and the many suggestions as to their physical cause(s) are reviewed here. The driving force of the instability appears to be a tapping of the shear energy of the differentially rotating fluid by modes which transport angular momentum outwards. In the most violent modes this is achieved through interactions between waves propagating around the rotation axis near the inner and outer radii of the torus.

No general global stability criteria exist, but what can be gleaned from the theory of rotating stars is presented here. In particular the general limits on instability growth rates and "almost" corotation theorems are still valid, and both of these can be improved upon for particular classes of tori.

In the special case of non-self-gravitating, constant specific angular momentum, homentropic slender tori one may calculate the full normal mode oscillation spectrum and this gives a complete analytic description of the instability for this case. This is in fact the most violent mode and is now known to be stabilized in Newtonian slender tori when the specific angular momentum distribution is steeper than $\varpi^{2-\sqrt{3}}$. This result is generalized to pseudo-Newtonian tori, which could be of some practical significance if the less violent modes which exist beyond this point do not actually disrupt the torus.

The surface interaction nature of the instability is demonstrated by studying two-dimensional annular flows. Pseudo-Newtonian cusps are found to be stabilizing in incompressible flows because they cannot support wave motion at the inner edge. The extra degrees of feedom existing in a compressible flow are, however, immediately destabilizing.

Finally, the effects of accretion on the instability can be studied by constructing a continuous sequence of two-dimensional relativistic models going from a marginally bound annulus (which is unstable) to a pure radial infall from infinity (which is stable). The location of the marginal stability point is still unknown at the present time.

CONTENTS

I. THICK ACCRETION DISK THEORY

The idea that accretion disks can be geometrically thick in the vertical direction has received great interest from theorists in the past decade. The natural astrophysical environment of such objects is around a black hole, and they may turn out to be important for understanding the central engines of active galactic nuclei and exotic Galactic sources such as SS433. Given these proposed applications it is however understandable that observational evidence for the existence of thick accretion disks is rather scarce. Indeed even the current theoretical models must be said to rest on shaky foundations, partly because they are extremely simple and contain a large number of unknown free parameters and functions, and partly because they may be subject to dynamical instabilities. These instabilities will form the subject of this thesis, but suffice to say for now that their role in real astrophysical flows is far from certain at the present time.

This chapter reviews the theory of thick accretion disks, leaving aside the question of their dynamical stability. At the heart of the theory lie the equilibria of perfect fluid rings rotating around a central mass. After a full discussion of their properties, we briefly turn to the simplest imperfect fluid configuration, that of the thin Keplerian accretion disk. The theory of thick accretion disks proper is then reviewed; concentrating primarily on the radiation pressure supported variety. Finally, alternative models supported by gas pressure are briefly discussed.

Earlier reviews of thick disks have been written by Paczyński (1982) and Wiita (1982b). For applications of the theory to active galactic nuclei see Begelman (1984); Begelman, Blandford and Rees (1984); Blandford (1985) and Rees (1984). Calvani and Nobili (1981) have applied the theory to SS433 and Margon (1984) cites observations which indicate that this system may contain a thick disk.

I.1 Perfect Fluid Tori

The relativistic equilibrium configurations of perfect fluid tori rotating around a black hole have been derived and discussed by Fishbone and Moncrief (1976); Fishbone (1977); Abramowicz, Jaroszyński and Sikora (1978); Kozłowski,

Jaroszyński and Abramowicz (1978) and Chakrabarti (1985).

Consider the Newtonian case to begin with, first discussed by Fishbone and Moncrief. Here the fluid obeys Newtonian hydrodynamics and rotates around a central point mass M. Hydrostatic equilibrium requires

$$\frac{1}{\rho}\nabla p = \underline{g}_{eff} = -\nabla\Phi + \Omega^2 \varpi \hat{\underline{\varpi}} \qquad (1.1)$$

where $\underline{g}_{eff}$ is the effective gravitational acceleration due both to gravity and centrifugal forces (figure 1-1).

Virtually all discussions of the equilibrium structure of thick disks assume that they are barotropic, i.e. that surfaces of constant pressure and constant density coincide:

$$p = p(\rho) \qquad (1.2)$$

This assumption simplifies the problem enormously, as $\underline{g}_{eff}$ is then the gradient of a potential and the specific angular momentum ℓ and angular velocity Ω are constant on cylinders centred about the rotation axis (the Poincaré - Wavre theorem, see e.g. ch. 4 of Tassoul 1978):

$$\ell = \varpi^2\Omega = \ell(\varpi) \qquad (1.3)$$

Defining a rotational potential Φ_{rot} and the total effective gravitational potential w by

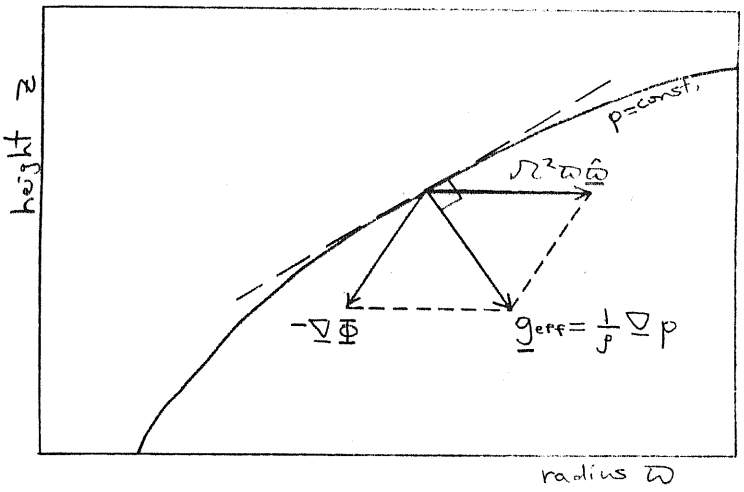

Figure 1-1. The balance of forces in a torus (adapted from Paczynski 1982).

$$\Phi_{rot} \equiv -\int \Omega^2 \varpi \, d\varpi \tag{1.4}$$

$$W \equiv -\int \frac{dp}{\rho} \tag{1.5}$$

then equation (1.1) is easily solved to give

$$W = \Phi + \Phi_{rot} + C \tag{1.6}$$

where C is a constant.

Specification of the rotation law (1.3) and the gravitational field determines the shape of the isobaric (or "equipotential") surfaces. The problem is usually simplified still further by assuming that the torus self-gravity is negligible compared with the gravitational field of the central mass. Figure 2 illustrates the equipotential surfaces for non-self-gravitating tori with $\ell = (GM\varpi_o)^{\frac{1}{2}}$ = constant and $\ell = (GM\varpi_o)^{\frac{1}{2}}(\varpi/\varpi_o)^{.45}$.

At $(\varpi=\varpi_o, z=0)$ the pressure gradient vanishes as fluid elements rotate with the Keplerian angular velocity - this is the central pressure maximum of the torus. Depending on the actual $p=p(\rho)$ relation, the fluid will fill one of the toroidal equipotential surfaces around ϖ_o. Inside the pressure maximum, $\ell > (GM\varpi)^{\frac{1}{2}}$, so that the pressure gradient forces must be directed inwards to balance the excess centrifugal force. Outside ϖ_o, $\ell < (GM\varpi)^{\frac{1}{2}}$, and the situation is reversed - pressure acts outwards to make up for the deficient centrifugal force. Note that increasing the slope of ℓ tends to stretch the equipotential surfaces out in the radial direction. If one continues increasing the slope towards a Keplerian distribution one is left with the classical thin disk discussed later in this chapter.

Figure 1-3(a) depicts the specific angular momentum distribution near the pressure maximum. Another interesting topological feature occurs when $\ell > (GM\varpi)^{\frac{1}{2}}$ outside a Keplerian point ϖ_{cusp} and $\ell < (GM\varpi)^{\frac{1}{2}}$ inside. Here the pressure gradients are reversed and one has a cusp in the equipotential surfaces. Figure 1-4 depicts a case where both Keplerian points exist. One may continue to play with $\ell(\varpi)$ and produce other topological features, further discussion of which may be found in Abramowicz, Calvani and Nobili (1980).

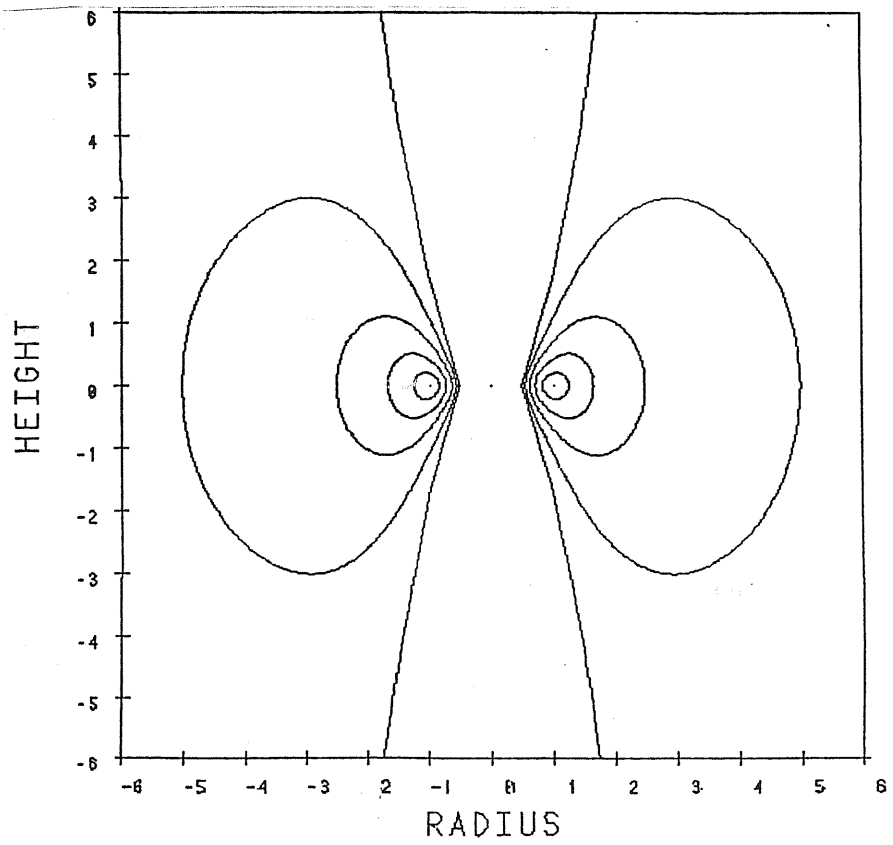

(a)

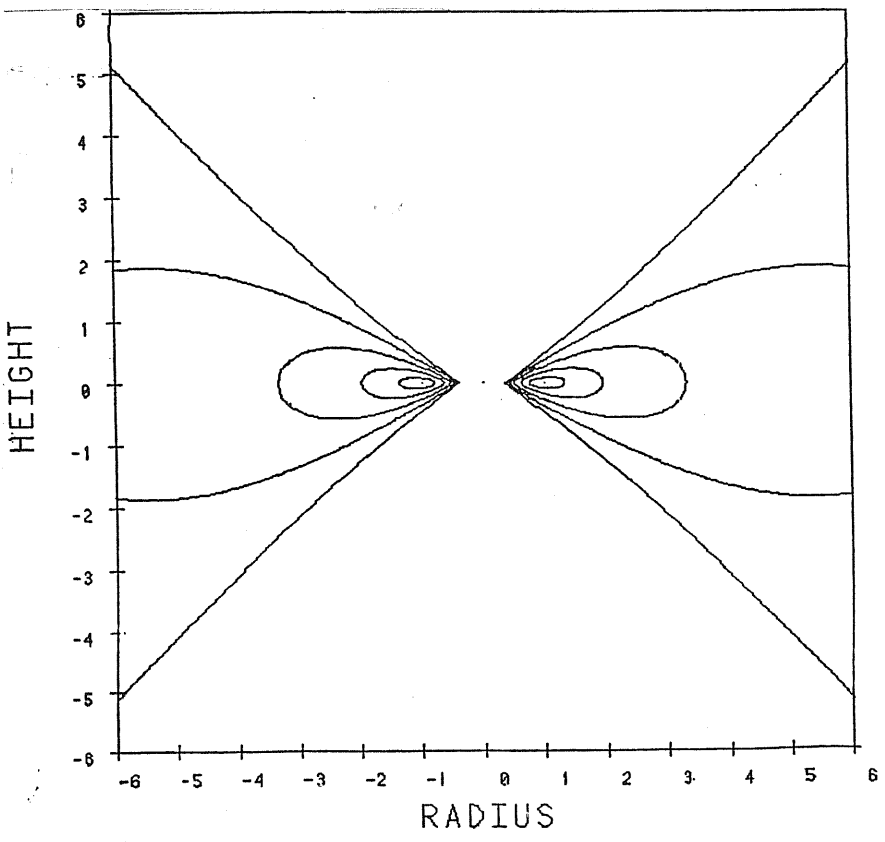

(b)

Figure 1-2. The equipotential surfaces for a Newtonian potential and specific angular momentum ℓ given by (a) $\ell = (GM\varpi_o)^{\frac{1}{2}}$ and (b) $\ell = (GM\varpi_o)^{\frac{1}{2}}(\varpi/\varpi_o)^{.45}$. Distances in the figure are scaled with respect to the radius ϖ_o of the central, pressure maximum ring.

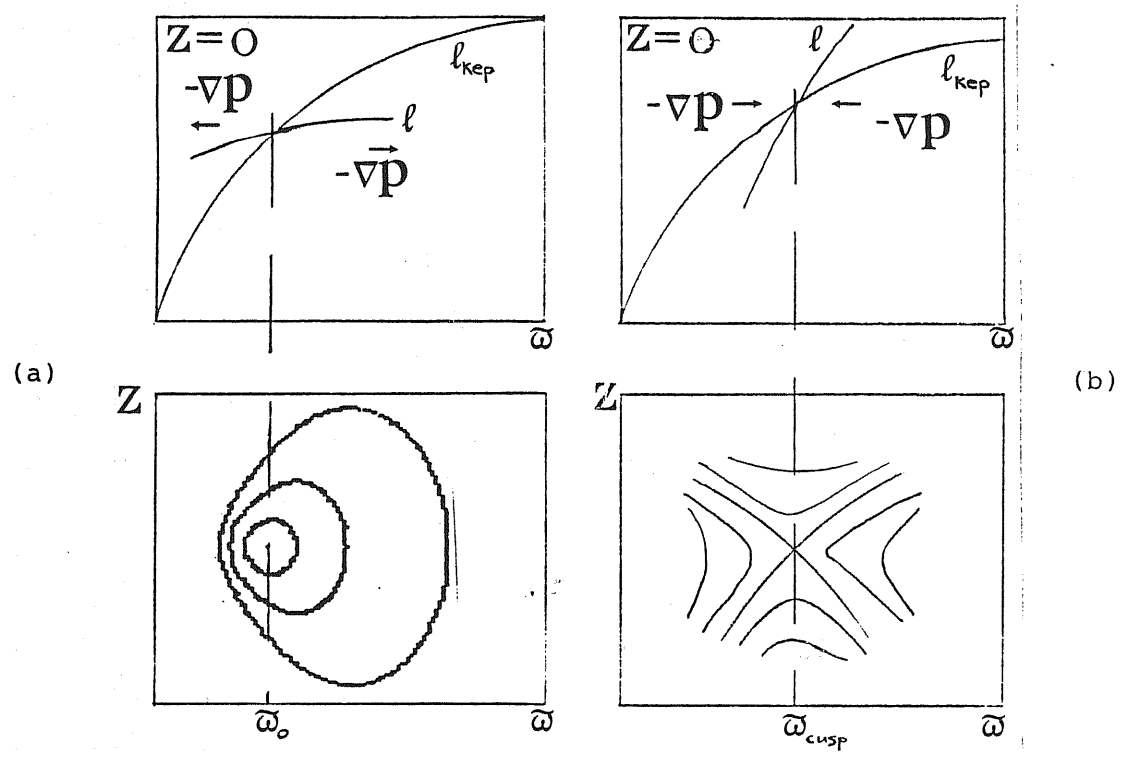

Figure 1-3. The distribution of specific angular momentum ℓ and the equipotential surfaces near (a) the pressure maximum and (b) a cusp.

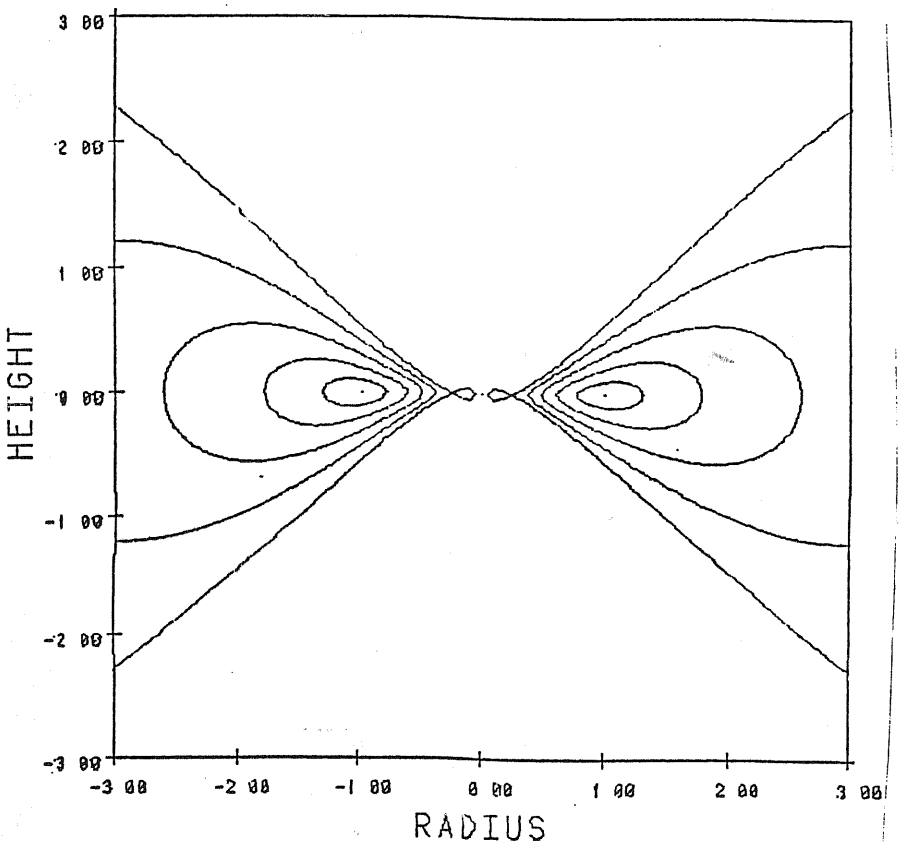

Figure 1-4. The equipotential surfaces for a Newtonian potential and specific angular momentum distribution $\ell = \frac{(GM\varpi_0)^{1/2}}{2-\sqrt{2}}\left[\left(\frac{\varpi}{\varpi_0}\right)^{1/4} + 1 - \sqrt{2}\right]$

A cusp exists at $\varpi_{cusp} = \varpi_0/4$.

Fully relativistic tori rotating in stationary, axisymmetric spacetimes have broadly similar properties. The usual barotropic assumption is that the surfaces of constant pressure and constant total energy density coincide:

$$p = p(\mathcal{E}) \tag{1.7}$$

This again implies that the surfaces of constant ℓ and constant Ω coincide[1]:

$$\ell = \ell(\Omega) \tag{1.8}$$

However, the spacetime geometry distorts these surfaces (the so-called "von Zeipel surfaces") from their Newtonian cylindrical shape, though they still retain a cylindrical topology (figure 1-5).

For a static gravitational field, such as that of a Schwarzschild black hole, the von Zeipel cylinders are independent of the relation $\ell = \ell(\Omega)$. This is not the case for a stationary field such as that of a Kerr black hole (or a self-gravitating torus).

As in Newtonian theory both $\ell(\Omega)$ and the gravitational field are required to determine the equipotential surfaces. Figure 1-6(a) depicts the case ℓ = constant and a Schwarzschild metric, again neglecting the fluid self-gravity. An inner cusp is present, due to the fact that the specific angular momentum of a Keplerian orbit is non-monotonic (figure 1-6(b))[2]. This makes the cusp a generic feature of general relativistic fields, in contrast to the Newtonian case where cusps are produced only for special choices of ℓ.

The cusp equipotential surface is the largest that a fluid in hydrostatic equilibrium can fill. In fact, if the cusp lies inside the marginally bound test particle orbit ω_{mb}, then the fluid cannot even fill this surface.

---

[1] In the present discussion ℓ and Ω are defined by

$$\ell = -\frac{u_\phi}{u_t} \qquad \Omega = \frac{u^\phi}{u^t}$$

where u^i is the four velocity of the fluid in the standard, spherical polar coordinate system. For coordinate independent definitions see, e.g., appendix 1 of Kozłowski, Jaroszyński and Abramowicz (1978).

[2] In papers on thick disks the word "Keplerian" often simply refers to a circular test particle orbit, regardless of the gravitational field. This is a common source of confusion, especially with those who study, say, rotation curves of disk galaxies.

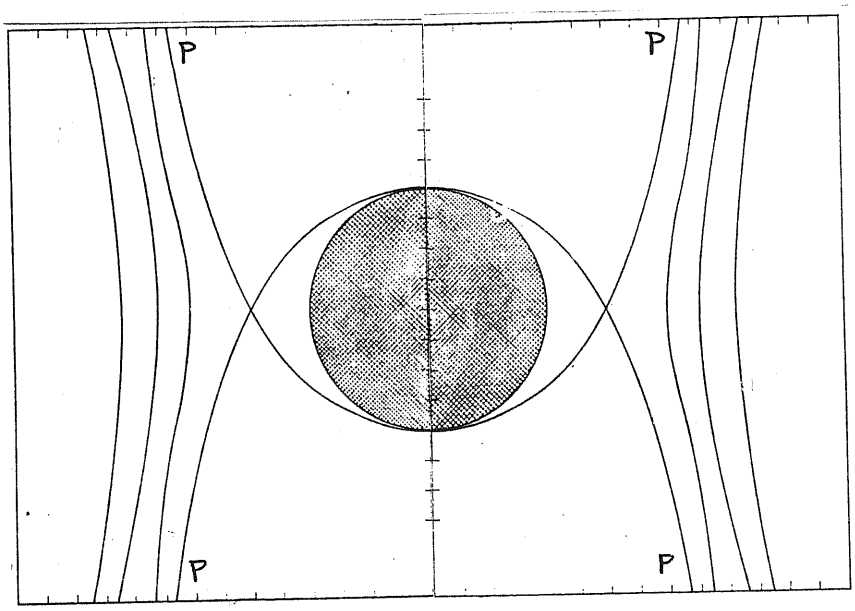

Figure 1-5. The von Zeipel surfaces for a Schwarzschild spacetime. Note the $\omega \simeq$ constant behaviour as one goes away from the hole, in agreement with Newtonian theory. (Inside the critical surface P the surfaces do not have cylindrical topology, but they lose their significance here because matter cannot rotate in hydrostatic equilibrium in this region.)
(from Kozłowski, Jaroszyński and Abramowicz 1978)

(a)

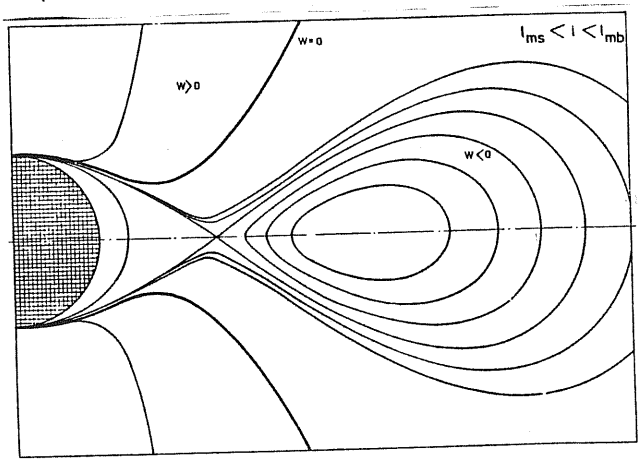

(b)

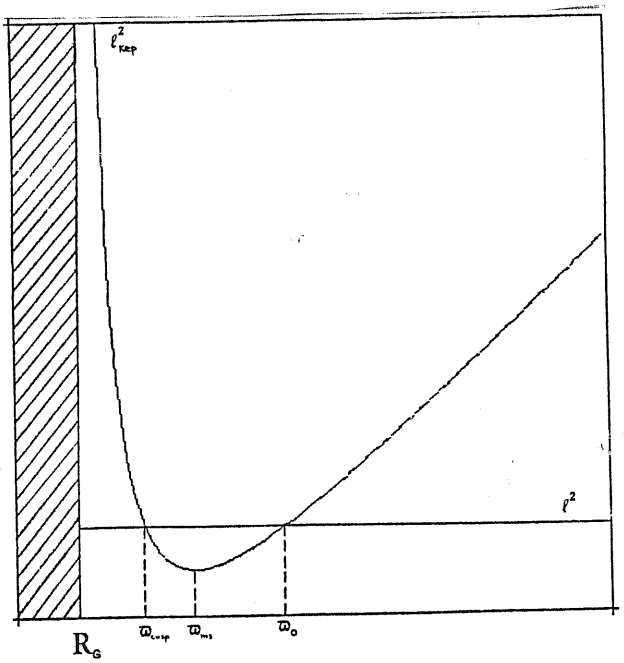

Figure 1-6. (a) Equipotential surfaces and (b) the specific anglular momentum distributions for an ℓ =constant test fluid rotating around a Schwarzschild black hole. (fig. a from Abramowicz, Jaroszyński, and Sikora 1978)

This is because surfaces whose inner edges are inside this radius are open at infinity, regardless of the spacetime and regardless of the specific angular momentum distribution (atleast provided it is continuous and stable).

Consider a configuration which fills the cusp equipotential surface. If in addition to being outside ϖ_{mb}, the cusp is inside the last stable test particle orbit ϖ_{ms}, then a process similar to Roche lobe overflow in close binaries occurs. A fluid ring at the cusp rotates in a Keplerian orbit. This orbit is unstable if $\varpi_{cusp} < \varpi_{ms}$ because on perturbing the fluid axisymmetrically inwards, its specific angular momentum is less than the local Keplerian value and so it will continue to fall inwards. Note that this overflow mechanism will not occur in Newtonian cusps, where ℓ_{kep} is monotonically increasing, or indeed in relativistic cusps if $\varpi_{cusp} > \varpi_{ms}$.

Near an unstable cusp the assumption of hydrostatic equilibrium clearly breaks down. A stream of fluid will flow from the torus into the black hole and, like in spherical accretion, this flow is transonic. Further discussion of this process will be found in chapter VI of this thesis, where the stability of accreting flows will be examined.

Paczyński and Wiita (1980) pointed out that the essential features of a Schwarzschild spacetime with regard to accretion flows can be mimicked with a pseudo-Newtonian potential

$$\Phi = \frac{-GM}{(\varpi^2 + z^2)^{\frac{1}{2}} - R_G} \tag{1.9}$$

The specific binding energy and angular momentum of Keplerian orbits in such a potential are

$$e_{kep} = \tfrac{1}{2}GM \left[\frac{\varpi - 2R_G}{(\varpi - R_G)^2} \right] \tag{1.10}$$

and

$$\ell_{kep} = \frac{(GM\varpi^3)^{\frac{1}{2}}}{\varpi - R_G} \tag{1.11}$$

so that

$$\frac{de_{kep}}{d\varpi} = -\tfrac{1}{2}GM \left[\frac{\varpi - 3R_G}{(\varpi - R_G)^3} \right] \tag{1.12}$$

and
$$\frac{d\,\ell_{kep}}{d\,\varpi} = \tfrac{1}{2}(GM\varpi)^{\frac{1}{2}}\ \frac{\varpi - 3R_G}{(\varpi - R_G)^2} \tag{1.13}$$

Hence orbits are bound ($e_{kep} > 0$) if $\varpi > 2R_G$ and stable ($d\,\ell_{kep}/d\varpi > 0$) if $\varpi > 3R_G$. The pseudo-Newtonian potential thus produces the same marginally stable and marginally bound orbits as a Schwarzschild black hole. In addition, the specific binding energy is a maximum at the last stable orbit, just as in the Schwarzschild case, and equals $.0625c^2$ compared with the correct value $.0572c^2$. The equipotential surfaces also have very similar topologies to those of the Schwarzschild case. Given the huge uncertainties in the physics of real accretion, this potential has often been used to capture the essential dynamical features of non-rotating black holes without the mathematical complexities.

Although the qualitative discussion presented so far in this section holds even for self-gravitating disks, the figures have only illustrated the non-self-gravitating case. Self-gravitating configurations are very difficult to actually compute, as one must solve the Euler equations and Poisson's equation (or, in relativity, the full set of Einstein's equations) simultaneously. Abramowicz et al. (1984a) have qualitatively examined the global consequences of self-gravity in Newtonian theory. Their discussion centres on the fact that self-gravity changes the Keplerian distribution of specific angular momentum. Figure 1-7, adapted from this paper, illustrates this for a slender, self-gravitating ring. Inside the ring the self-gravity is directed outwards, so that a rotating test particle needs less specific angular momentum to stay in equilibrium. Outside the ring the situation is reversed. Note that the Keplerian distribution can be non-monotonic so that self-gravitating Newtonian tori may have unstable cusps.

Finally, it should be emphasized that <u>all</u> the discussion in this section relies on the assumption that the configurations are barotropic. If this is not the case (a "baroclinic" torus), constant pressure and constant density surfaces do not coincide and the von Zeipel cylinders no longer have any significance. A procedure for constructing baroclinic models adopted by Frank (private communication) has been to assume pressure and density distributions and then work out the rotation law which gives hydrostatic equilibrium. The configuration is then checked <u>a posteriori</u> for self-consistency.

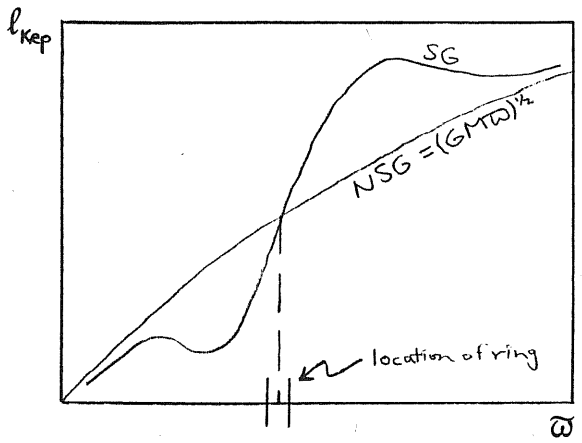

Figure 1-7. The Keplerian specific angular momentum distributions for non-self-gravitating (NSG) and self-gravitating (SG) slender rings around a central Newtonian mass M.

This is a bit like specifying the potential of a self-gravitating configuration and working out the density, though of course obtaining self-consistency is much more straightforward.

Of course the perfect fluid tori which are of primary interest are those which resemble the products of the accretion process, and it is to this which we shall now turn.

I.2 Thin Disks

Apart from the cusp overflow, the idealized fluid tori of the last section are all nonaccreting. However, these configurations are differentially rotating, and so actually viscous friction between the shearing layers will produce a slow infall. Although quite complecated in general, the behaviour of a viscous disk becomes much easier to treat if the disk is thin. As already pointed out, this occurs if the rotation law is approximately Keplerian. Indeed, vertical hydrostatic equilibrium gives the ratio of disk height to radius as roughly

$$\frac{H}{\varpi} \sim \frac{v_s}{v_{Kep}} \tag{1.14}$$

where v_s is the sound speed. A thin disk must have v_s small everywhere, and this implies that radial pressure gradients are small compared with gravitational and centrifugal forces. The rotation law must therefore be Keplerian.

Thin accretion disks are the most widely studied models of accretion with angular momentum, and they are reasonably successful in interpreting observations, particularly those of cataclysmic variables. The standard model of such disks was developed by Pringle and Rees (1972), Shakura and Sunyaev (1973) and Lynden-Bell and Pringle (1974). A relativistic treatment was presented by Novikov and Thorne (1973). An excellent review of thin disk theory is by Pringle (1981).

Inside the disk, gas rotates in circular orbits with the Keplerian angular velocity. Viscosity slows down the rapidly rotating inner regions and speeds up the slowly rotating outer regions, causing an outward transport of angular momentum and energy. In addition viscosity dissipates mechanical energy into heat, most of which is radiated locally from the disk surface. If the disk rotates around a black hole, matter slowly drifts inwards until it reaches the last stable orbit. At this point the disk breaks up and matter simply falls into the hole (the thin disk cusp overflow!).

Because the disk is thin, it is convenient to distinguish between its vertical and radial structure. The latter is determined by height-averaging the disk and imposing local mass, angular momentum and thermal energy balance. Then, at every radius, one computes the vertical structure from hydrostatic equilibrium and the vertical energy transport required to balance the viscous heat generation with the heat losses at the surface.

The greatest problem in disk modelling is the unknown nature of the viscosity. The most widespread convention is to lump all the uncertainty into a single parameter α defined by

$$\nu = \alpha H v_s \tag{1.15}$$

where ν is the kinematic viscosity. For a Keplerian disk this is roughly equivalent to taking the $w\phi$ component of the viscous stress tensor to be proportional to the pressure. General physical arguments imply $0 < \alpha < 1$.

The standard stationary black hole disk model of Shakura and Sunyaev (1973) and Novikov and Thorne (1973) assumes an alpha viscosity and radiative energy diffusion in the vertical direction. Depending on the central mass and accretion rate, the disk model may be broadly divided into three zones.

In the outer two zones the disk is gas pressure dominated, while in the innermost zone radiation pressure dominates. The opacity in the two inner zones is electron scattering dominated while in the outermost zone free-free absorption and other mechanisms are important.

Real disks need not be stationary, as either the external mass supply could vary or the disk itself could be unstable. There are several different evolution timescales: the dynamical, the thermal (the time it takes the heat content to be viscously generated) and the viscous (the time it takes a fluid element to be viscously transported through the disk):

$$t_{dyn} = \Omega_{Kep}^{-1} \qquad t_{therm} = \alpha^{-1} t_{dyn} \qquad t_{visc} = \alpha^{-1}\left(\frac{H}{\varpi}\right)^{-2} t_{dyn} \tag{1.16}$$

Note that $t_{visc} \gg t_{therm} \gtrsim t_{dyn}$.

Pringle, Rees and Pacholczyk (1973), Lightman and Eardley (1974) and Lightman (1974) discovered that stationary accretion disks are subject to local instabilities. Shakura and Sunyaev (1976) unified the previous studies in an analysis of the standard model. Assuming that the perturbations are axisymmetric and have a wavelength Λ in the range $H \ll \Lambda \ll \varpi$, then the only relevant equations are those for radial viscous mass diffusion and thermal energy balance. Two modes of instability, thermal and viscous, were found in the inner radiation pressure dominated region. Piran (1978) considered more general models and found two necessary conditions for local stability:

$$\left.\frac{d\ \ln Q^{+}}{d\ \ln H}\right|_{\Sigma} < \left.\frac{d\ \ln Q^{-}}{d\ \ln H}\right|_{\Sigma} \tag{1.17}$$

$$\left.\frac{\partial}{\partial \Sigma}(\nu\Sigma)\right|_{Q^{+}=Q^{-}} > 0 \tag{1.18}$$

Here Q^{+} and Q^{-} are the local heating and cooling rates and Σ is the surface density. The first condition expresses the fact that if a perturbation in the disk height causes Q^{+} to increase faster than Q^{-} then the disk will heat and swell further (thermal instability). The second condition is simply a statement that the perturbed mass diffusion coefficient is positive. Violation of this criterion means that regions of high density will get denser while

regions of low density will become more rarified, and the disk will therefore tend to break up into rings.

These instabilities have since been the subject of intense theoretical study in the hope that they can help explain the outbursts of cataclysmic variables (see e.g. Smak 1984 for a review).

It should be emphasized that the above criteria are local in that perturbations are assumed to be concentrated at a given radius. Taam and Lin (1984) have studied the global, nonlinear evolution of locally unstable disks. Radial energy transport by advection and radiative diffusion were included and it was found that this could stabilize the disk even when the local criteria were violated. Piran (1978) also noted that mass loss in the form of a wind could have a stabilizing effect. For disks around black holes, Abramowicz (1981) used this idea to show that mass loss at the inner disk boundary is stabilizing.

I.3 Radiation Tori - Formation and Stationary Structure

In the inner radiation pressure dominated zone of the standard thin disk model, the ratio of height to radius reaches a maximum value which satisfies (Shakura and Sunyaev 1973; Jaroszyński, Abramowicz and Paczyński 1980, hereafter JAP)

$$\left(\frac{H}{\varpi}\right)_{max} > \frac{4}{9}\frac{\dot{M}}{\dot{M}_E} \tag{1.19}$$

where $\dot{M}_E$ is the "critical" accretion rate required to produce the Eddington luminosity,

$$L_E \equiv \frac{4\pi GMc}{\kappa} \tag{1.20}$$

Clearly, the disk cannot remain thin and in hydrostatic equilibrium if the accretion rate is too high. In addition even subcritical radiation pressure dominated thin disks may be subject to thermal instabilities which will tend to make the disk puff up. Two things can happen - either hydrostatic equilibrium breaks down and material is blown off in a wind driven by radiation pressure

(Shakura and Sunyaev 1973) or the thinness assumption breaks down and a thick radiation pressure supported disk is formed. Assuming the former possibility to be the course which nature chooses, Meier (1979, 1982 a,b,c) has made detailed models of supercritical winds. In this section the latter possibility will be discussed. The real situation might of course lie somewhere in between, with both a thick disk and a wind or jet, but 2D radiation hydrodynamical simulations are required to explore the matter fully.

Tidal disruption of individual stars by black holes with mass $\lesssim 10^6 M_\odot$ has also been suggested as a mechanism for producing radiation supported tori (Frank 1979).

The assumption of hydrostatic equilibrium immediately places a great constraint on the viscosity in a thick disk (JAP). Rough calculations of the accretion velocity give

$$v \approx \alpha v_s \left(\frac{H}{\varpi}\right) \tag{1.21}$$

where α is the viscosity parameter. Because the disk is thick, equation (1.14) implies that v_s is now of order v_{kep} (pressure gradients are dynamically important), and so α must be small in order for hydrostatic equilibrium to remain valid. This is in contrast to the thin disk case where the smallness of H/ϖ and v_s ensured dynamical equilibrium.

Modelling thick accretion disks is a much more difficult business than in thin disks because mass, energy and angular momentum will in general be transported both vertically and radially. The initial approach adopted in the early works of Paczyński and Wiita (1980, hereafter PW); JAP and Abramowicz, Calvani and Nobili (1980, hereafter ACN) was to drop entirely any discussion of the disk interior and to use instead global conservation laws to elucidate general features. They envisaged a stationary configuration consisting of a thin Keplerian outer disk which swelled into a thick disk at radius ϖ_{out}. This in turn extended down to an unstable cusp where a thin stream of matter overflowed into the black hole (figure 8). Full general relativity was used by JAP whereas Newtonian and pseudo-Newtonian potentials were used by ACN and PW.

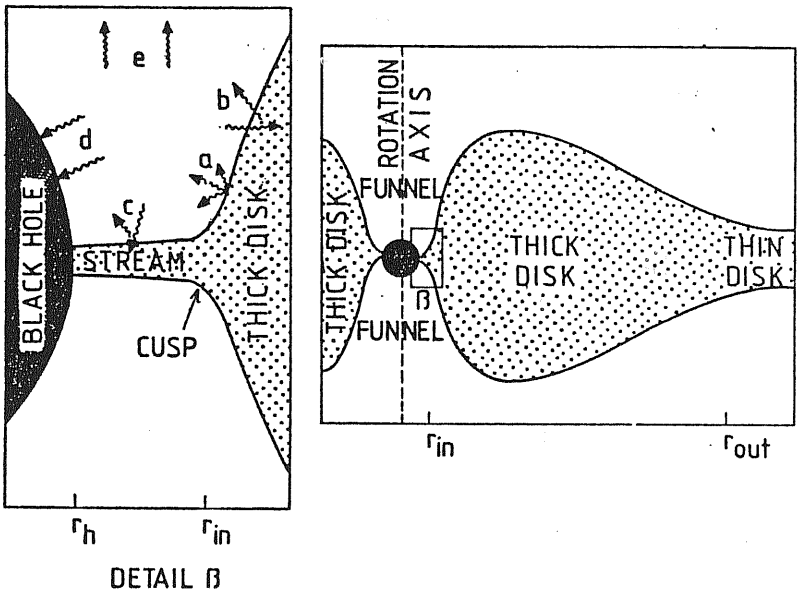

Figure 1-8. (taken from JAP) The supercritically accreting disk model of PW, JAP and ACN. The left hand panel illustrates the possible fates of radiation emitted in the inner funnel region. The bloated form of the thick disk which is illustrated here was not in fact a general feature of the models. PW calculated several cases in which the disk height increased monotonically with radius.

Assuming that the disk surface can be well approximated by a zero pressure surface, its shape can be calculated given the inner cusp radius ($\varpi_{mb} \leq \varpi_{in} \leq \varpi_{ms}$), the height at the cusp, and the surface distribution of specific angular momentum $\ell(\varpi)$. Because the thick portion is everywhere radiation pressure dominated, the above papers also assumed that its surface was radiating at some given fraction $C(\varpi)$ of the local Eddington flux $\underline{F}_{Edd} = -c\underline{g}_{eff}/\kappa$, which is already known once the shape of the surface is known. Integrating the flux over the surface gives the radiated luminosity.

The outer thin disk can be modelled in the way outlined in the previous section using local conservation of mass, angular momentum and energy. In the thick portion, where details of the accretion flow become uncertain, global conservation laws may be invoked . Neglecting winds from the disk surface, the rate at which mass enters the disk through ϖ_{out} must equal the rate at which it flows out at ϖ_{in} . The viscous torque applied to the thick disk must equal the net rate at which angular momentum leaves by advection and radiation. Finally, neglecting the advection of heat into

and out of the thick portion and additional possible internal sources such as nuclear burning, then thermal equilibrium implies that the thick disk luminosity is equal to the rate of work done by the viscous torque on the disk plus the rate at which mechanical energy is lost in the flow from ϖ_{out} to ϖ_{in}.

Neglecting the viscous torque produced by the transonically accreting stream, the above laws enable one to determine the stationary accretion rate and the viscous torque at ϖ_{out}. If one also assumes that the luminosity produced by the stream is negligible, then applying global thermal equilibrium to the whole (thick and thin) disk configuration gives the total luminosity:

$$L = \dot{M} e_{in} \tag{1.22}$$

where e_{in} is the binding energy at the cusp. Note that thick disks will in general be less efficient than thin disks in converting rest mass into radiated energy because the binding energy of a Keplerian orbit <u>decreases</u> inside the marginally stable orbit ϖ_{ms}. Of course equation (1.22) does not take into account the fate of the radiation after it initially leaves the surface (see figure 1-8).

Even though thick disks may be inefficient, their total luminosities can in principle exceed the Eddington limit by as much as a hundred in the case of a 10^8 $M_\odot$ black hole (ACN). ACN have also shown that this is <u>not</u> due to the nonspherical geometry of the torus, as one might initially guess, but to the centrifugal contribution to the effective gravity. Indeed, configurations with big shear and small vorticity can easily have luminosities in excess of equation (1.3) and still remain in hydrostatic equilibrium.

Most of the luminosity is radiated in the central funnel region and this fact is the source of most interest in thick disks. Lynden-Bell (1978) proposed that the intense radiation field in the funnel region could accelerate a pair of collimated jets, and that radiation pressure supported thick disks could thus be the central powerhouses of some active galactic nuclei and quasars. (For further work in this area, see Nobili, Calvani and Turolla 1985 and references quoted therein.)

The approach adopted by ACN, JAP and PW is useful but only zeroth order. No assumptions about the viscosity mechanism (except that it must be small) and the equation of state or flow pattern in the interior were made.[3] However, this is done at the price of specifying two free functions $\ell(\varpi)$ and $C(\varpi)$ on the disk surface, in addition to the height at the inner edge. Topological and stability ($d\ell/d\varpi > 0$) arguments can restrict $\ell(\varpi)$ somewhat, and PW also use local thermal equilibrium at ϖ_{ad} to provide an additional constraint. Clearly, though, it is the accretion flow which determines these functions, and one must study the disk interior to proceed further.

The earliest attempt to model the accretion flow was by Paczyński (1980). Using a pseudo-Newtonian potential, he considered an extreme case where the viscosity was large only close to the disk surface, so that the flow was confined to a thin layer there. Hydrostatic equilibrium was assumed to hold; and the shape of the disk was again determined by specifying the surface distribution of $\ell(\varpi)$. However, $\ell(\varpi)$ was in turn determined by the structure of the accreting layer. This layer is like a thin disk tacked onto the thick disk, and local conservation of mass, energy and angular momentum determine its radial structure. All the heat dissipated in the layer was assumed to be locally radiated out of the disk at a constant fraction C of the Eddington flux. The inner cusp boundary was assumed to have zero height while at large radii the solution was matched onto a thin disk.

Given these assumptions the disk height, surface angular momentum distribution and inner radius could be calculated once $(\dot{M}/C)$, or equivalently the outer transition radius, was specified. Beyond the fact that it did not participate in the accretion, no assumptions were made about the disk interior. Subcritical (with C=1) models all had $\varpi_{in} = \varpi_{ms}$, as in thin disk models, whereas ϖ_{in} gradually moved inwards to ϖ_{mb} at higher supercritical accretion rates. At the same time the disk became thicker with narrower funnels. At very high accretion rates regions were formed in which $d\ell/d\varpi < 0$ and which were therefore dynamically unstable.

---

[3] PW actually assumed that the disk interior was barotropic. However, none of their results depend on this assumption.

Paczyński and Abramowicz (1982) studied a complementary model in which viscosity was assumed to be important only on the equatorial plane of the disk. They proposed that in such a case the disk would be convectively unstable, and argued by analogy with stellar interiors that the convection would be very efficient in transporting heat and angular momentum. This means that along a convective flow line the fluid would be very close to its marginally stable state, i.e. the specific entropy and specific angular momentum ℓ would be constant. They were thus led to consider so-called "gyrotropic" configurations:

$$s = s(\ell) \tag{1.23}$$

As convection occurs primarily in the vertical direction, the constant entropy surfaces have the topology (but not the exact shape) of cylinders. Assuming hydrostatic equilibrium over long enough timescales, pseudo-Newtonian gravity, an α-viscosity and a mixture of perfect gas and radiation they were able to construct models with critical and twice critical accretion rates. Both of these turned out to be stable to the Høiland criterion (even radially) and they were able to confirm a posteriori that the contribution of nuclear burning was negligible.

Some of the most detailed models constructed so far were by Wiita (1982). Taking the models of PW, he beefed them up by placing uniform and exponential atmospheres on the surface, adopted a polytropic interior, and assumed explicit α-viscosity laws. This permitted an investigation of the structure of the interior and checks to be made on its self-consistency, in particular the assumptions that nuclear burning and self-gravity were negligible. In addition, one set of models was constructed under the assumption that the ratio of gas to radiation pressure was constant in the atmosphere and then the distribution of α was calculated, permitting a check on whether it was low. In another set of models the reverse procedure was taken whereby a distribution of α was assumed and a check was made on whether the atmosphere would be radiation pressure dominated.

In both sets of models the most serious constraint was caused by self-gravity, a problem which became worse as the inner edge moved closer to the marginally bound orbit. Indeed it was claimed that it was hard to

have non-self-gravitating disk models around non-rotating black holes more massive than about 10^7 $M_\odot$, although more elaborate models might change this conclusion.

Finally, Begelman and Meier (1982) examined the extreme case where the accretion rate is very supercritical, so supercritical in fact that the trapping radius R_T (the radius below which photons are advected with the accretion flow faster thatn they can diffuse outwards) lies well outside the cusp radius. Inside R_T most of the heat would be advected with the flow except in the surface layers. Investigations were made of the region well inside R_T and outside the cusp and pressure maximum under the assumptions that the flow would be self-similar and that infall velocities would be small enough to maintain hydrostatic equilibrium. Diffusion of radiation was neglected compared with advection, but allowance was made for the diffusive surface regions by treating them as a boundary layer.

The models depended on essentially five parameters which measured the pressure gradients, the spatial variation of viscosity, the thickness of the diffusing boundary layer, and the degree of pressure support. Extensive numerical exploration of this parameter space was made. Vertical as well as radial shear was fully allowed for in the self-similar form of the rotation law, and a generic feature of the models was the high vertical shear near the surface. Other interesting features included models in which the angular velocity actually changed sign in the disk and possible thermal instabilities in the surface layers. Also, all disk models were convectively unstable (to the Høiland criterion) in part or all of their volume.

Apart from detailed models, radiation tori have also been studied phenomenologically by workers investigating their utility as models for the central engines of active galactic nuclei. Figure (1-9), from Begelman (1984), illustrates the physical state of the interior near the pressure maximum for various central densities and black hole masses. The upper region of the diagram is excluded for all the previous models because nuclear burning is expected to be an efficient source of energy of self-gravity becomes important.

Lines of constant optical depth and constant α (computed by assuming

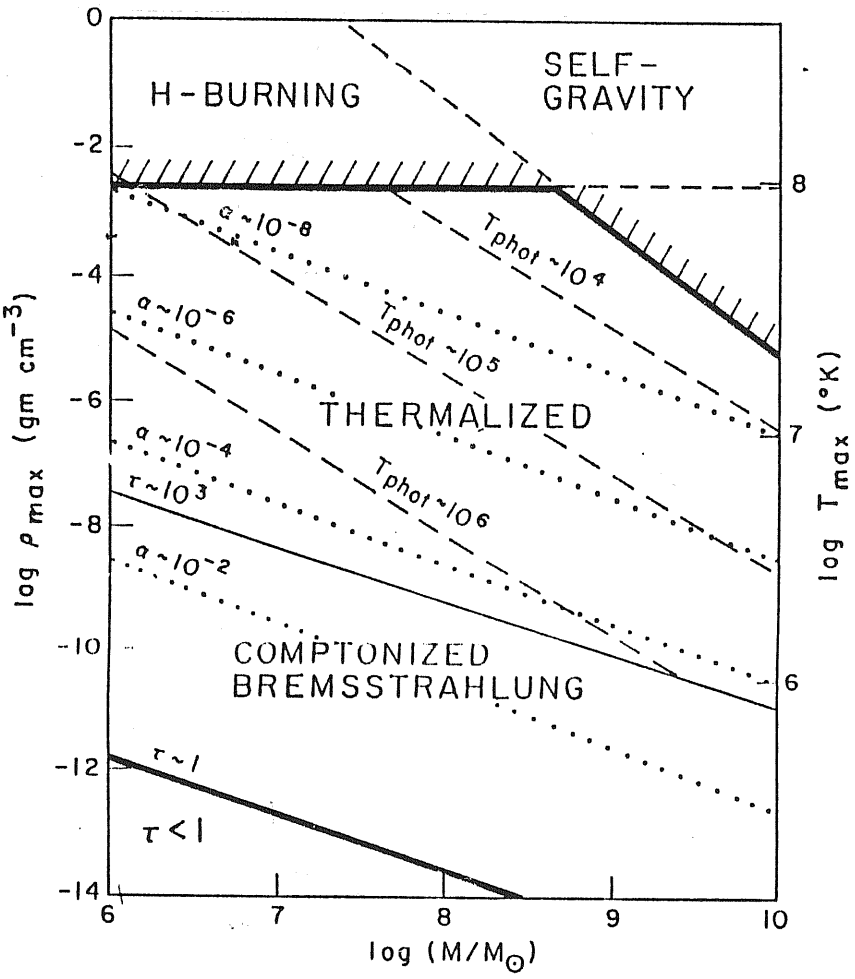

Figure 1-9. (taken from Begelman 1984) The physical state of the interiors of radiation-supported thick disks around supermassive black holes.

that viscosity is generating approximately an Eddington luminosity of heat per unit volume near the pressure maximum) are also plotted. Radiation supported tori are completely excluded from the lower left hand corner where the optical depth becomes less than unity (and α exceeds unity).

Finally, lines of constant photospheric temperature are also shown. These were computed by assuming a homentropic torus, though a stable entropy gradient would simply shift these lines further upwards. If the so-called "blue bump" that is seen in some quasars is thermal radiation with temperature of order 10^4 K, then α must be exceedingly small ($\lesssim 10^{-8}$) in order for a radiation torus to produce it. Note also that even LTE requires $\alpha \lesssim 10^{-3}$ (see also Rees 1984). Hence if the instabilities to be discussed in this thesis do not actually destroy the disk but form turbulence in the nonlinear regime, the effective viscosity thereby produced may be high enough to rule out radiation tori as viable quasar central engine models.

I.4 Radiation Tori - Secular Evolution

There is of course no reason why the infall of material into a thick disk should exactly compensate the radiative losses and outflow of material through the cusp, as is assumed in the stationary models of the previous section. Indeed, one could even imagine an isolated torus left as a remnant from the collapse that produced the black hole or produced by individual tidal disruptions of stars (Frank 1979, Rees 1983).

From equation (1.16) the secular evolution timescales in a thick disk ($H/\varpi \sim 1, \alpha \ll 1$) are much longer than the dynamical timescale. This led Abramowicz, Henderson and Ghosh (1983)[4] to suggest a simple method for computing the evolution of tori which has been recently implemented, with some modifications, by Abramowicz, Blaes and Turolla (1986, in preparation). Briefly, it assumes that the disk is always in a state of dynamical equilibrium which can be well approximated throughout its evolutionary history by a four parameter pseudo-Newtonian model. For disks without cusps and which are therefore nonaccreting these "structural" parameters are

r_G: the ratio of the Schwarzschild radius to the inner radius of the disk.

λ: the ratio of the specific angular momentum at the inner edge to the Keplerian value at this radius.

B : gives the power of the assumed specific angular momentum distribution

$$l = \lambda\, l_{kep}(\varpi_{in})(\varpi/\varpi_{in})^{B/2 + 1} \tag{1.24}$$

β : the ratio of gas pressure to total pressure, assumed constant throughout the disk.

Accreting tori with cusps automatically have λ=1 and for these cases λ is replaced by h_{in} , the height of the disk surface at the cusp, as a structural parameter. Evolution is then determined by bookkeeping the total mass M, angular momentum J, internal energy E_I and mechanical energy E_M using the equations

$$\frac{dM}{dt} = \frac{\partial M}{\partial x_i}\dot{x}_i = D_M \qquad \frac{dJ}{dt} = \frac{\partial J}{\partial x_i}\dot{x}_i = D_J$$

$$\frac{dE_I}{dt} = \frac{\partial E_I}{\partial x_i}\dot{x}_i = D_{EI} \qquad \frac{dE_M}{dt} = \frac{\partial E_M}{\partial x_i}\dot{x}_i = D_{EM} \tag{1.25}$$

---

[4] This paper, by the way, contains an enormous number of errors - the interested reader should be wary.

where x_i (i=1,2,3,4) represents the four structural parameters. The D's and the partial derivatives are all functions only of the x_i's so that equations (1.25) form a closed set which may be integrated numerically from any initial data $\{x_i\}$. D_M and D_J are simply the rate of mass loss and the rate of angular momentum advection, respectively, through the inner edge. In addition to advection, D_{EM} and D_{EI} include the viscous dissipation of mechanical energy into heat, modelled using an α-prescription with constant α. Finally, the torus is assumed to be radiating at the local Eddington flux (with an electron scattering opacity) over its entire surface and D_{EI} also includes this.

Equations (1.25) thus describe the evolution of an isolated torus without external viscous torques or the accretion of material from an external supply such as a thin disk. Given some prescription for handling these effects, they could easily be included in the scheme (though this has not been done yet).

The structural parameters r_G, λ and B determine the equipotential function and span only a limited range of values determined by local stability, $\omega_{in} \geq \omega_{cusp}$, and $\omega_{out} < \infty$. The quantity β, on the other hand, is limited by the self-consistency of the model. It cannot be too high, otherwise the torus would be self-gravitating, and it cannot be too low or the torus would no longer be optically thick. Typically, $\beta \sim 10^{-4}$ for $10^8 M_\odot$ black holes. In any case the code checks at every timestep that the torus is sufficiently optically thick ($\tau > 5000$) and non-self-gravitating. The height at the inner edge is in addition required not to be too large, as otherwise the assumption of hydrostatic equilibrium would break down. The only other parameter which needs to be specified initially is α - the consistency requirements of the previous section give an upper limit $\sim 10^{-4}$.

A full exploration of the initial data space has yet to be made, but it is already clear that nonaccreting tori have only two basic evolutionary behaviours determined by the relative importance of viscous heating to radiative cooling. If heating is dominant, then the specific angular momentum distribution steepens towards Keplerian and the torus inner edge moves inwards and forms a cusp. This is in agreement with the intuitive idea that viscosity is acting to transport angular momentum outwards (even though

this is not explicitly forced by the scheme). If cooling is dominant then the reverse tends to happen - ℓ gets flatter and the torus inner edge retreats from the black hole. At the same time, however, β tends to increase which in turn strongly increases the heating (which goes as β^4). Provided α is not too low and the torus starts off far enough away from the bounds on the parameter space, its evolution thus reverses and it moves to an accreting state.

A full evolution with an accreting transition is depicted in figures 1-10 and 1-11. The starting parameters were $r_{\ell_0}=.35$, $B_\varepsilon=-1.6$, $\alpha=10^{-4}$, $\lambda_0=1.028$ and $\beta_0=10^{-4}$. Time is measured in units of 1.8×10^7 seconds $\simeq$ ½ year. As the disk makes the transition to an accreting configuration, the height at the inner edge and the accretion rate grow rapidly but then stabilize. As time proceeds, the torus loses mass and shrinks down towards a Keplerian thin disk until the height at the inner edge is no longer negligible compared to the torus height. At this point the accretion rate grows rapidly and the torus presumably gets rapidly swallowed by the black hole.

These results are preliminary and further work is in progress. The method is of course very naïve and a number of objections may be raised. First and foremost is that constraining the disks to remain within a four-parameter family may be far too inadequate to model the possibly complicated evolutionary behaviour of real disks. A second criticism is that α is assumed to be constant. The fact that α could vary spatially inside the torus does not really matter as the scheme only uses α as a global conversion factor from the integrated product of stress and strain to the actual heat production. The assumption that α is a constant in time may, however, be much more serious. Finally, the dynamical instability to be discussed later must be taken into account, if indeed there are any configurations which are stable enough to evolve on a secular timescale.

Blandford, Jaroszyński and Kumar (1985) have examined the local secular stability of radiation tori in full general relativity. They find that the Goldreich-Schubert-Fricke instability should be sufficient to maintain

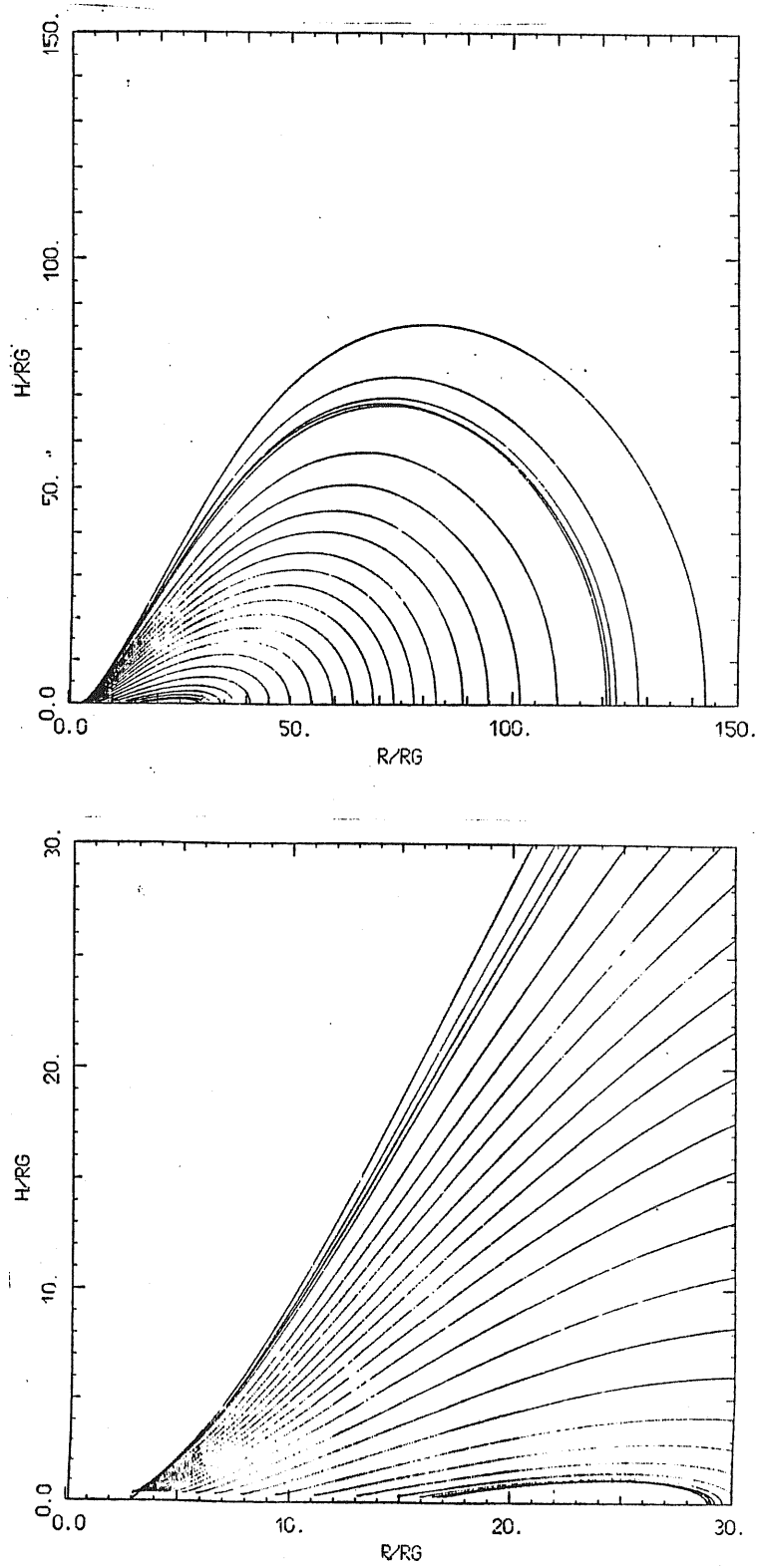

Figure 1-10. The shrinking of the torus surface as it evolves with time. The lower figure shows the cusp region in more detail.

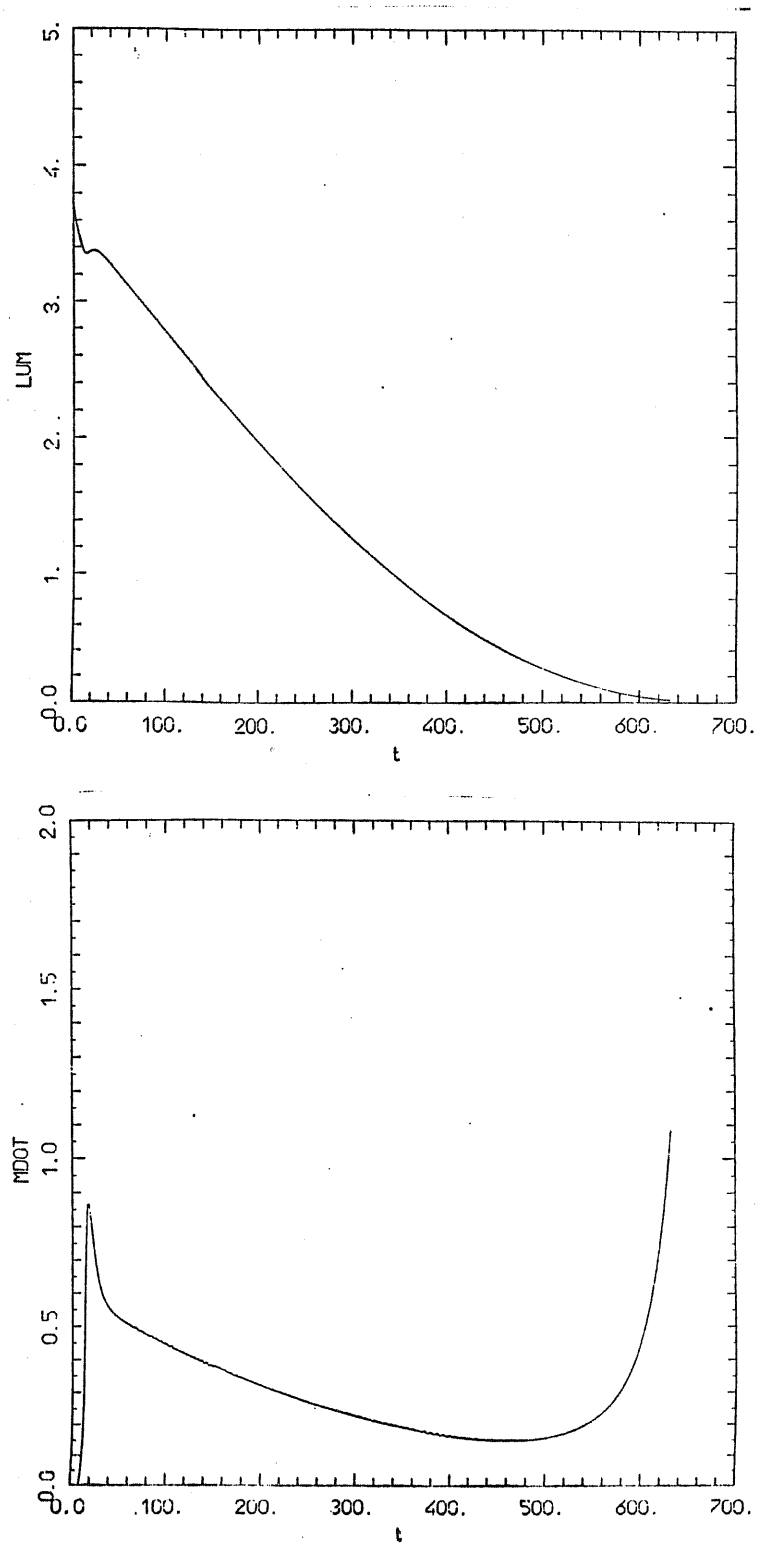

Figure 1-11. The luminosity (upper) and accretion rate (lower) scaled with respect to the Eddington values (an efficiency of 1% is assumed in this scaling).

barotropicity in a radiative zone provided it is sufficiently optically thick. Also, they confirm the assumption made by Paczyński and Abramowicz (1982) that angular momentum and entropy transport should be efficient enough to maintain a convective zone in a gyrotropic state, atleast in the deep interior. Suggestions were made as to how these results could be used to construct an alternative numerical scheme for the secular evolution of tori.

I.5 Ion Tori

Rees, Begelman, Blandford and Phinney (1982) pointed out that most extended radio galaxies emit very little radiation from their nuclei even though they produce highly energetic jets which transfer an enormous amount of power to their radio lobes. A radiation supported torus is highly unsuited to perform such a task because even though it might be able to accelerate the jets, it would inevitably produce too much isotropic emission ($\sim L_E$) to remain below the observed upper limits on the core luminosities. These authors proposed instead that a hot, optically thin gas pressure supported torus might be involved.

The temperature required for gas pressure to be dynamically significant and support a thick disk is given roughly by the local virial temperature $T_{vir} = (GMm_p/3k\varpi)$. Inside $\varpi \sim 2000\ R_G$, however, this temperature exceeds that associated with the electron rest mass energy and electrons will then be subject to very efficient relativistic cooling processes, particularly Compton scattering. Therefore to maintain a thick disk the ions must not be able to transfer their thermal energy to the electrons.

Coulomb interactions alone are insufficient to couple the electrons and ions if $\dot{M}$ is low enough to satisfy

$$\dot{M}\alpha^{-2} < 50\dot{M}_E \qquad (1.26)$$

Collective plasma processes may do the job, but these are apparently so poorly understood that Rees et al. contented themselves with assuming that it is possible for the ions to be much hotter and so support the torus.

Unlike the radiation torus, the ion torus is a very inefficient radiator, but it could nevertheless provide the catalyst for tapping a rotating black

hole's spin energy in order to accelerate a jet.

Note from equation (1.26) that α cannot be too low otherwise the disk would cool. Hence if the plasma physics works out, ion tori may be less vulnerable to any turbulent viscosity which may be generated by a nonlinear saturation of Papaloizou and Pringle's instability.

II. REVIEW OF THE PAPALOIZOU AND PRINGLE INSTABILITY

The thick disk models of the previous chapter cover a reasonably wide range of physical possibilities concerning the physical state of the plasma, the viscosity distribution, energy transport and the accretion flow pattern. All of them, however, rest on the fundamental (and untested at the time) assumption that thick disks can actually exist in stable dynamical equilibrium. To help ensure this the more detailed models were all checked against the Høiland stability criterion (see section 3.3 below) and some, particularly the self-similar flows of Begelman and Meier (1982), were found to be unstable. However, this criterion is simply a check that local buoyancy and centrifugal forces act to push individual perturbed fluid elements back to their equilibrium positions, and although it is a necessary condition for stability for perfect fluids in pure rotation, it is certainly not sufficient. In addition, its applicability to thick disks is limited to regions where the flow pattern is to a good approximation azimuthal, and it therefore says nothing about the fluid near an overflowing cusp.

With the view of exploring the applicability of this criterion further, Abramowicz et al. (1984b) derived a gigantic general local dispersion relation for axisymmetric perturbations on non-self-gravitating fluids. This relation is only valid if the perturbation wavelengths are much smaller than any local scale height, but interesting results could still be found. Although straightforward to derive, however, its sheer size and complexity have meant that a full exploration of the solution space has not yet been performed.

II.1 The Discovery

Hacyan (1982) studied the stability of thick disks from the (much more difficult!) global point of view. Lagrangian displacement trial functions which were linear in the Cartesian coordinates were used in the variational principle of Lynden-Bell and Ostriker (1967) to obtain approximate normal mode eigenfrequencies. Non-self-gravitating polytropic tori with adiabatic index $\gamma = 4/3$ and different specific angular momentum distributions were studied, and it was found that all these models were subject to instabilities with growth rates

$$\mathrm{Im}\,\sigma = A\,(\omega_{in}/\omega_{out})^{1/4}\,\Omega_{in} \qquad (2.1)$$

where A is a slowly varying function of ω_{in}/ω_{out} and is of order unity. The instabilities thus act on the dynamical timescale and pose serious problems for the self-consistency of thick disk models. However, the results are uncertain due mainly to the choice of trial function. This is in fact an exact solution for uniformly rotating, homogeneous bodies but is unlikely to be accurate for strongly differentially rotating, inhomogeneous configurations like thick disks (see e.g. chapter 6 of Tassoul 1978).

Papaloizou and Pringle (1984, 1985; hereafter PPI and PPII respectively) made another attempt with a study of non-self-gravitating, homentropic tori. In contrast to the previous approach of Hacyan, they used the Eulerian perturbation equations and actually attempted to solve them. In this way they were able to demonstrate conclusively the existence of a global non-axisymmetric instability which operates on the dynamical timescale. Tori subject to such an instability are unlikely to survive it and they concluded

> "These results imply that models of quasars which invoke accretion tori and models which imagine that centrifugal force can vacate a funnel up the rotation axis along which jets might originate are not viable."
>
> -PPII

Subsequent work has shown that this assertion may have been made a bit hastily, but even so thick disk theory will never be the same again.

PPI was confined to the study of constant specific angular momentum tori, for which the perturbation equations are much simpler than in the general case. Of course these configurations are only marginally stable to local perturbations anyway, but the global instability which was found has nothing to do with this. The actual results of this paper were as follows:

(1) By imposing artificial boundary conditions on tori with nonzero surface pressures, it was proven that incompressible tori are stable, and so any instability must somehow result from the fluid having a finite sound speed.

(2) An ingenious though rather tortuous argument was presented which demonstrated that every configuration is unstable to modes with high enough

azimuthal wavenumber.

(3) Two analytic calculations were performed on simple, but unrealistic, equilibrium models. Instabilities were found which grow on the dynamical timescale.

(4) Numerical calculations of the growth of arbitrary perturbations in realistic tori revealed the fastest growing unstable modes which grow on the dynamical timescale.

The first result is now known to be completely incorrect (Blaes 1985; Goldreich, Goodman and Narayan 1986,hereafter GGN) due to the fact that the effectively rigid boundary conditions precluded the existence of gravity waves on the (actually free) surface of the torus. Indeed, it is these surface waves which provide the key to understanding the most destructive mode of the instability.

The second piece of analysis, although proving the existence of instabilities, does not give any indication of their growth rate. Moreover, it again relies on the same incorrect boundary conditions and thus produces a criterion which requires compressible flow for an instability. PP support their choice of boundary conditions by arguing that if the density is low enough on the surface, it should not matter what precise boundary conditions are adopted, providing the perturbations are regular. Subsequent calculations do in fact support them on this, but of course it only works for compressible configurations[1]. This is important, however, because it shows that the inevitably complicated surface structure of a real thick disk will not have much effect on the instability.

Of more practical interest are the analytic calculations, but these have been superseded by later analytic work which will be discussed below. This leaves the numerical results which are worth describing in some detail.

The technique involved following the time evolution of arbitrary initial

---

[1] It's not that incompressible tori are actually supposed to be realistic, but that they give an easy physical understanding of the nature of some of the unstable modes. To state that the instability is due to finite sound speeds, simply because one can alter the boundary conditions in compressible tori and thereby rule out unstable incomprssible tori with the same altered boundary conditions, is clearly misleading.

perturbations corresponding to a particular azimuthal wavenumber m. After a period of time the fastest growing unstable mode dominates the perturbations and one can measure its growth time from the rate of increase of the perturbation amplitude.

In order to check the results, two different grids were employed in the spatial difference scheme. One (grid A) was a rectangular (ϖ ,z) grid and the other (grid B) used an orthogonal coordinate system in which one of the coordinates (f) was proportional to the effective potential (fig. 2-1). The boundary conditions employed on the torus surface were also different in the two cases.[2]

Figures 2-2 and 2-3, taken from PPI, illustrate the structure of the fastest growing modes for various m and torus thicknesses (represented here by a parameter β which approaches zero for slender tori and unity for infinitely thick tori). Both methods give more or less the same results. The contours are lines of constant absolute value of the perturbed velocity potential normalized such that the maximum value is one. Only modes which are symmetric with respect to the equatorial plane were considered. The most striking fact is the lack of vertical structure, especially in ths slender tori. In all cases the perturbation is concentrated towards the inner and outer radii, this effect becoming more pronounced as the torus becomes thicker (β increasing) or as m increases.

The growth times for each of the cases are listed in table 1 - all are within an order of magnitude of the dynamical timescale. Note that the higher m modes are faster in the slender torus. For the m=2 mode, the growth rate first increases with β but apparently seems to fall again as the torus gets even thicker.

PPII extended the analytic work of the first paper to configurations with power-law specific angular momentum distributions:

---

[2] Contrary to what is stated, PPI actually used the correct free surface boundary condition in grid B, because they require

$$\left(f^n \frac{\partial W}{\partial f}\right)_{f=0} = 0$$

This rules out unphysical solutions because they go as f^{1-n} (see section 4.2 below).

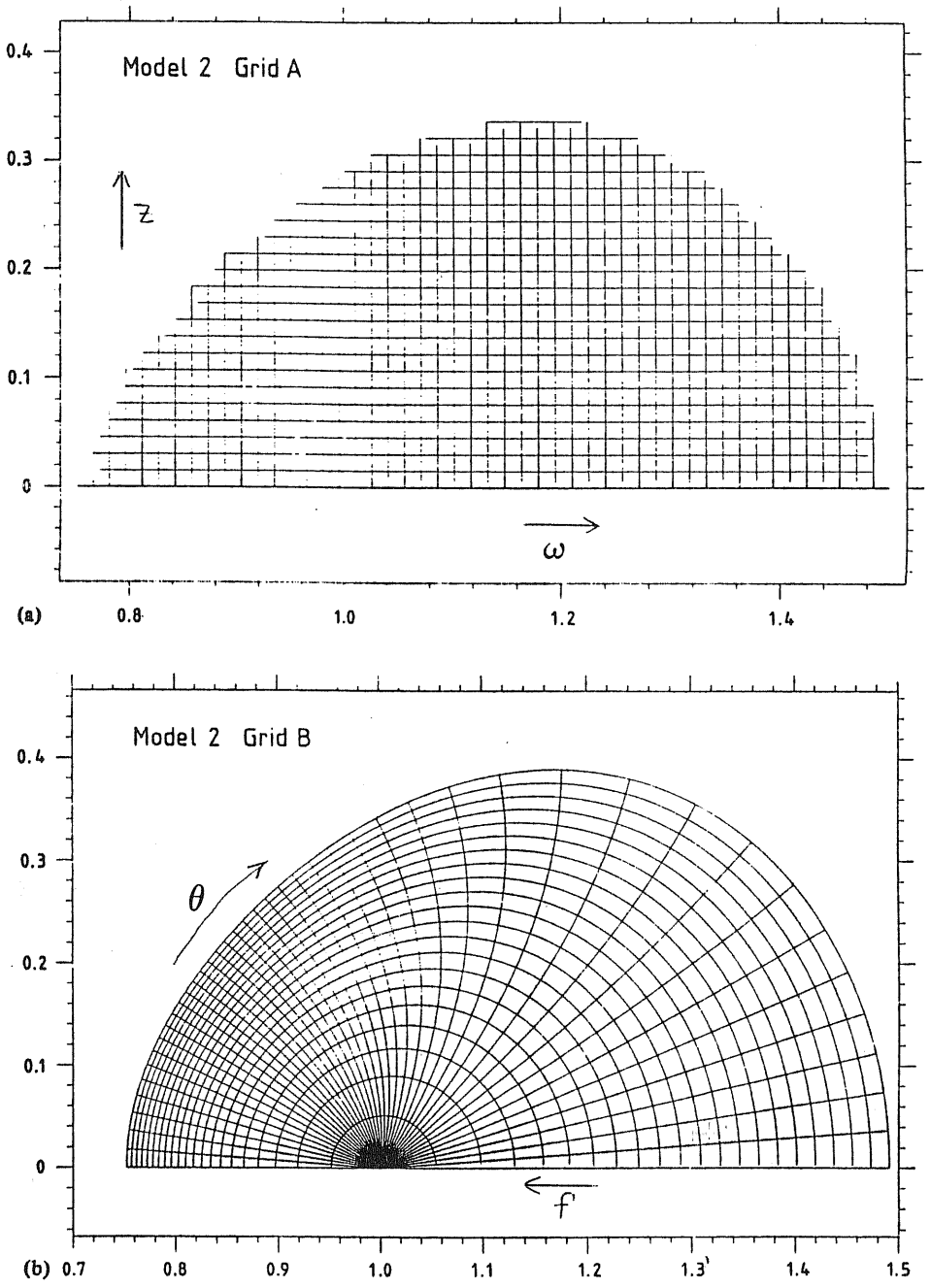

Figure 2-1. The grids used in the numerical calculations of PPI.

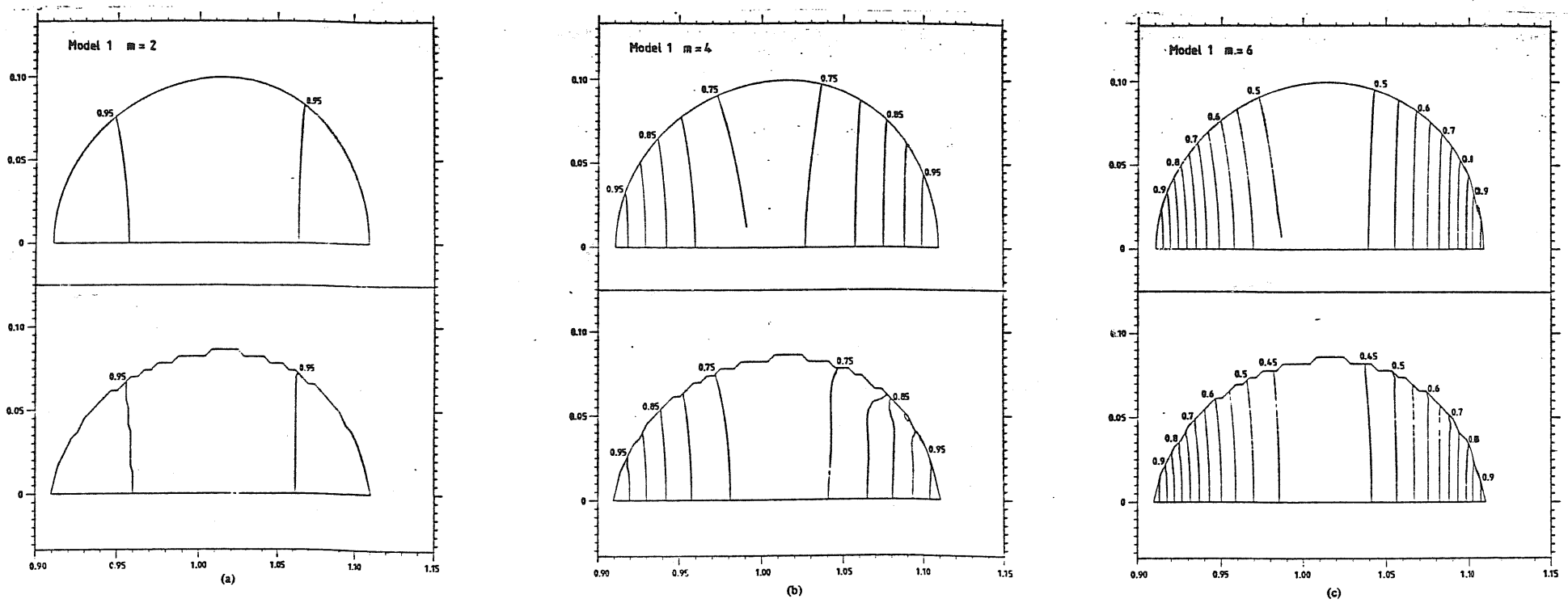

Figure 2-2. Structure of the fastest growing modes in the β =0.0995 torus for (a) m=2, (b) m=4 and (c) m=6. The upper and lower frames correspond to grids B and A respectively.

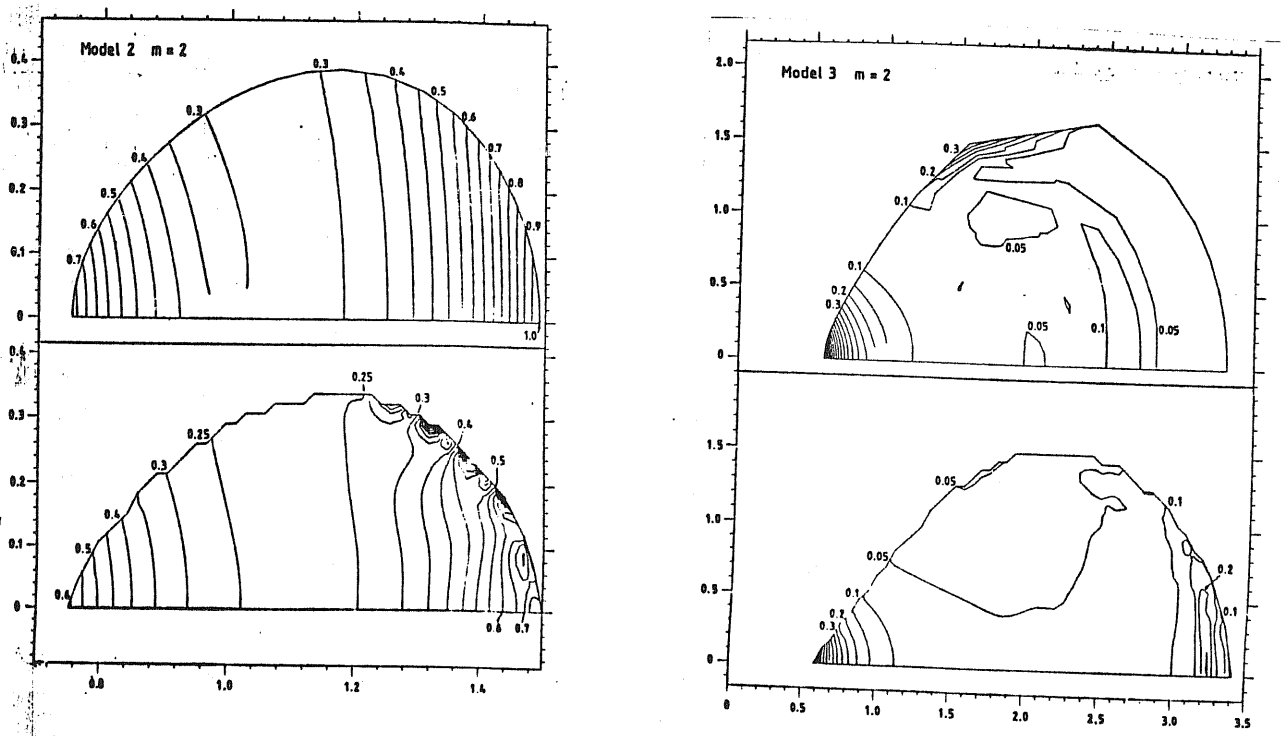

Figure 2-3. Structure of the fastest growing m=2 modes in the (a) β =0.333 and (b) β =0.707 tori. The upper and lower frames correspond to grids B and A respectively.

Table 1. Growth times in units of Ω_o^{-1} from the numerical calculations of PPI.

β	m	Grid A	Grid B
0.0995	2	8.0	8.5
	4	3.9	4.7
	6	2.9	4.0
0.333	2	4.0	4.6
0.707	2	8.5	10.7

$$\ell = \ell_{R_0}(\varpi/\varpi_0)^{2-q} \quad , \quad 1.5 < q \leq 2 \tag{2.2}$$

The results were as follows:

(1) All unstable modes must corotate with the equilibrium flow somewhere.

(2) Perturbation theory was employed near the (q=2) constant specific angular momentum limit to show that the instabilities of PPI were not an artifact of the special choice of rotation law, but persisted in a continuous manner when the rotation law was changed.

(3) For slender tori there exists a mode which is symmetric with respect to the equatorial plane and is stable for $q < \sqrt{3}$ while unstable for $q \geq \sqrt{3}$. Antisymmetric modes, on the other hand, are stable. This apparently innocuous result turns out to be of absolutely vital practical importance as we shall see later.

(4) High m modes in near-Keplerian thin disks are unstable, but no indication of their growth time was given.

PP interpreted these instabilities as being of two types, one sonic in origin and the other simply a compressible version of the classic Kelvin-Helmholtz instability. This viewpoint was taken on the basis of the important work by Grinfeld (1984) on the stability of compressible plane parallel shear flows. PPII presented an extension of this analysis to two-dimensional rotating flows and the following sufficient criterion for stability was derived. If there exists a constant quantity Ω_c for which

$$(\Omega - \Omega_c)\frac{d}{d\varpi}\left(\frac{\omega}{\rho}\right) > 0 \tag{2.3}$$

and

$$\varpi^2(\Omega - \Omega_c)^2 < v_s^2 \tag{2.4}$$

throughout the fluid, then the flow is stable. In the first inequality ω is the vorticity, and this condition can only be violated if the gradient of ω/ρ vanishes somewhere in the flow. This generalizes the famous inflexion point theorem of Rayleigh[3] to rotating, compressible flows. The

[3] This theorem was originally derived for a two-dimensional plane-parallel shear flow of incompressible fluid confined between two rigid plates. It

second inequality has no such analogue, and indeed rules out instabilities in zero vorticity (i.e. constant specific angular momentum) incompressible flows. As already stated above, this is incorrect, and it again arises because these stability criteria were derived under the assumption of rigid boundary conditions.

It can be shown, however, that the same criteria result from free boundary conditions, provided the fluid is incompressible. In this case, though, inequality (2.3) is always violated and the full criterion, which is only sufficient for stability, loses its utility. PP's physical interpretation is terms of these criteria is again misleading, and indeed GGN have shown that the so-called Kelvin-Helmholtz mode near $q=\sqrt{3}$ is in fact the same mode which is present in the slender constant specific angular momentum torus.

II.2 The Energy Source

Papaloizou and Pringle's instability is dynamical - after the torus is slightly perturbed it will thereafter preserve its total energy (and angular momentum). An exact (nonlinear) expression for this is

$$E_{Tot} = \int_{M_{Tot}} \tfrac{1}{2}(\delta v_\varpi^2 + \delta v_z^2)\,dM + \int_{M_{Tot}} \left[\tfrac{1}{2}(v_\phi + \delta v_\phi)^2 + (u + \delta u) + \Phi \right] dM \equiv E_1 + E_2 \qquad (2.5)$$

where v , u and Φ are time-independent distributions of azimuthal velocity, specific internal energy and gravitational potential energy of the original equilibrium torus. The perturbations and mass distribution are of course time-dependent. Note that the first integral E_1 is non-negative. Initially its magnitude will be close to zero but if there is an instability then it will grow. The energy reservoir to fuel this growth is contained in the second integral E_2, which initially has a value close to the total equilibrium energy.

Another property of the unstable modes is that they are non-axisymmetric - all the m=0 modes are stable provided the Høiland criterion is satisfied

---

states that a necessary condition for instability is that the flow velocity have an inflexion point somewhere or, equivalently, that the vorticity gradient vanish at some point (see e.g. Drazin and Reid 1981).

throughout the torus (Fricke and Smith 1971). The main difference between axisymmetric and non-axisymmetric perturbations is that the former conserve a fluid element's angular momentum whereas the latter do not. This fact led to a telling remark made at the end of PPI:

> "It is the ability of non-axisymmetric modes to transfer angular momentum which enables the tapping of the shear energy and so the growth of the mode."
>
> -PPI

To understand the meaning of this statement, consider how one might reduce E_2 in order to increase E_1. Suppose the density and specific internal energy distributions are kept constant. Then the only way to vary E_2 is to reduce the rotational kinetic energy term

$$T = \int_V \tfrac{1}{2} \rho v_\phi^2 dV \tag{2.6}$$

where, for the sake of brevity, v_ϕ is now the actual azimuthal velocity of the perturbed fluid. Because the density distribution is fixed, the moment of inertia

$$I = \int_V \rho \varpi^2 dV \tag{2.7}$$

is fixed. From the Schwarz inequality,

$$TI = \tfrac{1}{2}\left(\int_V \rho v_\phi^2 dV\right)\left(\int_V \rho \varpi^2 dV\right) \geq \tfrac{1}{2}\left(\int_V \rho v_\phi \varpi dV\right)^2 = \tfrac{1}{2}J^2 \tag{2.8}$$

where J is the total conserved angular momentum of the torus. Therefore

$$T \geq \frac{J^2}{2I} \tag{2.9}$$

with equality occurring only if v_ϕ and ϖ are linearly dependent, i.e. the fluid is <u>uniformly rotating</u> ($v_\phi \propto \varpi$). Hence every differentially rotating fluid has "shear energy" which can be tapped to fuel the growth of perturbations. Note that this does not depend on the fact that ρ and u were kept fixed - they could be changed as one pleased but if the flow were

still differentially rotating one could extract further energy from it by making it rotate uniformly.

For tori which have angular velocities which decrease outwards, it is therefore possible to release energy by transferring angular momentum from the rapidly rotating inner regions to the more slowly rotating outer regions, something only non-axisymmetric modes can do. Students of accretion disk theory will recognize this energy argument from Lynden-Bell and Pringle (1974). Viscosity dissipates mechanical energy in an accretion disk for precisely the same reason.[4] The corotation theorem of PPII (and generalizations discussed in chapter III below) gives an intuitive confirmation that this is indeed the driving force behind the instability, because inside the corotation radius the perturbations will be moving more slowly than the equilibrium flow, while outside they will be moving faster.

II.3 The Tapping Mechanism

Having identified a possible energy source, one still needs to discover what are the essential global conditions which allow some non-axisymmetric modes to tap it. In order to shed some light on this problem, Goldreich and Narayan (1985) studied isothermal perturbations on an infinitely thin, homogeneous gas sheet with a constant velocity gradient and an artificial Coriolis force to simulate the effects of rotation. For such a system the perturbation equations may be solved exactly, with the wave-like asymptotic forms of the solutions being used to impose boundary conditions and determine the eigenfrequencies. The entire procedure is essentially equivalent to a WKB analysis of a differentially rotating disk and has been used in the study of spiral arm formation in disk galaxies (Goldreich and Lynden-Bell 1965).

---

[4] Indeed, this discussion is actually a consequence of a rather profound fact - fluid equilibria are not necessarily configurations of extremal energy, as there is no unconstrained action principle for the fluid equations in Eulerian variables (Schutz and Sorkin 1977). If the perturbations conserve particle number, entropy, and are axisymmetric, then the energy of an axisymmetric rotating configuration is an extremum. This is why one can derive energy principles for axisymmetric stability (Tassoul 1978, ch.6) but also why they do not work for nonaxisymmetric perturbations - such a principle would be impossible to derive.

Goldreich and Narayan found that if reflecting boundaries were placed on either side of the corotation radius then an instability was generated. If the reflection coefficients were reduced then the growth rates decreased. This is simply the standard wave amplifier of spiral density wave theory (Mark 1976) and can be intuitively understood as follows (see figure 2-4).

A wave incident on the corotation region from the inner parts of the disk will produce a reflected wave and a transmitted wave. Now, the incident and reflected waves have negative angular momentum relative to the equilibrium flow because their pattern speeds are lower. The transmitted wave, on the other hand, has positive angular momentum. Because of angular momentum conservation, the outward angular momentum transfer to the transmitted wave causes a reduction, and therefore amplification, of the reflected wave. A reflecting boundary at the inner edge is needed simply to provide a feedback so that the process can continue. Alternatively, a reflecting boundary at the outer edge will produce similar results, while two reflecting boundaries could produce correlated amplification on both sides of the corotation region.

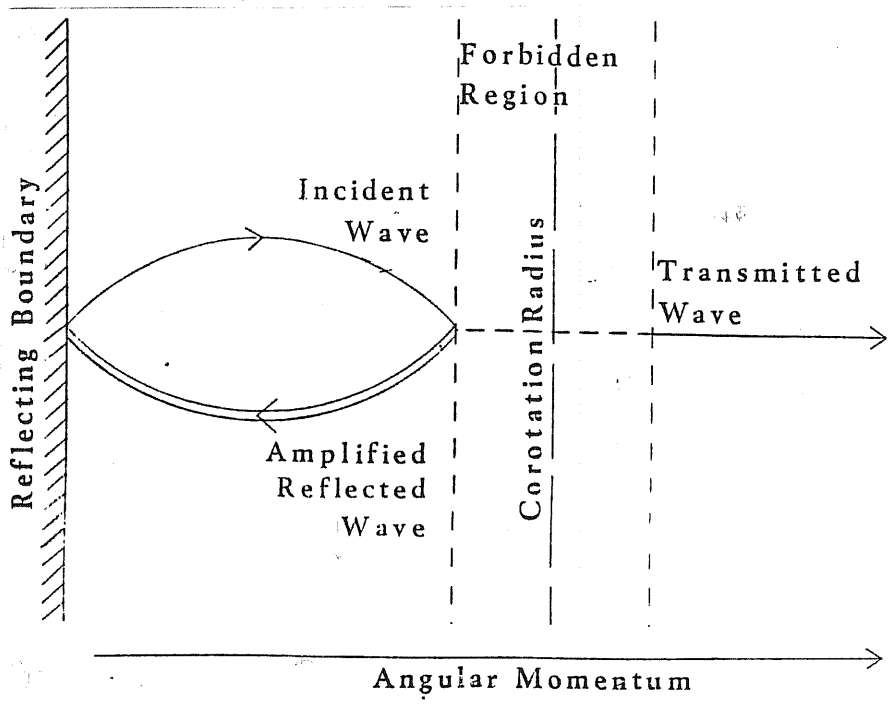

Figure 2-4. The wave-amplifier picture of Goldreich and Narayan (1985). Outside the so-called "forbidden region" the perturbations have a wave-like character, and it is the interaction of these waves across the corotation radius that drives the instability.

That is the physical idea, but whether or not it actually works in more general configurations than that considered by Goldreich and Narayan was studied by Drury (1985). By examining conditions near the corotation radius in cylindrical but otherwise quite general non-self-gravitating flows it was found that a necessary condition for this region to be able to amplify waves is that

$$Ri < 1/4 \tag{2.10}$$

where Ri is the Richardson number defined by

$$Ri \equiv \frac{(k_z^2 + m^2/r^2\omega^2)N^2 + k_z^2\kappa^2}{m^2(d\Omega/dr\omega)^2} \quad . \tag{2.11}$$

Here k_z is the vertical wavenumber, N is the Brunt Väisälä frequency and κ is the epicyclic frequency. This criterion is well-known as a necessary condition for instability in flows between rigid boundaries (Sung 1974). Drury shows in addition that a <u>sufficient</u> condition for the corotation region to act as an amplifier is that Ri vanishes there. Note that for modes which are approximately independent of height (k_z small), condition (2.10) can be satisfied if N^2 is small, i.e. either the specific entropy gradient or the pressure gradient vanishes locally.

If the wave amplifier picture works in fully three-dimensional tori, then it would suggest that instabilities would always be present as the Richardson number can be made as small as one likes by taking high m modes corotating near the pressure maximum ($N^2 \sim 0$). However, in addition to a corotating amplifier, "reflecting boundaries" are required. Goldreich and Narayan state that if the density cuts off near the inner and outer surfaces of the torus on scales shorter than the radial wavelength of the mode, then they will behave as perfect reflectors. This is probably correct if the WKB waves are sonic in character.

The main trouble with these ideas, however, is that the fastest growing perturbations tend to have characteristic radial scales which are much larger than the entire torus cross-section! It is therefore difficult to interpret them as waves - a more realistic discussion would centre around how the

true boundary conditions act to set up a corotating eigenfunction which by its very nature would transport angular momentum outwards and be self-amplifying. Fortunately, there now exists such an interpretation.

II.4 The Instability as a Surface Wave Interaction

In the special case of a slender, non-self-gravitating constant specific angular momentum torus one can calculate all the normal modes analytically (Blaes 1985b, Jaroszynski 1985, chapter IV). The fundamental mode corotates with the equilibrium flow and exists for every value of the azimuthal wavenumber. It is this mode which causes the instability in slender tori, and calculations of the growth rate and perturbation amplitude agree well with the numerical computations of PPI. However, in contrast to the statements made in PPI and II, this mode is not sonic in character and does not go away when the incompressible limit is taken.

The realization that incompressible configurations could share the same unstable behaviour as tori led Blaes and Glatzel (1976) and GGN independently to study two-dimensional incompressible annuli (chapter V). Their methods of treatment differ, but the essential point is the same. For a given azimuthal wavenumber there exist four modes which, when the boundaries are sufficiently far apart, represent surface gravity waves propagating upstream and downstream at the inner and outer edges, the amplitudes of the waves decaying with depth inside the annulus.

Due to the differential rotation, the two inner modes have much higher "pattern speeds" than the two outer modes. The slower upstream inner mode and the faster downstream outer mode have the closest speeds, and each of these two modes has a corotation point inside the annulus. As the boundaries are brought closer together, the faster outer mode catches up with the slower inner mode, their corotation points coincide, and they merge to form a single mode which has high amplitude at both edges and a corotation point in between - this mode is unstable.

Of course the boundaries play a crucial role here simply because the annulus is incompressible, and so wave motion can only be supported at the free edges. Indeed, the instability can be killed off in this case by placing

the inner edge on a cusp. The effective gravity then vanishes there and no wave motion can be supported.

That compressible, three-dimensional tori share the same instability was shown convincingly by GGN. These authors were able to construct a continuous sequence of models from two-dimensional incompressible annuli to compressible three dimensional tori by height-averaging the perturbation equations. Figure (2-5), taken from this paper, illustrates the behaviour of this mode in a torus with polytropic index n=3.[5] Contours of constant growth rate (scaled with the angular velocity at the pressure maximum) are plotted, and it is clear that this is the mode which is stabilized in slender tori at $q=\sqrt{3}$. Moreover a comparison between table 1 and this figure shows that this is the mode which was found numerically in PPI's two slender models. Note that the eigenfunctions of figures (2-2) and (2-3) are in agreement

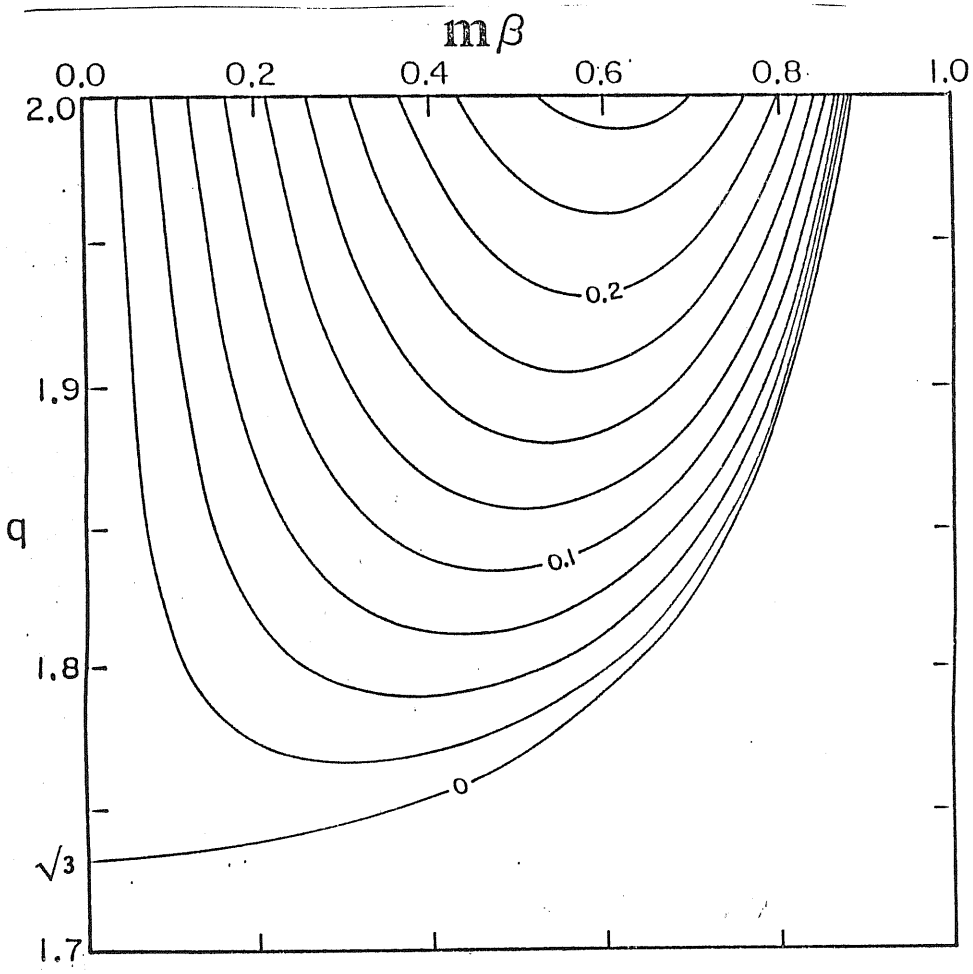

Figure 2-5. The surface interaction mode in a compressible torus (from GGN).

[5] Note that the curves in this diagram depend on the product of m and the thickness parameter β, and not on m alone. This is a consequence of the fact that GGN's analysis is strictly valid only for high m modes in slender tori.

with the surface interaction picture.

As the torus becomes thicker the surface interaction modes stabilize, with the low m modes surviving the longest. In a numerical study of thick, two-dimensional annuli with polytropic index 2.5, Glatzel (1986) has shown however that the additional modes present in a compressible fluid can play the same game, and this extends the instability to even the thickest configurations (figure 2-6, see also section 5 of GGN). The first hump in each diagram represents the incompressible interaction while the later humps are produced by the compressible modes. Slower instabilities of a completely different character were also found (the smaller humps in the m=2 and 10 diagrams) and it may be possible to interpret these in the way that PP originally imagined. These latter instabilities are not removed by angular momentum gradients although their growth rates are decreased.

Specific angular momentum gradients do kill off the surface interaction modes and this occurs faster if the annulus is thick. Figure (2-7) depicts the value of q required to stabilize an infinitely thick configuration. (Glatzel could not find any other unstable modes in the infinitely thick configurations - it could be that such configurations are absolutely stable beyond a certain angular momentum gradient.)

Kojima (1986) has shown that thick compressible tori have qualitatively similar behaviour (see figure 2-8, taken from this paper). The main difference is that the growth rate appears to decrease with the torus thickness (compare the m=1 modes in figures 2-6 and 2-8). This behaviour has also been found in numerical calculations by Frank (private communication), who has in addition explored true baroclinic configurations with a variety of boundary conditions. The latter do not appear to affect the instability in any serious way. Nonzero entropy gradients, however, can drastically alter the structure of the instability, though they never actually remove it.

To summarize, the principal unstable mode of Papaloizou and Pringle's instability in neither sonic nor Kelvin-Helmholtz in origin, nor does it arise from "reflecting boundaries". Instead, it seems best to interpret it as an interaction between two surface modes. It is stabilized by specific

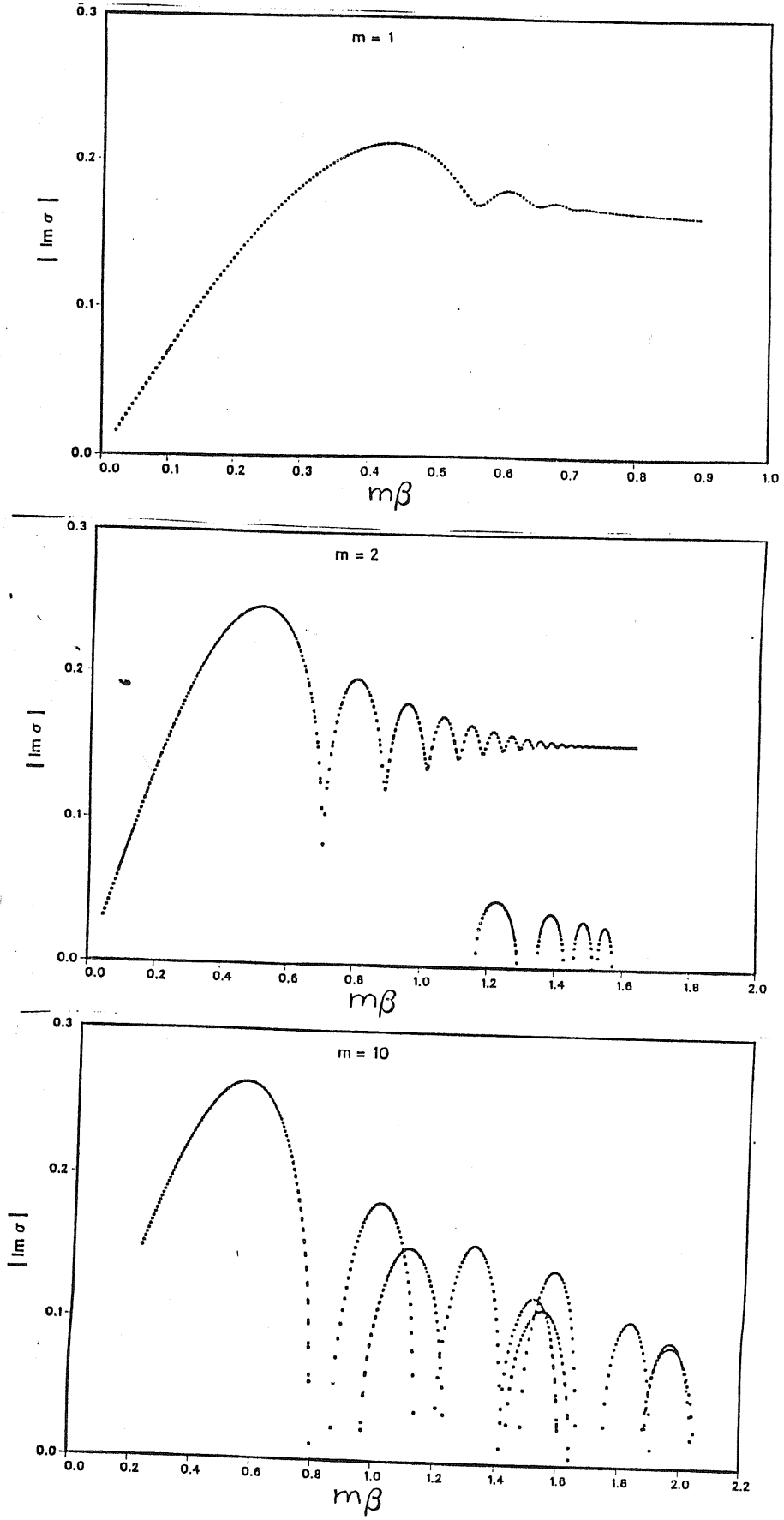

Figure 2-6. (from Glatzel 1986) Unstable growth rates, scaled with respect to the angular velocity at the pressure maximum, for two-dimensional, constant specific angular momentum, n=2.5 annuli.

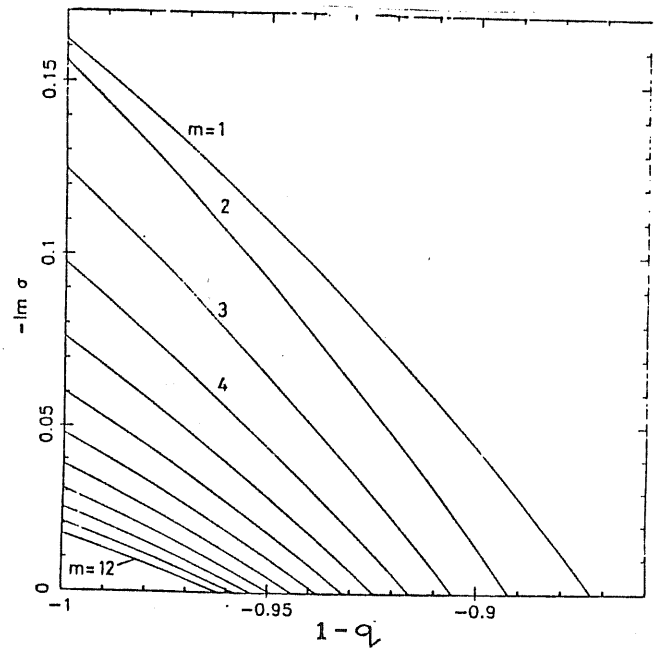

Figure 2-7. (from Glatzel 1986) the value of the specific angular momentum index q required to stabilize the "surface interaction mode" in an infinitely thick n=2.5 annulus. (No other modes were found in these configurations!)

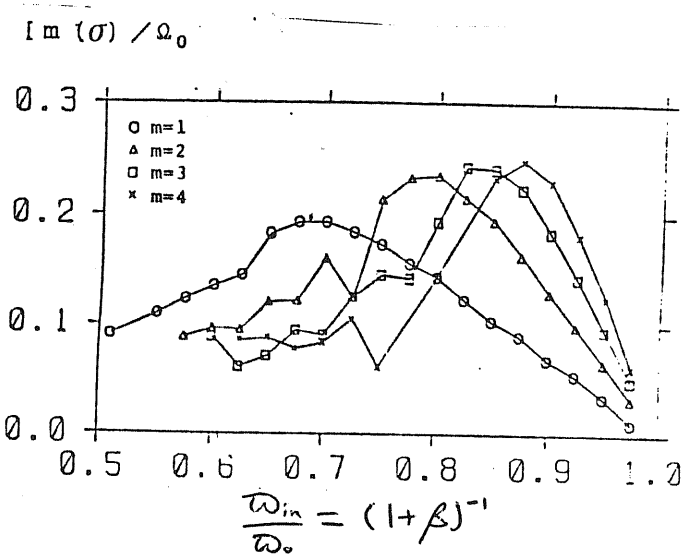

Figure 2-8. (from Kojima 1986) Unstable growth rates in a constant specific angular momentum, n=3 torus. The left and right hand sides correspond to infinitely thick and infinitely slender tori respectively.

angular momentum gradients, this becoming easier as the configuration gets thicker (atleast in the 2D models by Glatzel). Slower instabilities may generally exist in tori, however.

II.5 Nonlinear Evolution

Zurek and Benz (1986) hav studied the development of the instability into the nonlinear regime using a 3D smooth particle hydrodynamics code. Non-self-gravitating, polytropic (n=3) configurations rotating in a Newtonian potential well were investigated. Two simulations were presented which started with constant specific angular momentum tori of two different thicknesses (β = 0.74, corresponding to ω_{rot}/ω_m =6.7, and β =0.88, corresponding to ω_{rot}/ω_m =15.7). Both of these were violently unstable, with perturba-

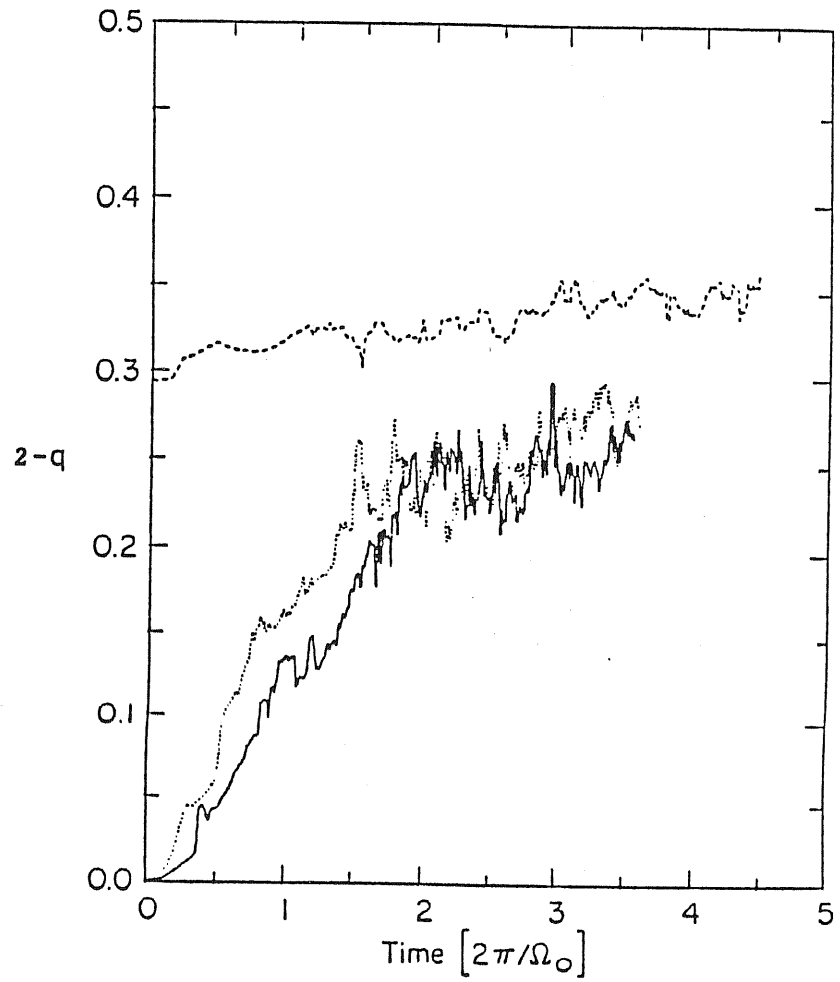

Figure 2-9. The development with time of the (power-law fit) specific angular momentum index in the three simulations of Zurek and Benz (1986).

tion rise times in good agreement with the linear theory. Within two rotation periods the tori evolved to configurations with approximately $q=\sqrt{3}$ power-law specific angular momentum distributions, after which the evolution time dramatically increased to $\sim$ 10-20 rotation periods. Moreover, a third simulation of a torus starting off with q near $\sqrt{3}$ exhibited similar slow unstable growth times (see figure 2-9).

These results are in good agreement with expectations from the linear theory, which shows that the most violent "surface interaction" instability is stabilized at $q=\sqrt{3}$. It is however somewhat surprising that the nonlinear evolution should produce power-law distributions of specific angular momentum - these were only chosen for convenience in the linear analyses.

Beyond $q=\sqrt{3}$, other slower dynamical instabilities act. Zurek and Benz point out, however, that their existence could be a numerical artifact of the "molecular viscosity" associated with the smooth particle hydrodynamics scheme, and much more careful numerical work needs to be done to explore and understand the nonlinear regime.

This completes the review part of the thesis. The next chapter will present all the mathematical linear stability theory along with the most general results which have been obtained. Chapters IV and V then explore the particularly simple configurations of slender tori and annuli from which most of the current physical understanding is based. A pseudo-Newtonian potential is used wherever possible to gauge the effects of relativity. Chapter VI then outlines a way of approaching the problem of accretion, which is likely to modify the instability drastically. Finally some tentative conclusions are presented.

III. LINEAR STABILITY OF PERFECT FLUID TORI - GENERAL THEORY AND RESULTS

Most of the work on the stability of thick accretion disks has concentrated on the non-accreting, perfect fluid tori of section (1.1). The stability theory of rotating fluids, and especially rotating stars, can be used to obtain some general results for these configurations (see Tassoul 1978 and Schutz 1983 for two complementary reviews). However, this theory is still in pretty poor shape, especially with regard to non-axisymmetric perturbations on differentially rotating fluids, and there are no general global stability criteria. This chapter is devoted to a derivation of the perturbation equations and a discussion of the general results which may be applied to perfect fluid tori.

III.1 The Perturbation Equations

All discussion in this chapter is based on the Newtonian equations of motion for an ideal fluid (for the relativistic equations, see e.g. Blandford, Jaroszyński and Kumar 1985).

$$\frac{\partial \rho}{\partial t} + \nabla\cdot(\rho \underline{v}) = 0 \qquad \text{(mass conservation)} \qquad (3.1)$$

$$\frac{\partial \underline{v}}{\partial t} + \underline{v}\cdot\nabla\underline{v} + \frac{1}{\rho}\nabla p + \nabla(\Phi_{int} + \Phi_{ext}) = 0 \qquad \text{(momentum conservation)} \qquad (3.2)$$

$$\frac{\partial s}{\partial t} + \underline{v}\cdot\nabla s = 0 \qquad \text{(adiabatic flow)} \qquad (3.3)$$

$$p = p(\rho, s) \qquad \text{(equation of state)} \qquad (3.4)$$

$$\nabla^2 \Phi_{int} = 4\pi G \rho \qquad \text{(gravitational field)} \qquad (3.5)$$

Here Φ_{int} is the gravitational field due to the thick disk itself while Φ_{ext} is the fixed external gravitational field of the central mass[1]. All other symbols have their usual meanings (see appendix E).

---

[1] Throughout this thesis it is assumed that the central mass is unaffected by the evolution of the torus. For completeness we retain the torus self-gravity in this chapter - it will be neglected in the remainder of the thesis.

Suppose now that one has a stationary perfect fluid disk and that at time t=0 the flow is everywhere perturbed by infinitesimal amounts. The equations describing the initial evolution of these perturbations, written out in cylindrical polar coordinates (ϖ,ϕ,z), are

$$\frac{\partial \delta\rho}{\partial t} + \Omega\frac{\partial \delta\rho}{\partial \phi} + \nabla\cdot(\rho\,\delta\underline{v}) = 0 \tag{3.6}$$

$$\frac{\partial \delta v_\varpi}{\partial t} + \Omega\frac{\partial \delta v_\varpi}{\partial \phi} - 2\Omega\delta v_\phi - \frac{1}{\rho^2}\frac{\partial p}{\partial \varpi}\delta\rho + \frac{1}{\rho}\frac{\partial \delta p}{\partial \varpi} + \frac{\partial \delta\Phi_{int}}{\partial \varpi} = 0 \tag{3.7}$$

$$\frac{\partial \delta v_\phi}{\partial t} + \Omega\frac{\partial \delta v_\phi}{\partial \phi} + \frac{1}{\varpi}\delta\underline{v}\cdot\nabla l + \frac{1}{\rho\varpi}\frac{\partial \delta p}{\partial \phi} + \frac{1}{\varpi}\frac{\partial \delta\Phi_{int}}{\partial \phi} = 0 \tag{3.8}$$

$$\frac{\partial \delta v_z}{\partial t} + \Omega\frac{\partial \delta v_z}{\partial \phi} - \frac{1}{\rho^2}\frac{\partial p}{\partial z}\delta\rho + \frac{1}{\rho}\frac{\partial \delta p}{\partial z} + \frac{\partial \delta\Phi_{int}}{\partial z} = 0 \tag{3.9}$$

$$\frac{\partial \delta s}{\partial t} + \Omega\frac{\partial \delta s}{\partial \phi} + \delta\underline{v}\cdot\nabla s = 0 \tag{3.10}$$

$$\delta p = \left(\frac{\partial p}{\partial \rho}\right)_s \delta\rho + \left(\frac{\partial p}{\partial s}\right)_\rho \delta s \tag{3.11}$$

$$\nabla^2\delta\Phi_{int} = 4\pi G\,\delta\rho \tag{3.12}$$

where δQ represents the "Eulerian change" in a fluid variable Q, defined as the difference between the values of Q evaluated at the same time and place in the perturbed and unperturbed flows:

$$\delta Q(r,t) \equiv Q(r,t)_{\text{perturbed}} - Q(r,t)_{\text{unperturbed}} \tag{3.13}$$

Another useful way to treat perturbations is through the "Lagrangian change" ΔQ. This is the change in Q as one goes from an unperturbed fluid element to the corresponding perturbed fluid element at the same time t. If these two elements are connected by a vector $\underline{\xi}$, called the Lagrangian displacement, then the two types of perturbation are related in the following way (Friedman and Schutz 1978a):

$$\Delta Q = \delta Q + \mathcal{L}_\xi Q \tag{3.14}$$

where $\pounds$ is the Lie derivative[2]. The Lagrangian displacement itself is related to the perturbed velocity field by

$$\Delta \underline{v} = \frac{\partial \underline{\xi}}{\partial t} \tag{3.15}$$

or

$$\delta v_m = \frac{\partial \xi_m}{\partial t} + \Gamma \frac{\partial \xi_m}{\partial \phi} \tag{3.16}$$

$$\delta v_\phi = \frac{\partial \xi_\phi}{\partial t} + \Gamma \frac{\partial \xi_\phi}{\partial \phi} - \omega \underline{\xi} \cdot \nabla \Gamma \tag{3.17}$$

$$\delta v_z = \frac{\partial \xi_z}{\partial t} + \Gamma \frac{\partial \xi_z}{\partial \phi} \tag{3.18}$$

Because the equilibrium tori have zero pressure surfaces, the perturbed surface must also remain at zero pressure. This gives the boundary condition that the Lagrangian change in pressure vanish on the equilibrium surface:

$$\Delta p\Big|_{p=0} = (\delta p + \underline{\xi} \cdot \nabla p)\Big|_{p=0} = 0 \tag{3.19}$$

In addition, the gravitational force must be continuous across the perturbed boundary, so that $\Delta \nabla \Phi$ must be continuous on the equilibrium surface.

The partial differential equations (3.6) - (3.12) and (3.16) - (3.18) together with the boundary conditions form a closed system for the evolution of any arbitrary initial perturbation data[3]. Note that this system is both linear and homogeneous - a consequence of the assumption that the initial perturbations are infinitesimal, and therefore nonlinear terms are negligible and have been dropped.

---

[2] Thus tensor components are measured with respect to a Lagrangian frame, i.e. a frame dragged by the perturbed flow. This choice of frame is not necessary, but it is perhaps more natural than an Eulerian frame where one would simply use the Taylor expansion $\Delta = \delta + \underline{\xi} \cdot \nabla$ and $\Delta \underline{v} = \partial \underline{\xi} / \partial t + \underline{v} \cdot \nabla \underline{\xi}$.

[3] In fact there exists a set of trivial solutions to these equations in which the Eulerian perturbations vanish but $\underline{\xi}$ remains nonzero (Friedman and Schutz 1978a). Physically this simply corresponds to a relabelling of fluid elements in the equilibrium flow. Provided we continue to work with the Eulerian variables, however, this will not cause problems.

If there exists a single set of initial perturbations which produces a solution of these equations which grows with time then the equilibrium configuration will be linearly unstable and nonlinear terms will have to be included to determine its eventual fate. On the other hand, if all sets of initial perturbations produce solutions which oscillate or decay with time, then the configuration is linearly stable and is a physically realizable possibility in nature. Note that even unstable models can be interesting from a physical point of view, provided the growth timescale of the instability exceeds that of other physically interesting timescales.

III.2 Symmetries and Normal Modes

The equilibrium tori all possess two symmetries which make it useful to split any arbitrary initial perturbation into certain fundamental components. Axisymmetry implies that all the coefficients of the perturbation equations are independent of ϕ. It is therefore sensible to Fourier analyze the perturbations such that

$$\delta Q \sim \exp(im\phi) \tag{3.20}$$

where m is an integer. Similarly, the equatorial symmetry of the tori makes it useful in some cases to consider the perturbations to be even or odd functions of z. No loss of generality occurs here as any arbitrary perturbation can be expanded in terms of these fundamental components.

There is, of course, another symmetry in any equilibrium configuration - the time invariance. Again this implies that all the coefficients in the above equations are independent of time so that one is naturally led to consider "normal mode" perturbations of the form

$$\delta Q \sim \exp(i\sigma t) \tag{3.21}$$

where σ is treated as an unknown complex eigenvalue. Clearly, if $\mathrm{Im}\,\sigma < 0$ for any solution of the perturbation equations, then the configuration is linearly unstable. On the other hand, even if $\mathrm{Im}\,\sigma \geq 0$ for all the solutions of the form (3.21), it cannot be argued that the model is linearly stable to arbitrary initial perturbations unless the solutions form a complete set.

The usual method of treating the time dependence in greater generality is to apply a Laplace transform to the perturbation equations, assuming that the time behaviour is not too extreme so that the transform converges in some region of the transform plane. Then on inversion, the singularities of the transform solution give rise to individual modes in the time-dependent solution. Simple poles give rise to the usual complex exponential normal modes, but higher order poles give rise to polynomials in time multiplied by complex exponentials and other singularities produce further complications.

Dyson and Schutz (1979) adopted this approach to investigate the completeness problem in rotating stars. They showed that provided the density vanishes in addition to the pressure on the surfaces of the equilibrium configuration, then every solution of the perturbation equations is bounded in time by $\exp(\lambda_0 t)$, i.e.

$$\int_0^\infty |\delta Q(t)|^2 e^{-2\lambda_0 t} dt < \infty \tag{3.22}$$

where λ_0 is any real number greater than the largest $(-\mathrm{Im}\,\sigma)$ to be found amongst the normal mode eigenvalues. In particular, if $\mathrm{Im}\,\sigma \geq 0$ for all eigenvalues, then there can be no exponentially growing perturbations. This does not, however, preclude the existence of perturbations which grow more slowly with time. A common example are those modes which have a polynomial dependence on t, associated with points of normal mode "marginal stability" (Schutz 1980).

With the boundedness condition (3.22) in hand I shall for the most part limit the discussion to normal modes from now on. The perturbation equation set (3.6) - (3.12) and (3.16) - (3.18) becomes

$$i\bar{\sigma}\delta\rho + \nabla\cdot(\rho\delta\underline{v}) = 0 \tag{3.23}$$

$$i\bar{\sigma}\delta v_\varpi - 2\Omega\delta v_\phi - \frac{1}{\rho^2}\frac{\partial p}{\partial \varpi}\delta\rho + \frac{1}{\rho}\frac{\partial \delta p}{\partial \varpi} + \frac{\partial \delta\Phi_{int}}{\partial \varpi} = 0 \tag{3.24}$$

$$i\bar{\sigma}\delta v_\phi + \frac{1}{\varpi}\delta\underline{v}\cdot\nabla l + \frac{im}{\rho\varpi}\delta p + \frac{im}{\varpi}\delta\Phi_{int} = 0 \tag{3.25}$$

$$i\bar{\sigma}\delta v_z - \frac{1}{\rho^2}\frac{\partial p}{\partial z}\delta\rho + \frac{1}{\rho}\frac{\partial \delta p}{\partial z} + \frac{\partial \delta\Phi_{int}}{\partial z} = 0 \tag{3.26}$$

$$i\bar{\sigma}\delta s + \xi_r \cdot \nabla s = 0 \tag{3.27}$$

$$\delta p = \left(\frac{\partial p}{\partial \rho}\right)_s \delta\rho + \left(\frac{\partial p}{\partial s}\right)_\rho \delta s \tag{3.28}$$

$$\nabla^2 \delta\Phi_{int} = 4\pi G\delta\rho \tag{3.29}$$

$$\xi_\varpi = -\frac{i}{\bar{\sigma}}\delta v_\varpi \tag{3.30}$$

$$\xi_\varphi = -\frac{i\delta v_\varphi}{\bar{\sigma}} - \frac{\varpi}{\bar{\sigma}^2}\delta v \cdot \nabla\Omega \tag{3.31}$$

$$\xi_z = -\frac{i}{\bar{\sigma}}\delta v_z \tag{3.32}$$

where $\bar{\sigma} \equiv \sigma + m\Omega$ (3.33)

and all the perturbations are now functions of ϖ and z only. Note that $\bar{\sigma}$ is also a function of ϖ and z because of differential rotation.

It is straightforward to show that given the solution

$$(\sigma, m, \delta\rho, \delta p, \delta s, \delta\Phi_{int}, \delta v_\varpi, \delta v_\varphi, \delta v_z, \xi_\varpi, \xi_\varphi, \xi_z)$$

then

$$(\sigma^*, m, \delta\rho^*, \delta p^*, \delta s^*, \delta\Phi^*_{int}, -\delta v^*_\varpi, \delta v^*_\varphi, -\delta v^*_z, \xi^*_\varpi, -\xi^*_\varphi, \xi^*_z)$$

$$(-\sigma, -m, \delta\rho, \delta p, \delta s, \delta\Phi_{int}, -\delta v_\varpi, \delta v_\varphi, -\delta v_z, \xi_\varpi, -\xi_\varphi, \xi_z)$$

$$(-\sigma^*, -m, \delta\rho^*, \delta p^*, \delta s^*, \delta\Phi^*_{int}, \delta v^*_\varpi, \delta v^*_\varphi, \delta v^*_z, \xi^*_\varpi, \xi^*_\varphi, \xi^*_z)$$

are also solutions. (The asterix denotes complex conjugate.) Hence to every growing ($\mathrm{Im}\,\sigma < 0$) solution with given azimuthal wavenumber m there exists a damped ($\mathrm{Im}\,\sigma > 0$) solution with the same m. In addition, to every growing (damped) solution with given m, there exists another solution for (-m) with exactly the same growth (damping) rate. Finally, note that all four of the above solutions have the same "pattern speed" $\Omega_p \equiv (-\mathrm{Re}\,\sigma/m)$.

These conclusions, based simply on the mathematical nature of the normal mode equations and boundary conditions, have been in dispute recently (Drury

1985; GGN and Glatzel 1986). These authors argue that corotation singularities in the equations (section III.4) mean that damped solutions require special treatment and so the symmetry between damped and growing solutions is broken. I do not wish to enter into details here because, however fundamental it may be to the general theory of stability, it is somewhat academic for the problem at hand: growing modes are completely unaffected and the $m \rightarrow -m$ correspondence remains valid. Given the latter fact, only non-negative azimuthal wavenumbers will be considered in the remainder of this thesis.

III.3 Local Stability and the Høiland Criterion

Consider now a local analysis of the above system in which

$$\delta Q \propto \exp\left[i(k_\varpi \varpi + k_z z) \right] \tag{3.34}$$

and the wavenumbers k_ϖ and k_z tend to infinity. In such a case one may neglect spatial variations of the equilibrium quantities along with the boundary conditions and obtain the following dispersion relation from equations (3.23) - (3.28):

$$\bar{\sigma}^2 = \frac{\frac{1}{\varpi^3}\left(\frac{\partial p}{\partial \rho}\right)_s (\underline{k} \times \hat{\underline{\varpi}}).(\underline{k} \times \underline{\nabla} l^2) - \frac{1}{\rho^2}\left(\frac{\partial p}{\partial s}\right)_\rho (\underline{k} \times \underline{\nabla} p).(\underline{k} \times \underline{\nabla} s)}{|k|^2 \left(\frac{\partial p}{\partial \rho}\right)_s} \tag{3.35}$$

where $\underline{k} = k_\varpi \hat{\underline{\varpi}} + k_z \hat{\underline{z}}$ is the wave vector. Transforming the quadratic form in the numerator to principal axes, one obtains

$$\bar{\sigma}^2 = \frac{\alpha_+ k_+^2 + \alpha_- k_-^2}{|k|^2} \tag{3.36}$$

where $k_\pm$ are the wave vector components along the principal axes and

$$\alpha_\pm = A \pm (A^2 + B)^{\frac{1}{2}} \tag{3.37}$$

with

$$A \equiv \tfrac{1}{2}\left[\frac{1}{\varpi^3} (\hat{\underline{\varpi}} \cdot \underline{\nabla} l^2) + \frac{1}{\rho} \underline{\nabla} p \cdot \left(\frac{1}{\rho} \underline{\nabla} \rho - \frac{1}{\gamma p} \underline{\nabla} p \right) \right] \tag{3.38}$$

$$B \equiv \frac{1}{\rho^2 \varpi^3} \left(\frac{\partial p}{\partial s} \right)_\rho (\underline{\nabla} p \times \hat{\underline{\varpi}}) \, (\underline{\nabla} l^2 \times \underline{\nabla} s) \tag{3.39}$$

and where use has been made of the equation

$$\nabla\left(\frac{1}{\rho}\right) \times \nabla p = \frac{1}{\omega^3}\nabla\ell^2 \times \hat{\omega} \tag{3.40}$$

derived by taking the curl of the hydrostatic equilibrium equation (1.1). Stability requires $\bar{\sigma}^2 > 0$ for all $\underline{k}$ with $|\underline{k}|$ large. Hence A and B must be positive or

$$\frac{1}{\omega^3}(\hat{\omega}\cdot\nabla\ell^2) + \frac{1}{\rho}\nabla p\cdot\left(\frac{1}{\rho}\nabla\rho - \frac{1}{\gamma p}\nabla p\right) > 0 \tag{3.41}$$

and

$$(\nabla p \times \hat{\omega})\cdot(\nabla\ell^2 \times \nabla s) > 0 \tag{3.42}$$

where $\gamma = \frac{\rho}{p}\left(\frac{\partial p}{\partial \rho}\right)_s$ is the adiabatic index. This is the well-known Høiland stability criterion. Although derived here through a local stability argument, the criterion in fact gives necessary and sufficient conditions for <u>global</u> stability to axisymmetric perturbations, provided the self-gravity of the fluid is negligible (Fricke and Smith 1971).

Note that the first inequality (3.41) may be rewritten

$$\kappa^2 + N^2 > 0 \tag{3.43}$$

where

$$\kappa^2 = \frac{1}{\omega^3}\frac{\partial\ell^2}{\partial\omega} = 2\Omega\left(2\Omega + \omega\frac{\partial\Omega}{\partial\omega}\right) \tag{3.44}$$

is the square of the "epicyclic frequency" of the torus and

$$N^2 = \frac{1}{\rho}\nabla p\cdot\left(\frac{1}{\rho}\nabla\rho - \frac{1}{\gamma p}\nabla p\right) \tag{3.45}$$

is the square of the Brunt-Väisälä frequency. These represent the characteristic local oscillation frequencies of rotating and stratified fluids respectively. The full Høiland criterion results from the combined effects of centrifugal and buoyancy forces. Together with the equilibrium condition (3.40), it places stability constraints on the vectors $\nabla\ell^2$, ∇p and ∇s. For the relativistic version see Seguin (1975) or Blandford, Jaroszyński and Kumar (1985).

If the Høiland criterion is satisfied, then equation (3.36) implies $\bar{\sigma}$ is real and lies in the range

$$-\sqrt{\alpha_+} < \bar{\sigma} < -\sqrt{\alpha_-} \tag{3.46}$$

or

$$\sqrt{\alpha_-} < \bar{\sigma} < \sqrt{\alpha_+} \tag{3.47}$$

depending on the ratio of the wavenumber components. The fact that this ratio can take any real value while keeping $|\underline{k}|$ large suggests the existence of a dense or continuous real spectrum of global modes with frequencies satisfying (3.46) or (3.47) for every point in the torus. Now B, and therefore α_-, always vanishes somewhere in the torus (e.g. at the centre), so that this spectrum will actually cover the range

$$-(\max \alpha_+)^{\frac{1}{2}} < \bar{\sigma} < (\max \alpha_+)^{\frac{1}{2}} \quad . \tag{3.48}$$

This generalizes the discussions of Papaloizou and Pringle (1982) for the case of uniform rotation and PPI for the case of homentropic configurations. The mathematical and physical significance of these inequalities will be discussed in the next section where particular classes of tori are examined.

The local analysis of this section considered the $|\underline{k}| \to \infty$ limit, and thus the results obtained here are generally valid for any rotating perfect fluid. Further useful results can be obtained by considering higher order terms in the dispersion relation, but for consistency $|\underline{k}|$ must always be much greater than the reciprocal of the local scale height, and this necessarily implies an examination of individual classes of configurations. Such an analysis for accretion disks and tori was begun by Abramowicz et al. (1984b) and much more work needs to be done in this area. The instabilities discovered by Papaloizou and Pringle cannot, however, be analyzed in this way as their lengthscales are typically much greater than then any scale height.

III.4 Equations for Particular Cases and Corotation Theorems

We turn now to the equations describing particular classes of tori and some general results associated with them.

(a) Non-self-gravitating, homentropic configurations ($\nabla s=0$, $G=0$)

This was the case treated originally by Papaloizou and Pringle in PPI and PPII. They succeeded in deriving a single perturbation equation by defining a quantity W as

$$W \equiv \frac{\delta p}{\delta \bar{\sigma}} \tag{3.51}$$

Equations (3.24)-(3.26), (3.28), and (3.30)-(3.32) may then be solved to express all the perturbations in terms of W:

$$\delta p = \delta \bar{\sigma} W \tag{3.52}$$

$$\delta \rho = \frac{\rho^2 \bar{\sigma}}{\gamma p} W \tag{3.53}$$

$$\delta v_\varpi = \frac{i}{D}\left[\bar{\sigma}^2 \frac{\partial W}{\partial \varpi} + \frac{K^2 \bar{\sigma} m W}{2\varpi\Omega}\right] \tag{3.54}$$

$$\delta v_\phi = \frac{1}{D}\left[-\frac{m\bar{\sigma}^2 W}{\varpi} - \bar{\sigma}\right] \tag{3.55}$$

$$\delta v_z = i \frac{\partial W}{\partial z} \tag{3.56}$$

$$\xi_\varpi = \frac{1}{D}\left[\bar{\sigma} \frac{\partial W}{\partial \varpi} + \frac{K^2 m W}{2\varpi\Omega}\right] \tag{3.57}$$

$$\xi_\phi = \frac{i}{D}\left[\frac{m\bar{\sigma} W}{\varpi} + 2\Omega \frac{\partial W}{\partial \varpi}\right] \tag{3.58}$$

$$\xi_z = \frac{1}{\bar{\sigma}} \frac{\partial W}{\partial z} \tag{3.59}$$

where $$D \equiv \bar{\sigma}^2 - K^2 \quad . \tag{3.60}$$

The perturbed continuity equation (3.23) and the boundary condition (3.19) may now be written

$$\frac{1}{\varpi}\frac{\partial}{\partial \varpi}\left[\frac{\rho \varpi \bar{\sigma}^2}{D} \frac{\partial W}{\partial \varpi}\right] + \frac{\partial}{\partial z}\left[\rho \frac{\partial W}{\partial z}\right] + W\left[\frac{\bar{\sigma}}{\varpi}\frac{\partial}{\partial \varpi}\left(\frac{\rho K^2 m}{2D\Omega}\right) - \frac{\rho m^2 \bar{\sigma}^2}{D\varpi^2} + \frac{\bar{\sigma}^2 \rho^2}{\gamma p}\right] = 0 \tag{3.61}$$

$$\left(W\rho\bar{\sigma} + \frac{\bar{\sigma}}{D}\frac{\partial W}{\partial \varpi}\frac{\partial p}{\partial \varpi} + \frac{1}{\bar{\sigma}}\frac{\partial W}{\partial z}\frac{\partial p}{\partial z} + \frac{Wm}{\varpi^2 D}\frac{\partial p}{\partial \varpi}\frac{dl}{d\varpi} \right)\Bigg|_{p=0} = 0 \qquad (3.62)$$

These two equations constitute the eigenvalue problem for σ.

The Hoiland criterion for local stability in this class of tori reduces simply to the Rayleigh (or Solberg) criterion:

$$K^2 = \frac{1}{\varpi^3}\frac{\partial l^2}{\partial \varpi} > 0 \qquad (3.63)$$

which is easy to understand physically. If a fluid element is perturbed outwards such that it conserves its angular momentum in a region where condition (3.63) is violated, it will have more angular momentum than its surroundings. Excess centrifugal forces will therefore drive it further outwards.

Inequalities (3.46) and (3.47) also suggest that in this case the above eigenvalue problem will produce a dense or continuous set of eigenfrequencies in the range

$$-K < \bar{\sigma} < K \qquad (3.64)$$

for every point in the torus.

Further properties of equation (3.61) have been elucidated by Balbinski (1985). Considering σ to be real, he examined the equation for the characteristic surfaces,

$$D\left(\frac{d\varpi}{dz}\right)^2 + \bar{\sigma}^2 = 0 \qquad (3.65)$$

and found that the perturbation equation is in general of mixed type, depending on the value of σ (figure 3-1). The surfaces across which the type changes correspond to the classical resonances of spiral density wave theory (Toomre 1977):

Corotation Resonance $\Omega_p = \Omega$ or $\bar{\sigma} = 0$ (3.66)

Inner Lindblad Resonance $\Omega_p = \Omega - \frac{K}{m}$ (3.67)

Outer Lindblad Resonance $\Omega_p = \Omega + \frac{K}{m}$ (3.68)

or $D = 0$

Here $\Omega_p = -\sigma/m$ is the "pattern speed" or angular velocity of the mode.

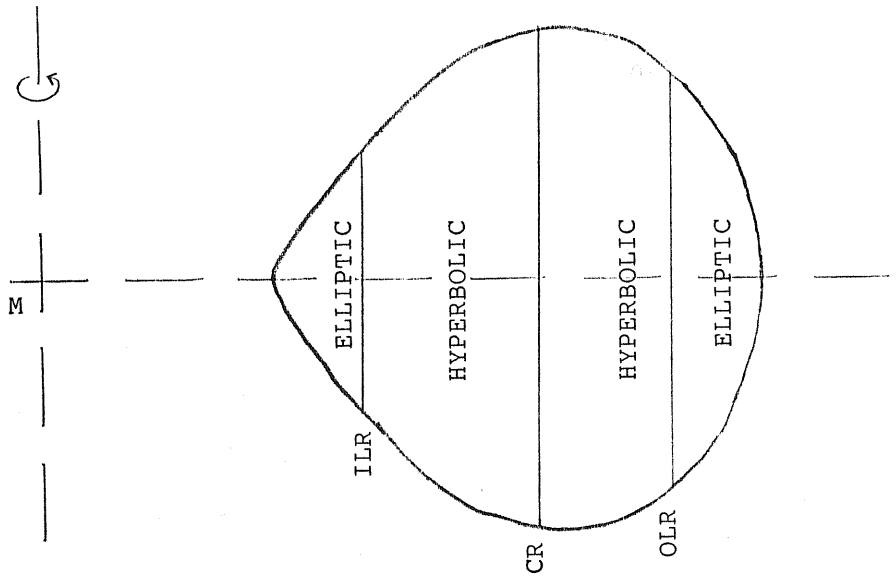

Figure 3-1. The inner Lindblad, corotation and outer Lindblad resonances for a homentropic torus.

Outside the two Lindblad resonances ($D>0$) the characteristics are complex and the equation is elliptic. Inside the Lindblad resonances ($D<0$) the characteristics are real and the equation is hyperbolic, apart from the corotation cylinder. This is itself a characteristic surface because both $\bar{\sigma}$ and $d\varpi/dz$ vanish here. Solutions in the neighbourhood of this surface are therefore non-analytic unless special conditions are imposed to avoid this. Because the torus is differentially rotating there is a continuous range of pattern speeds, and therefore of σ , which will be corotating. There will thus be a corresponding continuous set of singular eigenfunctions. Although each of these eigenfunctions might at first be thought unphysical,when combined together they represent nonsingular perturbations which must be included in a complete normal mode analysis. (Case 1960 and Balbinski 1984 emphasize this point and present simple analytic problems which illustrate it.)

Balbinski (1985) also suggests that the hyperbolic region may in general be related to the existence of a dense or continuous spectrum of modes as in (3.64) above. It is interesting to note that this inequality has also been found in the context of tightly-wrapped spiral denstity wave theory (Lin, Yuan and Shu 1969) where the waves are known to be trapped between the two Lindblad resonances.

Finally, it has been shown in PPII that, for power law distributions of specific angular momentum, any unstable mode must corotate with the equi-

librium flow somewhere, i.e.

$$\text{If } \mathrm{Im}(\sigma) \neq 0, \text{ then } \mathrm{Re}(\bar{\sigma}) = -m\Omega(\varpi) \tag{3.65}$$

at some radius ϖ inside the torus. It is still unknown whether or not this result applies to other forms of rotation law.

(b) Non-self-gravitating, constant specific angular momentum, pseudobarotropic configurations ($\nabla\Omega^2=0$, G=0)

The general baroclinic torus is quite difficult to treat due to the geometrical complications which arise when surfaces of constant pressure and density do not coincide. However, if one assumes that the specific entropy is constant along isobaric surfaces (a "pseudobarotrope") then density will also be constant along these surfaces and the geometrical simplicity of a barotropic torus (i.e. $\Omega = \Omega(\varpi)$) will be maintained. As mentioned in chapter I, gyrotropic configurations (i.e. with surfaces of constant specific entropy and constant specific angular momentum coinciding) may be more likely, but this is much more complicated and it seems reasonable to consider the pseudobarotropic case first.

For simplicity consider a constant specific angular momentum torus which has constant equilibrium adiabatic index $\gamma \equiv \rho/p\,(\partial p/\partial \rho)_s$. Then one may generalize the definition (3.51) of W to be

$$W = \frac{\delta p}{p^{1/\gamma}\bar{\sigma}} \tag{3.66}$$

It proves convenient to transform equations (3.23) - (3.32) from (ϖ, z) coordinates to a system where one of the coordinates f is constant on equipotential surfaces and the other is an orthogonal, angle-like, coordinate measured up from the inner equatorial plane and around the isobaric surfaces (see figure 2-1(b) for a diagram of the (f,θ) coordinates). In a similar fashion to the previous section one may then derive the following perturbation equation

$$\frac{|\nabla f||\nabla\theta|}{\varpi}\left[\frac{\partial}{\partial f}\left(\frac{\varpi|\nabla f|}{|\nabla\theta|}\frac{p^{2/\gamma}}{\rho}\frac{\bar{\sigma}^2}{\bar{\sigma}^2-N^2}\frac{\partial W}{\partial f}\right)\right.$$
$$\left.+\frac{\partial}{\partial\theta}\left(\frac{\varpi|\nabla\theta|}{|\nabla f|}\frac{p^{2/\gamma}}{\rho}\frac{\partial W}{\partial\theta}\right)\right]+W\left[\frac{p^{2/\gamma}\bar{\sigma}^2}{\gamma p}-\frac{m^2 p^{2/\gamma}}{\rho\varpi^2}\right]=0 \tag{3.67}$$

with boundary condition

$$\left(p^{1/\gamma}\bar{\sigma}W + \frac{p^{1/\gamma}}{\rho}\frac{\bar{\sigma}}{\bar{\sigma}^2 - N^2}\frac{dp}{df}\frac{\partial W}{\partial f}|\nabla f|^2\right)_{p=0} = 0 \tag{3.68}$$

The Høiland criterion for these tori reduces to the familiar Schwarzschild criterion for convective stability:

$$N^2 = \frac{1}{\rho}\nabla p \cdot \left(\frac{1}{\rho}\nabla\rho - \frac{1}{\gamma p}\nabla p\right) > 0 \tag{3.69}$$

or

$$-g_{\text{eff}} \cdot \nabla s > 0 \tag{3.70}$$

where g_{eff} is the effective gravitational acceleration. Physically, if a fluid element is adiabatically perturbed outwards in a region where condition (3.70) is violated, then it will have a higher specific entropy than its surroundings. Because it must remain in pressure equilibrium it will therefore have a lower density which will result in buoyancy forces driving it further outwards. Centrifugal forces play no role here because if the perturbed fluid element preserves its specific angular momentum, it will never have an excess of this over its surroundings as $\nabla \ell^2 = 0$.

One may carry on and derive analagous results to the previous section. A dense or continuous spectrum of real modes is expected from inequalities (3.46) and (3.47) in the range

$$-N < \bar{\sigma} < N \,. \tag{3.71}$$

In addition equation (3.67) is again of mixed type, being hyperbolic in the above range of $\bar{\sigma}$ and elliptic outside it.

Finally, one may prove that the corotation theorem (3.65) is also valid in this case. Multiplying (3.67) by $\frac{W^* \varpi}{|\nabla f||\nabla\theta|}$ and integrating over the cross-sectional area of the torus,

$$\int_0^{2\pi}\int_{f_{\text{surface}}}^{f_{\text{centre}}} W^*\left[\frac{\partial}{\partial f}\left(\frac{\varpi|\nabla f|}{|\nabla\theta|}\frac{p^{2/\gamma}}{\rho}\frac{\bar{\sigma}^2}{\bar{\sigma}^2 - N^2}\frac{\partial W}{\partial f}\right)\right.$$

$$\left. + \frac{\partial}{\partial\theta}\left(\frac{\varpi|\nabla\theta|}{|\nabla f|}\frac{p^{2/\gamma}}{\rho}\frac{\partial W}{\partial\theta}\right)\right] df d\theta + \int_0^{2\pi}\int_{f_{\text{surface}}}^{f_{\text{centre}}} |W|^2\left[\frac{p^{2/\gamma}\bar{\sigma}^2}{\gamma p} - \frac{m^2 p^{2/\gamma}}{\rho\varpi^2}\right]\frac{\varpi df d\theta}{|\nabla f||\nabla\theta|} = 0 \tag{3.72}$$

Integrating the first two terms by parts,

$$\int_0^{2\pi}\left[W^*\left(\frac{\varpi|\nabla f|}{|\nabla\theta|}\frac{p^{2/\gamma}}{\rho}\frac{\bar\sigma^2}{\bar\sigma^2-N^2}\frac{\partial W}{\partial f}\right)\right]_{f_{surface}}^{f_{centre}}d\theta-\int_0^{2\pi}\int_{f_{surface}}^{f_{centre}}\frac{p^{2/\gamma}}{\rho}\left[\frac{\bar\sigma^2}{\bar\sigma^2-N^2}|\nabla f|^2\left|\frac{\partial W}{\partial f}\right|^2\right.$$

$$\left.+|\nabla\theta|^2\left|\frac{\partial W}{\partial\theta}\right|^2+\frac{m^2|W|^2}{\varpi^2}-\frac{\rho\bar\sigma^2}{\gamma p}|W|^2\right]\frac{\varpi\,df\,d\theta}{|\nabla f||\nabla\theta|}=0 \tag{3.73}$$

where use has been made of the fact that W must be periodic in θ.

At the central pressure maximum of the torus the (f,θ) coordinate system is singular; $|\nabla\theta|$ blows up while $|\nabla f|\,\partial W/\partial f$ remains finite. Hence the f_{centre} term vanishes.

One might at first think that the $f_{surface}$ term also vanishes as p=0 and N^2 generally blows up there. However, the density may also vanish and W could in principle blow up. If we take the equipotential function f to be simply the pressure, then the boundary condition (3.68) implies

$$\int_0^{2\pi}\left[W^*\left(\frac{\varpi|\nabla f|}{|\nabla\theta|}\frac{p^{2/\gamma}}{\rho}\frac{\bar\sigma^2}{\bar\sigma^2-N^2}\frac{\partial W}{\partial f}\right)\right]_{f_{surface}}d\theta$$

$$=-\int_0^{2\pi}\left[p^{2/\gamma}|W|^2\bar\sigma^2\frac{\varpi}{|\nabla p||\nabla\theta|}\right]_{p=0}d\theta \tag{3.74}$$

and hence the imaginary part of equation (3.73) is

$$2\,Im(\sigma)\left\{\int_0^{2\pi}\left[\frac{p^{2/\gamma}|W|^2\varpi}{|\nabla p||\nabla\theta|}(Re(\sigma)+m\Omega)\right]\right|_{p=0}d\theta$$

$$\left.+\int_0^{2\pi}\int_0^{p_{max}}\frac{p^{2/\gamma}}{\rho}\left[\frac{N^2}{|\bar\sigma^2-N^2|^2}|\nabla f|^2\left|\frac{\partial W}{\partial f}\right|^2+\frac{\rho|W|^2}{\gamma p}\right]\frac{\varpi}{|\nabla p||\nabla\theta|}(Re(\sigma)+m\Omega)\,dp\,d\theta\right\}$$

$$=0 \tag{3.75}$$

Hence if $Im(\sigma)\neq 0$ then $Re(\sigma)=-m\Omega(\varpi)$ at some radius ϖ in the torus, because the $\{\ \}$ factor would be positive definite[4] were it not for the presence of $(Re(\sigma)+m\Omega)$ in the two integrals.

---

[4] Assuming $N^2>0$ for local stability.

It is not yet known whether or not the corotation theorems proved for these two classes of tori are generally valid. As already mentioned in chapter II, corotation points are extremely important physically and this suggests that a general theorem may be lurking somewhere. There does exist an "almost" corotation theorem (Friedman and Schutz 1978b) which states

$$\bar{\Omega}\left(1-\frac{1}{m}\right) \leq \Omega_p \leq \bar{\Omega}\left(1+\frac{1}{m}\right) \tag{3.76}$$

where

$$\bar{\Omega} \equiv \frac{\int |\xi|^2 \rho \Omega \, dV}{\int |\xi|^2 \rho \, dV} \tag{3.77}$$

is a mass-weighted angular velocity. Use of the mean value theorem then implies

$$\Omega_{min}\left(1-\frac{1}{m}\right) \leq \Omega_p \leq \Omega_{max}\left(1+\frac{1}{m}\right) \quad . \tag{3.78}$$

III.5 General Limits on Growth Rates

Dyson and Schutz (1979) derived general limits on the growth rates of unstable normal modes for configurations in which the density vanishes in addition to the pressure on the surface. These constraints are not very strong, especially for high m modes, but they are nevertheless useful in checking numerical results and have the advantage of being reasonably general.

Define the quantity

$$S \equiv (m+1)^2 \Omega_{max}^2 + 4\pi G \rho_{max} - N_{min}^2$$
$$- \min\left\{ \frac{\partial(\varpi\Omega^2)}{\partial \varpi}, \frac{1}{2}\Omega^2 - \frac{1}{2}\left[\Omega^4 + \left(\frac{\partial(\varpi\Omega^2)}{\partial z}\right)^2\right]^{1/2} \right\} \tag{3.79}$$

where, as mentioned previously, m is considered to be positive and the subscripts "min" and "max" refer to the minimum and maximum values, respectively, inside the torus. Dyson and Schutz proved that any complex normal mode frequency must satisfy

$$|\mathrm{Re}\,\sigma| \leq (m+1)\Omega_{max} \tag{3.80}$$

and
$$|\sigma| \leq \begin{cases} \sqrt{S} & \text{if } S \geq 0 \\ 0 & \text{if } S \leq 0 \end{cases} \tag{3.81}$$

One may strengthen these constraints still further by adding the corotation theorems of the previous section. In the most general case (figure 3-2(a))

$$(m - 1)\Omega_{min} \leq |\mathrm{Re}\,\sigma| \leq (m + 1)\Omega_{max} \tag{3.82}$$

which together with (3.81) implies

$$|\mathrm{Im}\,\sigma| \leq \left[S - (m - 1)^2\Omega_{min}^2\right]^{\frac{1}{2}} . \tag{3.83}$$

For strict corotation (figure 3-2(b)),

$$m\Omega_{min} \leq |\mathrm{Re}\,\sigma| \leq m\Omega_{max} \tag{3.84}$$

implying
$$|\mathrm{Im}\,\sigma| \leq \left[S - m^2\Omega_{min}^2\right]^{\frac{1}{2}} . \tag{3.85}$$

Finally, in the very special case of the non-self-gravitating, constant specific angular momentum, homentropic torus, one may replace inequality (3.81) with the stronger constraint (Blaes 1985a, Appendix A, figure 3-2(c))

$$|\sigma| \leq m\Omega_{max} \tag{3.86}$$

implying
$$|\mathrm{Im}\,\sigma| \leq m(\Omega_{max}^2 - \Omega_{min}^2)^{\frac{1}{2}} \tag{3.87}$$

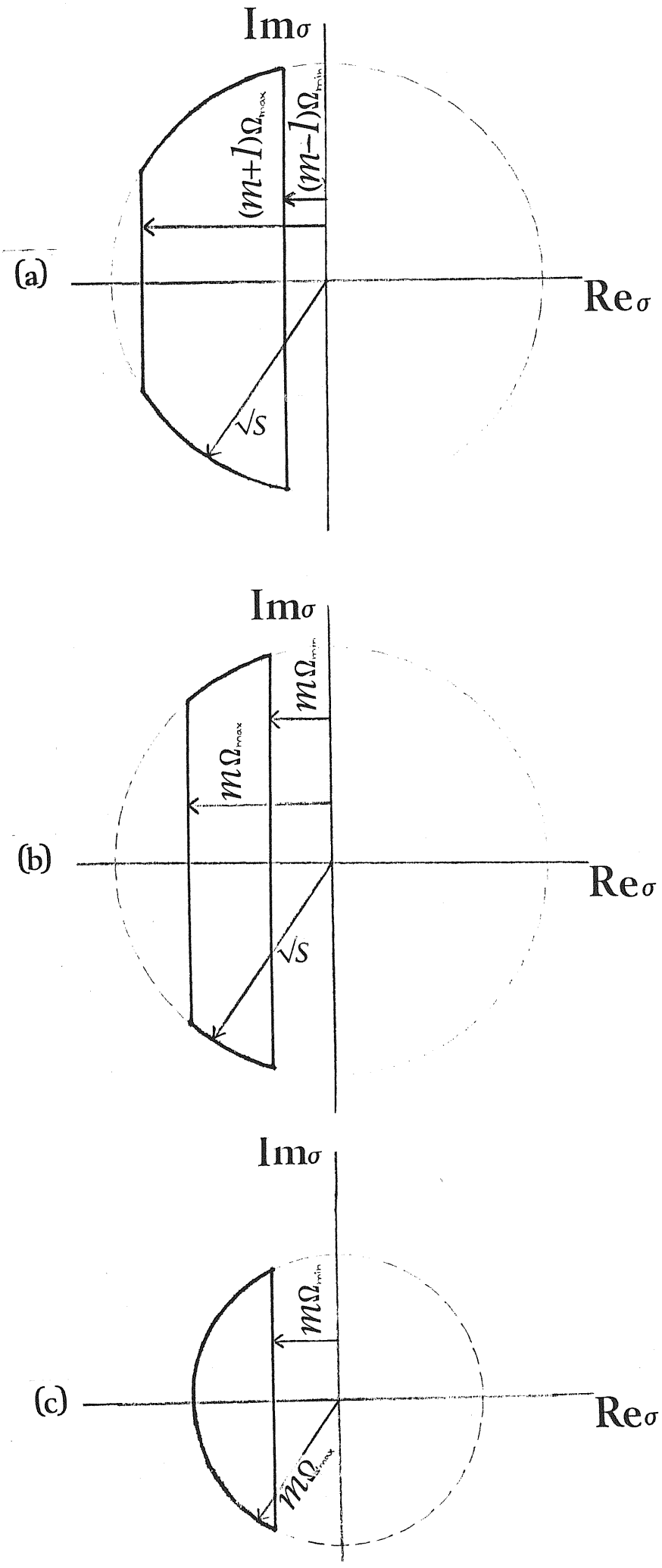

Figure 3-2. Constraints on complex frequencies for m 0: (a) general case; (b) strict corotation; (c) non-self-gravitating, constant specific angular momentum, homentropic torus.

IV. SLENDER TORI

The normal mode equations of the previous chapter are generally impossible to solve analytically because of the lack of separable coordinates for tori, the nonlinear nature of the eigenvalue problem (as formulated, e.g., by equations 3.61 and 3.67), and the presence of corotation singularities. Most of the analytic and quasi-analytic approaches have overcome these problems by studying simplified configurations. Slender, polytropic tori are considered in this chapter, while in the next chapter the vertical dimension is removed by studying annuli. Surprisingly, these two geometrically different models share many common features.

IV.1 Equilibrium Configurations

The equilibrium equation (1.6) may be rewritten as

$$w = w_o + (\Phi - \Phi_o) + (\Phi_{rot} - \Phi_{rot\,o}) \tag{4.1}$$

where the subscript zero denotes the value at the central pressure maximum. For polytropic tori,

$$p = k\rho^{1+1/n} = k\rho^{\Gamma} \tag{4.2}$$

where k, n, and Γ are constants. It is convenient to introduce the Lane-Emden function f by

$$\rho = \rho_o f^n \qquad \text{and} \qquad p = p_o f^{n+1} \ . \tag{4.3}$$

Equations (1.5), (4.1) and (4.3) then imply

$$f = 1 - \frac{\rho_o}{(n+1)p_o}\left[(\Phi - \Phi_o) + (\Phi_{rot} - \Phi_{rot_o})\right] \ . \tag{4.4}$$

The function f is one at the central pressure maximum of the torus and zero on the surface. It is also convenient to define a quantity η by

$$f = 1 - \eta^2 \tag{4.5}$$

such that η is zero at the centre and one on the surface.

Throughout this chapter and the next we shall consider pseudo-Newtonian configurations (cf section I.1) with power law distributions of specific angular momentum:

$$\Phi = -\frac{GM}{(\varpi^2 + z^2)^{\frac{1}{2}} - R_G} \tag{4.6}$$

$$l = l_{Kep_o}(\varpi/\varpi_o)^{2-q} = \frac{(GM\varpi_o^3)^{\frac{1}{2}}}{(\varpi_o - R_G)}(\varpi/\varpi_o)^{2-q} \tag{4.7}$$

where $R_G = 2GM/c^2$ is the Schwarzschild radius. Using equation (1.4) for Φ_{rot}, equation (4.4) may now be written

$$f = 1 - \frac{2}{\beta^2}\left[\frac{1}{1-\mathcal{R}_G} - \frac{1}{(r^2+z^2)^{\frac{1}{2}} - \mathcal{R}_G} + \frac{1 - r^{2-2q}}{(2-2q)(1-\mathcal{R}_G)^2}\right] \tag{4.8}$$

where

$$r \equiv \frac{\varpi}{\varpi_o} \quad z \equiv \frac{z}{\varpi_o} \quad \mathcal{R}_G \equiv \frac{R_G}{\varpi_o} \tag{4.9}$$

are the radius, height and Schwarzschild radius respectively scaled with the pressure maximum radius, and

$$\beta^2 \equiv \frac{2(n+1)p_o}{\rho_o}(\varpi_o/GM) \tag{4.10}$$

is a parameter measuring the ratio of thermal to kinetic energy at the pressure maximum. The topology of the equipotential surfaces is determined solely by q and $\mathcal{R}_G$, whereas the actual equipotential surface which the torus fills is determined by β. As $\beta \to 0$ the tori collapse to infinitely slender rings at $\varpi = \varpi_o$, and it is this limit which will be studied in this chapter.

To do this one must work in a coordinate system which itself collapses with the torus. One such is the orthogonal (f or η, Θ) coordinate system

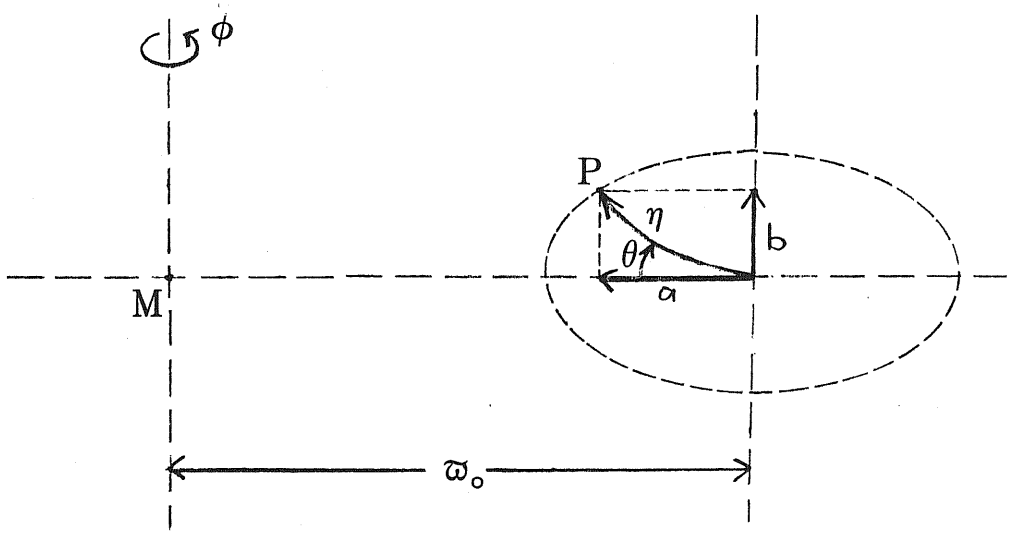

Figure 4-1. The (a,b) and (η , θ) orthogonal coordinates.

of figure 2-1 and used in the pseudobarotropic equations (3.67) and (3.68). The cylindrical polar coordinates (r, ζ) are also useful however and one may define a collapsing version (a,b) by

$$a \equiv \frac{1 - r}{\beta} = \frac{(\varpi_0 - \varpi)}{\beta \varpi_0} \tag{4.11}$$

$$b \equiv \frac{\zeta}{\beta} = \frac{z}{\beta \varpi_0} \tag{4.12}$$

These coordinates are illustrated in figure 4-1.

Expanding equation (4.8) about the slender $\beta = 0$ limit,

$$f = 1 - \left[\frac{b^2 + (2q - 1)a^2}{(1 - \mathcal{R}_0)^2} - \frac{2a^2}{(1 - \mathcal{R}_0)^3} \right] + \sigma(\beta) \tag{4.13}$$

Hence the surface of the torus is an ellipse with semimajor axis

$$a_s = \left[\frac{(1 - \mathcal{R}_0)^3}{(2q - 1)(1 - \mathcal{R}_0) - 2} \right]^{\frac{1}{2}} \tag{4.14}$$

and semiminor axis

$$b_s = 1 - \mathcal{R}_0 \ . \tag{4.15}$$

Equation (4.14) plus the fact that ℓ must increase outwards for local

stability implies that q must lie in the range

$$\frac{3 - \mathcal{R}_0}{2(1 - \mathcal{R}_0)} < q \leqslant 2 \quad . \tag{4.16}$$

The lower limit is in fact the value of q for which ℓ is locally Keplerian. This inequality further implies

$$0 \leqslant \mathcal{R}_0 < 1/3 . \tag{4.17}$$

As $\mathcal{R}_0 \to 1/3$ the torus lies on the marginally stable orbit and q can only take the value 2 because ℓ_{Kep} has a minimum there.

IV.2 The Oscillation Spectrum of the Newtonian $\nabla\ell = \nabla s = 0$ Slender Torus

Constant specific angular momentum, homentropic tori are marginally stable to the Høiland criterion and for them the perturbation equations are much simpler. From either the $K^2 \to 0$ limit of equations (3.61) and (3.62) or the $N^2 \to 0$ limit of equations (3.67) and (3.68) one may write

$$\nabla \cdot (\rho \nabla W) + \frac{\bar{\sigma}^2 \rho^2}{\gamma p} W = 0 \tag{4.18}$$

$$\left(W \rho \bar{\sigma} + \frac{1}{\bar{\sigma}} \nabla W \cdot \nabla p \right)\Big|_{p=0} = 0 \tag{4.19}$$

where, because $\nabla s = 0$, γ is equal to the polytropic value $\Gamma = 1 + 1/n$. The complicated mathematical structure of the more general cases disappears here - the equation is now entirely elliptic, there is no dense spectrum of modes (see also PPI), and there is no corotation singularity.[1] The reason these equations are simple is that the $\nabla\ell = \nabla s = 0$ torus is a potential flow, and in fact in this case W is simply the perturbed velocity potential, as may be seen from equations (3.54)-(3.56) with $K^2 = 0$.

As PPI point out, equation (4.18) is tantalizingly close to being a standard linear eigenvalue problem - the thing that prevents it is the differential rotation which makes $\bar{\sigma}$ a function of ϖ. However this problem

---

[1] Note that a $\bar{\sigma}^2$ has been cancelled out in passing to this limit so that a corotation continuum may still exist, though it does not affect equations (4.18) and (4.19).

completely disappears in the slender torus limit as then the variation in Ω across the torus vanishes.

Another fortunate thing occurs in the Newtonian ($\mathcal{R}_b=0$) case. Equation (4.13) then implies

$$f = 1 - \eta^2 = 1 - (b^2 + a^2) + \sigma(\beta) \tag{4.20}$$

so that the equipotentials have circular cross-sections! (This can be seen immediately from the central contour of figures 1-2(a) and 2-1). This extra symmetry makes the perturbation equation separable so that all the normal modes may be found analytically in the $\beta \to 0$ limit (Blaes 1985).

In (η, Θ) coordinates, the $\mathcal{R}_b=0$, $\beta \to 0$ limit of equations (4.18) and (4.19) is

$$\eta^2(1-\eta^2)\frac{\partial^2 W^{(0)}}{\partial \eta^2} + (1-\eta^2)\frac{\partial^2 W^{(0)}}{\partial \Theta^2} + \left[\eta(1-\eta^2) - 2n\eta^3\right]\frac{\partial W^{(0)}}{\partial \eta} + 2n\eta^2(\nu^{(0)} + m)^2 W^{(0)} = 0 \tag{4.21}$$

$$\left[f^n(\nu^{(0)} + m)^2 W^{(0)} + 2\eta^2 f^n \frac{\partial W^{(0)}}{\partial f}\right]_{f=0} = 0 \tag{4.22}$$

where the superscript (0) denotes the infinitely slender limit and ν is the ratio of σ to the angular velocity at the torus centre Ω_0. Equation (4.21) clearly admits even and odd (with respect to the equatorial plane) solutions of the form

$$W_k^{(0)} = V_k(\eta) \begin{cases} \cos k\Theta \\ \sin k\Theta \end{cases} \tag{4.23}$$

where k is a non-negative integer and $V(\eta)$ satisfies

$$\eta^2(1-\eta^2)\frac{d^2V}{d\eta^2} + \left[\eta(1-\eta^2) - 2n\eta^3\right]\frac{dV}{d\eta} + \left[2n\eta^2(\nu^{(0)} + m)^2 - k^2(1-\eta^2)\right]V = 0 \ . \tag{4.24}$$

If we let

$$V = \eta^k U(u) \tag{4.25}$$

where $u \equiv \eta^2$, then equation (4.24) becomes

$$u(1-u)\frac{d^2U}{du^2} + \left[(k+1) - (k+l+n)u\right]\frac{dU}{du} + \frac{n}{2}\left[(\nu^{(\infty)} + m)^2 - k\right]U = 0. \tag{4.26}$$

Provided $n > 0$, this equation together with the condition that U and its derivatives be finite at u=0 and 1 is a standard eigenvalue problem whose only solutions are the Jacobi polynomials $G_j(k + n, k + l, u)$ (Abramowitz and Stegun 1972). For nonzero k it might be expected that there are additional solutions of interest because really V and not U is required to be regular at $\eta = 0$. That this is not the case may be seen by performing a Frobenius series solution around u=0 in equation (4.26). Any alternative solution must have a leading term η^{-2k} (or $\ln\eta$ if k=0) which will make V (as well as U) blow up. Similar worries might be attached to the surface boundary condition (4.22), but a Frobenius series around u=1 in equation (4.26) shows that any additional solutions for W would have a leading term f^{1-n} (or ln f for n=1) so that this condition would be violated.[2]

The full eigenfunctions and corresponding eigenfrequencies are

$$W^{(\infty)}_{jkm} = A_{jk}\,\eta^k G_j(k + n, k + l, \eta^2)\begin{Bmatrix}\cos k\Theta \\ \sin k\Theta\end{Bmatrix}\exp\left[i(\sigma t + m\phi)\right] \tag{4.27}$$

$$\nu^{(\infty)}_{jkm} = -m \pm \left[\frac{1}{n}(2j^2 + 2jn + 2jk + nk)\right]^{\frac{1}{2}} \tag{4.28}$$

where the A's are constants. The three parameters j (a non-negative integer), k (a non-negative integer) and m (an integer) completely describe the solution. For $k > 0$ there is both an even and an odd eigenfunction associated with every eigenfrequency $\nu^{(\infty)}$, so there is a degeneracy. Note also that for every nonzero j or k, there are two eigenfrequencies associated with each eigenfunction,

---

[2] This is true even in thick tori (without cusps) as is easily seen from equations (4.18) and (4.19). Hence provided $n > 0$ one may always adopt the boundary condition that W and its derivatives be finite at the surface.

an ambiguity which arises because in the infinitely slender torus limit equation (4.21) is an eigenvalue problem for $(\nu^{\omega}+m)^2$, not ν^{ω}. One therefore expects that each zeroth order eigenfunction is the slender torus limit of two similar but distinct eigenfunctions with different frequencies. The pattern speed for each eigenfrequency is

$$\Omega_p = \Omega_0 \left\{ 1 \mp \left[\frac{1}{n}(2j^2 + 2jn + 2jk + nk) \right]^{\frac{1}{2}} \right\} \qquad (4.29)$$

showing that each eigenfunction is the limit of two modes propagating with similar speeds upstream and downstream relative to the equilibrium flow.

The spatial structure for given ϕ and t of three typical eigenfunctions is illustrated in figure 4-2. The significance of k is obvious - it is simply the number of wavelengths on a given isobaric surface so that there are 2k nodal lines radiating from the torus centre at $\eta=0$. In addition to the node at $\eta=0$ which occurs for $k\neq 0$, there are nodal surfaces at j other distinct values of η inside the torus.

Jaroszyński (1985) has classified the modes calculated here by analogy with the oscillations of nonrotating stars (see e.g. chapter 17 of Cox 1980). The k=0 modes are termed "radial". The j=0 modes have the special property

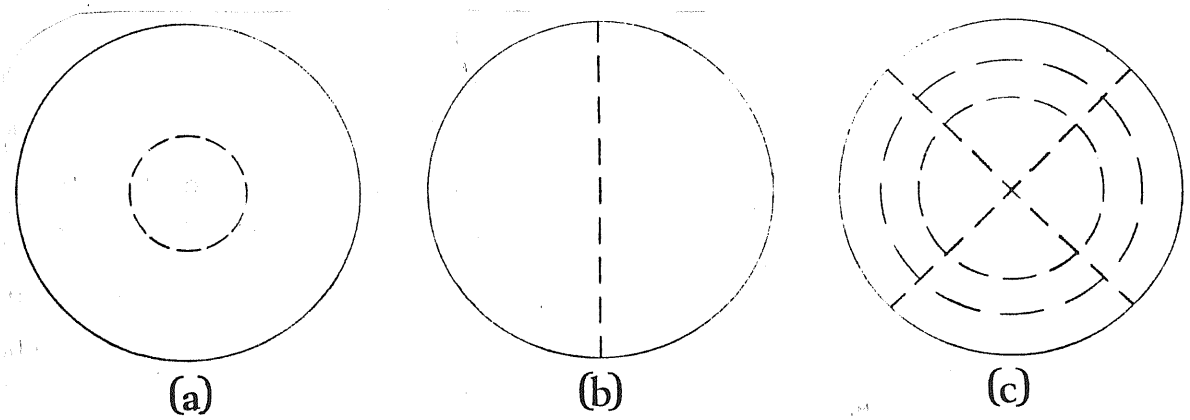

Figure 4-2. The spatial structure in a given cross-section of the torus for (a) the j=1, k=0 (radial); (b) the j=0, k=1 (f) and (c) the j=2, k=2 (p) even modes. The dashed lines indicate nodes of the eigenfunctions.

that

$$\Delta\rho^{(\infty)} = \delta\rho^{(\infty)} + \underline{\xi}^{(\infty)}\cdot\nabla\rho = \frac{\rho^2\tilde{\sigma}^{(\infty)}W^{(\infty)}}{\gamma p} + \frac{|\nabla\eta|^2}{\tilde{\sigma}^{(\infty)}}\frac{\partial W^{(\infty)}}{\partial\eta}\frac{\partial\rho}{\partial\eta} = 0 \qquad (4.30)$$

and hence the modes behave incompressibly. These are the Kelvin or "f-modes", and are the only solutions which survive the incompressible $n \to 0$ limit with finite eigenfrequency. Finally, the remaining $j\neq 0$, $k\neq 0$ eigenfunctions are termed "p-modes". Jaroszyński has also generalized the dispersion relation to include gravity of "g-modes" in the case of stratified tori.

Note that the expression under the square root in equation (4.28) is non-negative so that $\nu^{(\infty)}$ is real and all the modes are stable in this limit. This is fully expected from inequality (3.87) as there is no differential rotation in the slender torus. The fundamental j=0, k=0 mode is however only marginally stable:

$$\sigma^{(\infty)}_{00m} = -m\Omega_0 \qquad (4.31)$$

$$W^{(\infty)}_{00m} = A_{00}\exp\left[im(\phi - \Omega_0 t)\right] \qquad (4.32)$$

and corotates with the equilibrium flow. In the next section it will be shown that as the torus thickens this mode splits into a complex conjugate pair, producing the instability found in PPI.[3]

IV.3 The Papaloizou and Pringle Instability in the $\nabla\ell = \nabla s = 0$ Slender Torus

Ignoring the (t,ϕ) dependence, an important property of the zeroth order eigenfunctions is that they form a complete orthonormal set with respect to the inner product

---

[3] The slender torus is in fact stable only to exponentially growing modes. The fact that the zeroth order corotating mode is the marginally stable limit of a complex conjugate pair indicates the presence of a Jordan chain of unit length (a mode which grows linearly with time; Schutz 1980 and private communication). Indeed a Laplace transform treatment of the slender torus initial value problem shows the existence of modes that grow with time as t^N (N=1,2,3). These may either represent some limiting continuum spectrum or be a result of the fact that the $\nabla\ell = \nabla s = 0$ torus is itself marginally stable to the Høiland criterion. All this just shows the limitations of a normal mode analysis.

$$\langle W^{\omega}_{jk}, W^{\omega'}_{jk'} \rangle \equiv \int_0^{2\pi}\int_0^1 2n\eta\,(1-\eta^2)^{n-1} W^{\omega}_{jk} W^{\omega'}_{jk'}\, d\eta\, d\Theta = \delta_{jj'}\delta_{kk'} \qquad (4.33)$$

where the A_{jk}'s have been chosen to satisfy

$$A_{jk}^2 = \begin{cases} \dfrac{(2j+k+n)\Gamma^2(2j+k+n)}{n\pi\, j!(j+k)!\,\Gamma(j+k+n)\Gamma(j+n)} & \text{for } k \neq 0 \\ \dfrac{(2j+n)\Gamma^2(2j+n)}{2n\pi\,(j!)^2\Gamma^2(j+n)} & \text{for } k = 0 \end{cases} \qquad (4.34)$$

The completeness property may be seen from the well-known fact that the set $\{\exp(ik\Theta) : k=\text{integer}\}$ is complete as this is just a Fourier series. In addition, equation (4.24) together with the regularity conditions at $\eta=0$ and 1 constitute a Sturm - Liouville eigenvalue problem, so that for every given k the set of functions $V_{jk} = A_{jk}\eta^k G_j(k+n, k+1, \eta^2)$ is complete.

Any arbitrary piecewise continuous function $F(\eta, \Theta)$ defined over the torus cross-section and which is regular at $\eta=0$ and 1 and periodic in Θ may thus be expanded in terms of the eigenfunctions:

$$F(\eta, \Theta) = \sum_{jk} a_{jk} W^{\omega}_{jk} \qquad (4.35)$$

where

$$a_{jk} = \langle W_{jk}, F \rangle \quad . \qquad (4.36)$$

This means that perturbation theory may be used to tackle configurations away from the limit $\beta=0$.

Equation (4.18) may be rewritten

$$\mathcal{L}W + \left[2n\eta^2\bar{\nu}^2 - \frac{m^2\eta^2\beta^2}{r^2} f\right] W = 0 \qquad (4.37)$$

where $\mathcal{L}$ is a differential operator in η and Θ and $\bar{\nu} \equiv (\nu + m\frac{\Pi}{\Pi_0})$. Expanding the various quantities about the slender limit,

$$W = W^{(0)} + \beta W^{(1)} + \beta^2 W^{(2)} + \sigma(\beta^3)$$

$$\bar{v} = \bar{v}^{(0)} + \beta \bar{v}^{(1)} + \beta^2 \bar{v}^{(2)} + \sigma(\beta^3)$$

$$\mathcal{L} = \mathcal{L}^{(0)} + \beta \mathcal{L}^{(1)} + \beta^2 \mathcal{L}^{(2)} + \sigma(\beta^3) \qquad (4.38)$$

one may split equation (4.37) to different orders in β ;

$$\beta^0 : \quad \mathcal{L}^{(0)} W^{(0)} + 2n\eta^2 \bar{v}^{(0)2} W^{(0)} = 0 \qquad (4.39)$$

$$\beta^1 : \quad \mathcal{L}^{(1)} W^{(0)} + \mathcal{L}^{(0)} W^{(1)} + 4n\eta^2 \bar{v}^{(0)} \bar{v}^{(1)} W^{(0)} + 2n\eta^2 \bar{v}^{(0)2} W^{(1)} = 0 \qquad (4.40)$$

$$\beta^2 : \quad \mathcal{L}^{(2)} W^{(0)} + \mathcal{L}^{(1)} W^{(1)} + \mathcal{L}^{(0)} W^{(2)} + \left[4n\eta^2 \bar{v}^{(0)} \bar{v}^{(2)} + 2n\eta^2 \bar{v}^{(1)2} - m^2 \eta^2 f \right] W^{(0)}$$

$$+ 4n\eta^2 \bar{v}^{(0)} \bar{v}^{(1)} W^{(1)} + 2n\eta^2 \bar{v}^{(0)2} W^{(2)} = 0 \ . \qquad (4.41)$$

Equation (4.39) is simply the slender torus equation (4.21) and was solved in the last section.

The higher order eigenfunctions must be regular at η =0 and 1 (see footnote 2) and so may be expanded in terms of the zeroth order eigenfunctions:

$$W^{(1)} = \sum_{jk} a_{jk} W^{(0)}_{jk} \qquad W^{(2)} = \sum_{jk} b_{jk} W^{(0)}_{jk} \qquad (4.42)$$

The first order equation then becomes

$$\left[\mathcal{L}^{(1)} + 4n\eta^2 \bar{v}^{(0)} \bar{v}^{(1)} \right] W^{(0)} + 2n\eta^2 \sum_{jk} a_{jk} (\bar{v}^{(0)2} - \bar{v}^{(0)2}_{jk}) W_{jk} = 0 \ . \qquad (4.43)$$

Dividing by $2n\eta^2$ and taking the inner product of this equation with an arbitrary mode $W^{(0)}_{jk}$, we obtain

$$\left\langle W^{(0)}_{jk}, \left[(2n\eta^2)^{-1} \mathcal{L}^{(1)} + 2n \bar{v}^{(0)} \bar{v}^{(1)} \right] W^{(0)} \right\rangle + a_{jk} (\bar{v}^{(0)2} - \bar{v}^{(0)2}_{jk}) = 0 \qquad (4.44)$$

With the exception of the corotating fundamental, this equation may be used to calculate the first order changes is any zeroth order mode. The fact

that $\bar{v}^{(0)}$ is degenerate to even and odd pairs of modes is no problem as the equatorial symmetry of the torus ensures that the eigenfunctions remain even or odd to all orders. Note that equation (4.44) has real coefficients so that $\bar{v}^{(1)}$ and a_{jk} are real. This property of course extends to the higher order equations so that these modes remain stable to all orders.

For the corotating mode $\bar{v}^{(0)}_{00}=0$ so that this equation cannot be solved for $\bar{v}^{(1)}$. In addition $W^{(0)}_{00}$ is constant so that all the a_{jk}'s must be zero and the eigenfunction remains unchanged to this order. One must therefore proceed to the second order equation. Following the same procedure as before,

$$\left\langle W^{(0)}_{jk}, \left[(2n\eta^2)^{-1}\hat{L}^{(0)} + 2\bar{v}^{(0)}\bar{v}^{(0)} + \bar{v}^{(1)2} - m^2 f/2n\right] W^{(0)}\right\rangle$$

$$+ \left\langle W^{(0)}_{jk}, \left[(2n\eta^2)^{-1}\hat{L}^{(1)} + 2\bar{v}^{(0)}\bar{v}^{(1)}\right] W^{(1)}\right\rangle + b_{jk}(\bar{v}^{(1)2} - \bar{v}^{(0)2}_{jk}) = 0 \quad (4.45)$$

Hence for the corotating mode,

$$\left\langle W^{(0)}_{jk}, (\bar{v}^{(1)2} - m^2 f/2n) W^{(0)}_{00}\right\rangle - b_{jk}\bar{v}^{(0)2}_{jk} = 0 \quad (4.46)$$

For $j=k=0$, this gives

$$\bar{v}^{(1)} = \pm\, im\left[\frac{3}{2(n+1)}\right]^{\frac{1}{2}} \quad (4.47)$$

while for j or k different from zero, it implies

$$b_{jk} = \delta_{k0}\delta_{j1}\frac{(4n+1)n\pi m^2 A_{00}A_{10}}{2(n+1)^3(n+2)} + \delta_{k1}\delta_{j0}\bar{v}^{(1)}\frac{4\pi m A_{00}A_{01}}{(n+1)}$$

$$+ \delta_{k2}\delta_{j0}\frac{2\pi m^2 A_{00}A_{02}}{(n+1)(n+2)} \quad . \quad (4.48)$$

Hence the zeroth order corotation mode splits into two modes at first order, one growing and one decaying with time. This procedure may be repeated with the higher order equations, though further mode-splitting will not occur because all the equations will be linear in the unknown quatities.

The complete eigenfunction and eigenfrequency are

$$W = A_{00}\left\{1 + \beta^2 m^2\left[2\eta^2\cos^2\theta - \frac{3\eta^2}{4(n+1)} - \frac{(4n+1)}{4(n+1)^2} \pm 4i\left(\frac{3}{2n+2}\right)^{\frac{1}{2}}\eta\cos\theta\right]\right.$$
$$\left. + \sigma(\beta^3)\right. \tag{4.49}$$

$$\nu = -m \pm im\beta\left[\frac{3}{2(n+1)}\right]^{\frac{1}{2}} + \sigma(\beta^2) \tag{4.50}$$

Table 2 compares the predicted growth times from equation (4.50), neglecting terms of order β^2, with the numerically calculated values of the slender PPI model, for which n=3 and β =.0995. There is clearly excellent agreement, and this is also true for the eigenfunction. Neglecting terms of order β^3, the modulus of W is

$$|W| \doteq |A_{00}|\left\{1 + 2\beta^2 m^2\left[2\eta^2\cos^2\theta - \frac{3\eta^2}{4(n+1)} - \frac{(4n+1)}{4(n+1)^2}\right]\right\} \tag{4.51}$$

Hence |W| should have a minimum at the torus centre η=0 with the relative depth of the minimum increasing as m and/or β increase. In addition, the vertical structure of |W| will be rather weak due to the dominating influence of the $2\eta^2\cos^2\theta$ term. These properties are illustrated in figure 4-3 which should be compared with figure 2-2 from PPI. For thicker tori or higher azimuthal wavenumbers one would expect less agreement with the truncated expansions in equations (4.49) and (4.50) because higher order terms would become more important. In addition it is possible that at some finite β two stable modes merge to produce a complex conjugate pair, or vice-versa

Table 2. Growth times in units of Ω_o^{-1} - analytic versus numerical.

m	Predicted	Grid A	Grid B
2	8.2	8.0	8.5
4	4.1	3.9	4.7
6	2.7	2.9	4.0

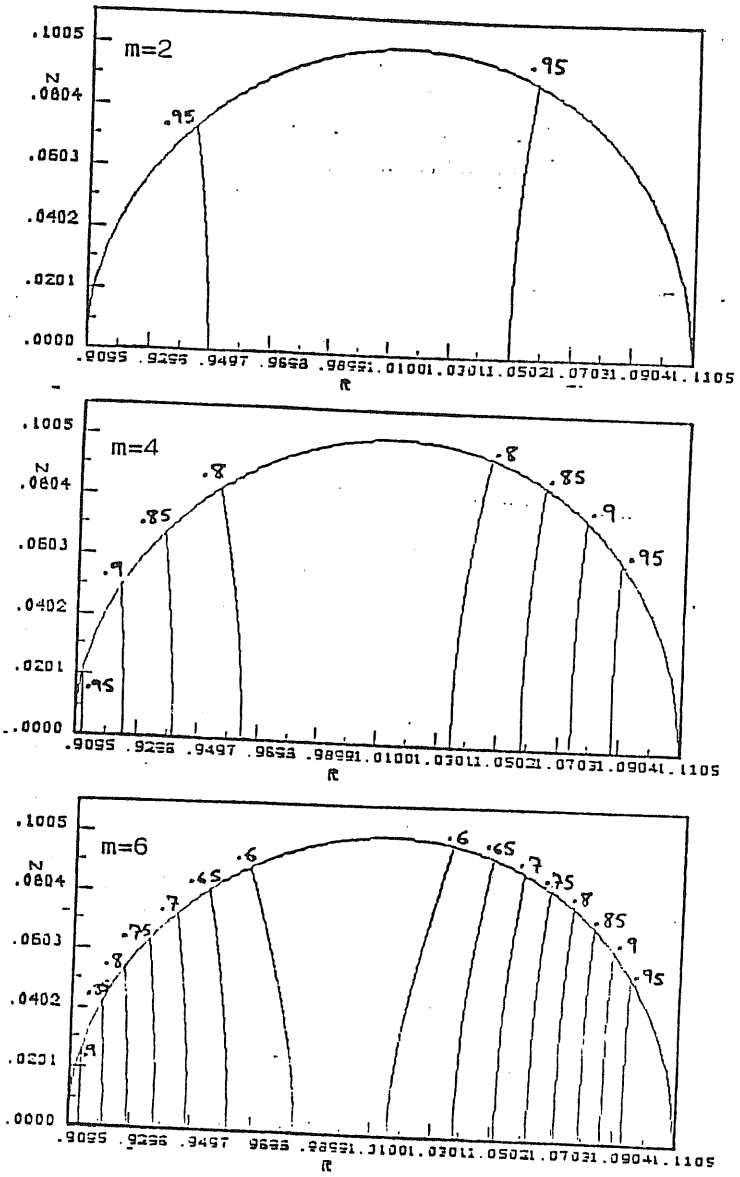

Figure 4-3. Structure of the unstable eigenfunctions in the β =0.0995, n=3 torus from the analytic solution.

(Schutz 1980); examples of this will be shown in the next chapter. Beyond such a point the perturbation expansion used here would of course no longer converge.

The perturbation in enthalpy $\delta p/\rho$ is given from equations (3.51), (4.49) and (4.50) by

$$\delta p/\rho = \bar{\sigma} W = \Omega_0 A_{00}{}^m \beta \left[2\eta\cos\theta \pm i \left(\frac{3}{2n+2} \right)^{\frac{1}{2}} \right] + \sigma(\beta^2) \qquad (4.52)$$

Including the ϕ-dependence, this has a phase

$$\tan^{-1}\left[\pm \left(\frac{3}{2n+2} \right)^{\frac{1}{2}} \frac{1}{2\eta\cos\theta} \right] + m\phi \qquad (4.53)$$

Examination of the surfaces where this is constant indicate that unstable modes (the minus sign in this expression) form leading spiral waves while damped modes are trailing (recall from fig. 4-1 that $\eta\cos\theta$ increases on moving <u>inwards</u> from the pressure maximum).[4]

Strictly speaking, the analysis in this section is only valid for compressible, $n>0$ tori. However, nothing appears to go wrong on taking the $n \to 0$ limit of equations (4.49) and (4.50), suggesting that incompressible tori are also unstable - contrary to the claims made in PPI and PPII. In Appendix B direct analysis of the n=0 case in the style of this section shows indeed that this conclusion is correct. As already discussed in chapter II, the reason for the discrepancy is that PPI and PPII invoked rigid boundary conditions instead of using the more physical free surface condition $\Delta p=0$.

All the above results are valid only for Newtonian tori. Pseudo-Newtonian tori are elliptical in cross-section so that the slender torus equation is not separable and one cannot calculate all the zeroth order modes analytically. Nevertheless, there still exists a constant corotating eigenfunction and the zeroth order modes will still form a complete set. One may therefore repeat most of the above analysis to show that the first order change in

---

[4] See also figure 3.3 of GGN for an excellent illustration of this fact.

the eigenfrequency is given by

$$\left\langle W_{00}^{(\infty)}, \left[\frac{\bar{\nu}^2}{(1-\mathcal{R}_c^2)} - \frac{m^2 f}{2n}\right] W_{00} \right\rangle = 0 \qquad (4.54)$$

(Here ν is scaled with the pseudo-Newtonian angular velocity at the torus centre Ω_c.) Because the torus cross-sections are no longer circular, it is convenient to rewrite the inner product (4.33) in (a,b) coordinates:

$$\left\langle W_{jk}^{(\infty)}, W_{j'k'}^{(\infty)} \right\rangle \equiv \oint\!\!\!\!\!\!\iint f^{(\infty)n-1} W_{jk}^{(\infty)} W_{j'k'}^{(\infty)} \, da\,db = 0 \qquad (4.55)$$

where $f^{(\infty)}$ denotes the $\beta \to 0$ expression (4.13) for f in terms of a and b. One then finds

$$\nu = -m \pm im\beta \left[\frac{(1-\mathcal{R}_c)^2(3-\mathcal{R}_c)}{(2n+2)(1-3\mathcal{R}_c)}\right]^{\frac{1}{2}} + O(\beta^2) \qquad (4.56)$$

For fixed β, the unstable growth rate increases as $\mathcal{R}_c$ increases from zero and relativity becomes more important. Note that as $\mathcal{R}_c \to 1/3$ the growth rate appears to blow up, but in fact β must be zero in this case as it is impossible to have a $\nabla\lambda = 0$ torus of nonzero thickness on the marginally stable orbit unless it has a cusp. We shall return to this point in the next chapter where the effect of a cusp will be discussed.

To summarize, for $\nabla\lambda = \nabla s = 0$ slender tori there exists one unstable mode for every nonzero value of the azimuthal wavenumber m. These modes are always symmetric with respect to the equatorial plane and represent leading "spiral waves". Relativity, atleast in the pseudo-Newtonian approximation, does not remove the instability.[5] Finally, the existence of these modes has nothing to do with compressibility, contrary to the claims of PPI and PPII.

IV.4 $\nabla\lambda \neq 0$, $\nabla s = 0$ Tori

Changing the rotation law makes the stability problem much more difficult

[5] Note by the way that it should be possible to treat slender tori in full general relativity using the methods in this section as the equations have a similar mathematical structure (Blandford, Jaroszyński and Kumar 1985).

for the reasons outlined in section (3.4), in particular the presence of a corotation singularity. This makes analytic results very difficult to obtain and one must in general resort to numerical work to get anything useful. One important analytic result was obtained in PPII, however - the fact that beyond a certain value for the specific angular momentum index $q=\sqrt{3}$, Newtonian slender tori are stable. In this section we outline the rather trivial procedure of generalizing this result to pseudo-Newtonian tori.

Consider first of all the perturbation equations for this case (3.61 and 3.62) written in (a,b) coordinates,

$$\frac{1}{1-\beta a}\frac{\partial}{\partial a}\left[\frac{f^n(1-\beta a)\bar{v}^2}{\Delta}\frac{\partial W}{\partial a}\right]+\frac{\partial}{\partial b}\left[f^n\frac{\partial W}{\partial b}\right]+$$

$$W\left[\frac{-\bar{v}\beta}{1-\beta a}\frac{\partial}{\partial a}\left(\frac{f^n\tilde{\kappa}^2 m}{2\Delta\tilde{\Omega}}\right)-\frac{m^2 f^n\bar{v}^2\beta^2}{\Delta(1-\beta a)^2}+\frac{2n\bar{v}^2 f^{n-1}}{(1-\mathcal{R}_6)^2}\right]=0 \qquad (4.57)$$

$$\left[\frac{2Wf^n\bar{v}}{(1-\mathcal{R}_6)^2}+\frac{\bar{v}f^n}{\Delta}\frac{\partial W}{\partial a}\frac{\partial f}{\partial a}+\frac{f^n}{\bar{v}}\frac{\partial W}{\partial b}\frac{\partial f}{\partial b}-\frac{Wm\beta f^n\tilde{\kappa}^2}{2\tilde{\Omega}\Delta(1-\beta a)^3}\frac{\partial f}{\partial a}\right]_{p=0}=0 \qquad (4.58)$$

where $\bar{v}$ and $\tilde{\Omega}$ are $\bar{\sigma}$ and Ω respectively scaled with the angular velocity at the pressure maximum Ω_0. Similarly,

$$\tilde{\kappa}^2\equiv\frac{\kappa^2}{\Omega_0^2}=2(2-q)(1-a\beta)^{-2q} \qquad (4.59)$$

and

$$\Delta\equiv\frac{D}{\Omega_0^2}=\bar{v}^2-\tilde{\kappa}^2 \ . \qquad (4.60)$$

For $n>0$, the boundary condition (4.58) may again be replaced with a regularity condition on W. Taking the slender torus limit,

$$\frac{\partial}{\partial a}\left[\frac{f^{\infty n}(\bar{v}^\infty+m)^2}{(\bar{v}^\infty+m)^2-2(2-q)}\frac{\partial W^\infty}{\partial a}\right]+\frac{\partial}{\partial b}\left[f^{\infty n}\frac{\partial W^\infty}{\partial b}\right]$$

$$+W^\infty\left[\frac{2n(\bar{v}^\infty+m)^2}{(1-\mathcal{R}_6)^2}f^{\infty n-1}\right]=0 \qquad (4.61)$$

As $q \to 2$ this reduces to the $\nabla\ell=0$ equation (4.21). A complete analytic solution to these equations does not exist but a few observations may still be made concerning the oscillation spectrum of these tori:

(1) From the discussion of chapter III one expects a dense spectrum of real modes with $(\nu^{\omega} + m)^2 < 2(2 - q)$ for which equation (4.61) is hyperbolic.

(2) The high order $\nabla\ell=0$ modes have high $(\nu^{\omega} + m)^2$ and so are unlikely to be affected by the epicyclic frequency $2(2 - q)$ in the first term. Instead, their frequencies will be modified solely due to the changing shape of the torus. Note that equation (4.61) is elliptic for these modes.

(3) Some modes which are separable in a and b can of course be found analytically (table 3). The first mode in the table is the only one which is independent of height (apart from the corotating mode which will be examined shortly). Interestingly enough, its frequency is independent of the angular momentum index q. Similarly, the second mode in the table is the only one which is independent of radius (apart from the last Lindblad resonance mode). Not surprisingly, its frequency is independent of both $\mathcal{R}_0$ and q. The last two modes in the table have no match to any of the $\nabla\ell=0$, $\mathcal{R}_0=0$ slender torus modes, as they tend to corotating modes but without constant eigenfunctions. These modes are in fact part of the dense spectrum and are marginally stable at $\nabla\ell=0$ - there they take on the character of modes growing as powers of t.

Table 3. Some $\nabla\ell\neq0$, $\nabla s=0$ Slender Torus Modes.

$(\nu^{\omega} + m)^2$	W	q=2, =0 limit
$\frac{(1 - \mathcal{R}_0)^2}{a_s^2} + 2(2 - q) = \frac{1 - 3\mathcal{R}_0}{1 - \mathcal{R}_0}$	a	j=0, k=1, even (f-mode)
1	b	j=0, k=1, odd (f-mode)
$\frac{(1 - 2\mathcal{R}_0)}{(1 - \mathcal{R}_0)} + \left[\frac{(1 - 2\mathcal{R}_0)^2}{(1 - \mathcal{R}_0)^2} - 2(2 - q)\right]^{\frac{1}{2}}$	ab	j=0, k=2, odd (f-mode)
$\frac{(1 - 2\mathcal{R}_0)}{(1 - \mathcal{R}_0)} - \left[\frac{(1 - 2\mathcal{R}_0)^2}{(1 - \mathcal{R}_0)^2} - 2(2 - q)\right]^{\frac{1}{2}}$	ab	No exponential normal mode limit
$2(2 - q)$	F(b)	No exponential normal mode limit

Finally, multiplication of equation (4.61) by $W^{(0)*}$ and integration over the torus cross-section indicates that there are no unstable modes provided $q < 2$, i.e. the Rayleigh criterion is satisfied. The corotation theorem of PPII implies that any $\beta > 0$ instability must therefore arise from a zeroth order corotating mode $\gamma^{(0)} = -m$. Note that for such a mode equation (4.61) is hyperbolic, implying that angular momentum gradients will affect the mode drastically. Because the analysis of this section and that of PPII is asymptotic for small β, $|\tilde{P}|^2$ will always be much less than $\tilde{\kappa}^2$, and this led Papaloizou and Pringle to the erroneous suggestion that the slender torus instability found in this case has a different physical origin (a "Kelvin-Helmholtz" instability) from the $\nabla\Omega = 0$ instability. GGN have however shown numerically that these two modes are the <u>same</u>.

The zeroth order corotating mode must satisfy

$$\frac{\partial}{\partial b}\left[f^{n} \frac{\partial W^{(0)}}{\partial b} \right] = 0 \quad . \tag{4.62}$$

The general solution which satisfies regularity on the surface is simply an arbitrary function of a:

$$W^{(0)} = W^{(0)}(a) \quad . \tag{4.63}$$

The fact that $W^{(0)}$ is undetermined at this level is purely a consequence of the fact that in addition to being the limit of any discrete unstable modes, the zeroth order corotation mode is also the limit of the corotating continuum.

Provided $q \neq 2$, the first order equation is also

$$\frac{\partial}{\partial b}\left[f^{n} \frac{\partial W^{(1)}}{\partial b} \right] = 0 \tag{4.64}$$

implying that W is unchanged to first order. The second order equation, again provided $q \neq 2$, is

$$\frac{\partial}{\partial b}\left[f^{(2n}\frac{\partial W^{(2)}}{\partial b}\right] + \frac{\partial}{\partial a}\left[\frac{f^{(2n}(\nu^{(1)} + mqa)^2}{-2(2-q)}\frac{dW^{(2)}}{da}\right]$$

$$+ \left[\frac{m}{2}(\nu^{(1)}+mqa)\frac{\partial f^{(2n}}{\partial a} + \frac{2n(\nu^{(1)} + mqa)^2}{(1-\mathcal{R}_0)^2} f^{(2n-1}\right] W^{(2)} = 0 \qquad (4.65)$$

$W^{(2)}$ may be eliminated from this equation by integrating it over b while keeping a fixed. One than obtains after some algebra

$$(1-x^2)\frac{d^2Q^{(2)}}{dx^2} - (2n+1)x\frac{dQ^{(2)}}{dx} + \left[\frac{2mxa_s(2n+1)}{(\nu^{(1)}+mqxa_s)} - \frac{2(2-q)(2n+1)a_s^2}{(1-\mathcal{R}_0)^2}\right]Q^{(2)} = 0 \qquad (4.66)$$

where
$$x \equiv \frac{a}{a_s} \qquad (4.67)$$

and
$$Q^{(2)} \equiv W^{(2)}(\nu^{(1)} + mqa) \qquad (4.68)$$

Equation (4.66) is difficult to solve analytically because of the corotation singularity at $\nu^{(1)} = -mqxa_s$ which gives rise to a continuum. However, following PPII one may ask whether there are any values of q for which the torus is marginally stable, i.e. $\nu^{(1)}=0$. For such a case equation (4.66) has Gegenbauer polynomials $C_j^n(x)$ as solutions where j is a non-negative integer and q must satisfy

$$\frac{2(2n+1)}{q} - \frac{2(2-q)(2n+1)a_s^2}{(1-\mathcal{R}_0)^2} = j(j+2n). \qquad (4.69)$$

Eliminating a_s from equation (4.14),

$$(1+2n)\left[q^2 - \frac{(3-\mathcal{R}_0)}{(1-\mathcal{R}_0)}\right] = j(j+2n)q\left[q - \frac{(3-\mathcal{R}_0)}{2(1-\mathcal{R}_0)}\right] \qquad (4.70)$$

which should be compared with equation (5.24) of PPII for the Newtonian $\mathcal{R}_0=0$ case. The discussion there is also valid here - j=0 gives the only permissable value of q which is

$$q_{crit} = \left(\frac{3-\mathcal{R}_0}{1-\mathcal{R}_0}\right)^{\frac{1}{2}} = (2q_{Kep})^{\frac{1}{2}} \qquad (4.71)$$

Perturbation theory shows that for $q > q_{crit}$ this mode is unstable while for $q < q_{crit}$ it is stable (see figure 4-4). GGN and Glatzel (1986) have shown numerically that this is in fact the same mode that was found in the $\nabla l = \nabla s = 0$ slender torus, and which is therefore removed by specific angular momentum gradients. Other unstable modes exist, however.

Finally, it should be pointed out that the analysis of this section and the corresponding one in PPII is actually valid for any analytic specific angular momentum distribution, simply because for a slender torus one may write

$$l = l_{Kep}\left[1 + \beta L_1 a + \sigma(\beta^2)\right] \tag{4.72}$$

where L_1 is a constant. For the power-law distribution (4.17), $L_1 = 2-q$ and the previous analysis still holds if q is everywhere replaced by $2-L_1$.

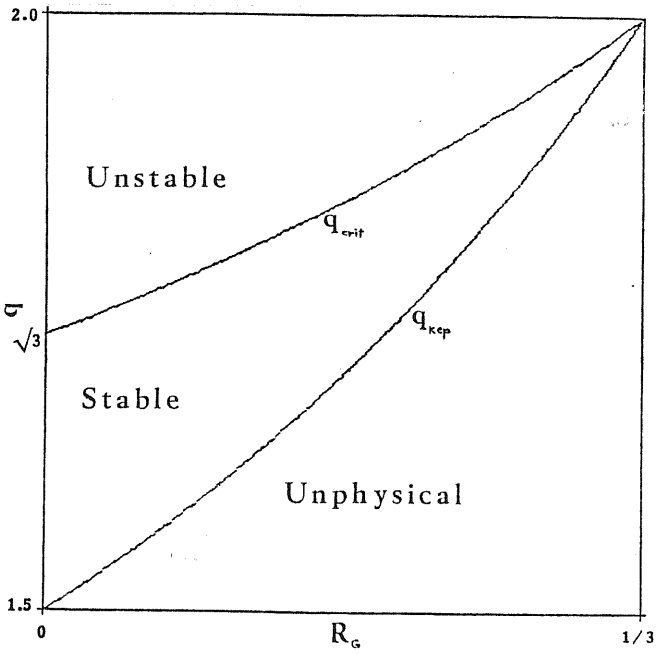

Figure 4-4. The critical value of the specific angular momentum index below which slender tori are stable to the $\nabla l = 0$ mode.

V. ANNULI AND CUSPS

Perhaps the most serious difficulty with studying the global stability of tori is the fact that one has to solve partial differential equations on asymmetric geometries. Given the approximate z-independent structure of the $\underline{\nabla} s = 0$ eigenfunctions from the previous section and Papaloizou and Pringle's numerical results, it is strongly tempting to just kill the z-dependence and work with two-dimensional annuli. In fact fluid dynamicists studying parallel shear flows do this quite often by invoking an extremely useful principle known as Squire's theorem (Drazin and Reid 1981). This states essentially that disturbances in a three dimensional flow can never be more unstable than those in a corresponding two dimensional flow.

Squire's theorem is not necessarily valid for rotating flows, however. Nevertheless the fact that studying annuli is so enormously easier than studying tori enables one to explore a wide range of configurations and gain some physical insight. In addition, GGN have shown that for slender configurations there is a direct transformation from two-dimensional annuli to three-dimensional tori.

This may easily be seen in the following way. No solution of equation (4.57) can be exactly independent of height for tori of nonzero thickness. However, if one integrates this equation vertically over b for fixed a, then the b-derivative term will vanish. Then assuming W is approximately independent of height (which by equation 3.56 is equivalent to assuming vertical hydrostatic equilibrium) one may take it outside the integrals. Now because slender tori have elliptical cross-sections,

$$\int_{-H(a)}^{H(a)} f^n db = (1 - a^2/a_s^2)^{n+\frac{1}{2}} \int_{-1}^{1} b_s (1 - x^2)^n dx \qquad (5.1)$$

where $H(a) = b_s(1 - a^2/a_s^2)^{\frac{1}{2}}$ is the height of the surface above the equatorial plane. Similarly,

$$2n \int_{-H(a)}^{H(a)} f^{n-1} db = 2(n + \tfrac{1}{2})(1 - a^2/a_s^2)^{n-\frac{1}{2}} \int_{-1}^{1} b_s (1 - x^2)^n dx \qquad (5.2)$$

Hence provided the torus is slender and vertical hydrostatic equilibrium is satisfied, the three-dimensional solutions can be obtained from the two-dimensional solutions by subtracting ½ from the two-dimensional polytropic index:

$$n_3 = n_2 - \tfrac{1}{2} \tag{5.3}$$

Only $\nabla s=0$ configurations will be considered in this chapter. Nonzero entropy gradients may produce strong deviations from z-independence, unless perhaps the torus is gyrotropic.

V.1 The Oscillation Spectrum of $\nabla l \neq 0$ Slender Annuli

On removing the z-dependence, equation (4.61) for $\nabla l \neq 0$ slender configurations is easy to solve analytically. Changing the independent variable to

$$u = \tfrac{1}{2}(1 + a/a_s) \tag{5.4}$$

this equation becomes the hypergeometric equation

$$u(1-u)\frac{d^2W^{(\omega)}}{du^2} + n(1-2u)\frac{dW^{(\omega)}}{du} + W\frac{2na_s^2}{(1-\mathcal{R}_0)^2}(\mathcal{V}^{(\omega)}+m)^2 - 2(2-q) = 0 \tag{5.5}$$

Solutions which are regular at the boundaries $a=\pm a_s$ occur only for

$$(\mathcal{V}^{(\omega)}+m)^2 = \frac{(1-\mathcal{R}_0)^2}{2na_s^2}J(2n-1+J) + 2(2-q) \tag{5.6}$$

where J is a non-negative integer. Note that a $(\mathcal{V}^{(\omega)}+m)^2$ has been cancelled to obtain equation (5.2) - the corotating mode which is the source of instabilities and the continuum cannot be determined at the zeroth level if $q\neq 2$, just as for $\nabla l \neq 0$ slender tori.

Comparing equation (5.6) with equation (4.28) and Table 3 for slender tori shows that J=0 and J=1 give slender torus modes, with J=0 corresponding to the (j=0,k=1,even) f-mode. Not surprisingly, these modes and the corotating mode are the only height independent modes of the infinitely slender torus. All other modes are lost or replaced with two-dimensional modes with different frequencies. This fact should be born in mind when comparing annuli with

tori. Instabilities involving the purely two-dimensional modes are likely to be quantitatively different from the three-dimensional case, although they might be similar qualitatively.

V.2 Equilibrium Configurations

Setting $\zeta = 0$ in equation (4.8), the Lane-Emden function for an annulus is

$$f = 1 - \frac{2}{\beta^2}\left[\frac{1}{1-\mathcal{R}_0} - \frac{1}{r-\mathcal{R}_0} + \frac{1 - r^{2-2q}}{(2-2q)(1-\mathcal{R}_0)^2}\right] \tag{5.7}$$

The boundaries r_{in} and r_{out} of the annulus are determined by setting $f=0$ in equation (5.7). Depending on the value of $\mathcal{R}_0$, the thickest annuli are of two types. Small values of $\mathcal{R}_0$ imply small deviations from Newtonian gravity and in these cases the outer boundary of the annulus extends to infinity when

$$\beta = \beta_{max} = \left[\frac{2q(1-\mathcal{R}_0) - 3 + 2\mathcal{R}_0}{(q-1)(1-\mathcal{R}_0)^2}\right]^{\frac{1}{2}} . \tag{5.8}$$

On the other hand, for large values of $\mathcal{R}_0$ the inner boundary can reach a critical radius where the effective gravity vanishes. This corresponds to the cusp of three dimensional tori and occurs when

$$\beta = \beta_{cusp} = \left[2\left(\frac{1}{1-\mathcal{R}_0} - \frac{1}{r_{cusp}-\mathcal{R}_0} + \frac{1 - r_{cusp}^{2-2q}}{(2-2q)(1-\mathcal{R}_0)^2}\right)\right] \tag{5.9}$$

where r_{cusp} is found by setting $(df/dr)_{r_{cusp}} = 0$. Thus, in addition to satisfying constraints (4.16) and (4.17), annuli can only exist if

$$0 < \beta < \min(\beta_{max}, \beta_{cusp}) \tag{5.10}$$

For constant specific angular momentum ($q=2$) annuli equations (5.8) and (5.9) become

$$\beta_{max} = \frac{(1-2\mathcal{R}_0)^{\frac{1}{2}}}{(1-\mathcal{R}_0)} \tag{5.11}$$

$$\beta_{cusp} = \left[2\left(\frac{1}{1 - R_0} - \frac{1}{r_{cusp} - R_0} + \frac{1 - r_{cusp}^2}{2 r_{cusp}^2 (1 - R_0)^2} \right) \right]^{\frac{1}{2}} \tag{5.12}$$

with

$$r_{cusp} = \frac{R_0}{2(1 - R_0)^2} \left[2 - R_0 + (4R_0 - 3R_0^2)^{\frac{1}{2}} \right] . \tag{5.13}$$

Note that β_{cusp} vanishes at $R_0 = 1/3$. In this case one has an infinitely thin cylinder rotating on the last stable orbit. When $R_0 \simeq .191$, $\beta_{max} = \beta_{cusp}$ and the thickest annulus extends to infinity while its inner edge lies on the marginally bound orbit (cf section I.1).

V.3 The Incompressible, $\nabla \ell = 0$ Annulus

This configuration, which when slender corresponds to a torus with polytropic index $-\frac{1}{2}$, is perhaps the furthest removed from reality of all the cases considered in this thesis. However, it is also the easiest to solve and instantly gives great physical insight.

Taking $\gamma \to \infty$ in the perturbation equations (4.18)-(4.19),

$$\nabla^2 W = \frac{1}{r} \frac{d}{dr}\left(r \frac{dW}{dr} \right) - \frac{m^2 W}{r^2} = 0 \tag{5.14}$$

$$\left(\bar{\nu}^2 W + g \frac{dW}{dr} \right)\Big|_{p=0} = 0 \tag{5.15}$$

where g is the dimensionless effective gravity:

$$g \equiv \frac{g_{eff}}{\omega_0^2 \zeta_0} = \frac{1}{r^3} - \frac{(1 - R_0)^2}{(r - R_0)^2} \tag{5.16}$$

Recalling that W is the perturbed velocity potential if $\nabla \ell = 0$ it is clear that these are simply the equations for surface gravity waves at the inner and outer edges of the annulus (see e.g. section 12 of Landau and Lifshitz 1959). The general solution to equation (5.14) is of course

$$W = \begin{cases} C_1 r^m + C_2 r^{-m} , & m \neq 0 \\ C_1 + C_2 \ln r , & m = 0 \end{cases} \tag{5.17}$$

Substitution of this solution into the boundary conditions (5.15) at the

two surfaces yields a quartic dispersion relation for ν . For axisymmetric modes this has the solution

$$\nu = 0,\ 0,\ \pm\left[\frac{r_{out}\, g_{in} - r_{in}\, g_{out}}{r_{in}\, r_{out}\,(\ln r_{out} - \ln r_{in})}\right]^{\frac{1}{2}} . \tag{5.18}$$

All four roots are real because the effective gravity is positive at the inner radius and negative at the outer. Hence there are no exponentially growing axisymmetric perturbations as is of course expected.

The dispersion relation for nonaxisymmetric modes,

$$\left[\left(\nu + \frac{m}{r_{in}^2}\right)^2 + \frac{m g_{in}}{r_{in}}\right]\left[\left(\nu + \frac{m}{r_{out}^2}\right)^2 - \frac{m g_{out}}{r_{out}}\right]$$

$$= (r_{out}/r_{in})^{2m}\left[\left(\nu + \frac{m}{r_{in}^2}\right)^2 - \frac{m g_{in}}{r_{in}}\right]\left[\left(\nu + \frac{m}{r_{out}^2}\right)^2 + \frac{m g_{out}}{r_{out}}\right] \tag{5.19}$$

is not so trivial to solve. Consider first the case where the outer boundary extends to infinity. Then only two solutions exist which are regular (C_1=0):

$$\nu = -\frac{m}{r_{in}^2} \pm \left(\frac{m g_{in}}{r_{in}}\right)^{\frac{1}{2}} \tag{5.20}$$

These represent gravity waves propagating around the inner boundary with equal and opposite pattern speeds relative to the equilibrium flow. We shall denote the slower upstream mode (the plus sign in equation 5.20) by f_I^- and the faster downstream mode by f_I^+ . Equation (5.19) also has a double zero root for which the eigenfunction blows up at infinity. This is in fact the limit of two modes which for large r_{out} have frequencies

$$\nu = -\frac{m}{r_{out}^2} \pm \left(\frac{-m g_{out}}{r_{out}}\right)^{\frac{1}{2}} \tag{5.21}$$

and thus represent gravity waves propagating around the outer boundary. As before we denote the slower upstream mode by f_O^- and the faster downstream mode by f_O^+.

Another interesting case occurs when the inner boundary lies on the cusp so that $g_{in}=0$. Then equation (5.9) admits a double root $-m/r_{in}^2$ in addition to the two roots

$$\nu = -\frac{m}{r_{out}^2} \pm \left[\frac{mg_{out}}{r_{out}} \left(\frac{\frac{2m}{r_{in}} + \frac{2m}{r_{out}}}{\frac{2m}{r_{in}} - \frac{2m}{r_{out}}} \right) \right]^{\frac{1}{2}} . \qquad (5.22)$$

The latter pair are clearly the $f_o^{\mp}$ outer gravity wave modes modified by the presence of the inner boundary - note that equation (5.15) indicates that these modes have zero amplitude at this boundary. Nonzero amplitudes at the inner edge only occur for the neutral, corotating inner modes because there is no restoring force to support wave motion.[1]

These two cases are very similar in that the inner and outer gravity waves do not influence each other - in the first case by separating the boundaries by large distances and in the second case by killing off wave motion at the inner edge. Note also that both of these cases are <u>stable</u>.

Figures (5-1) and (5-2) present the real parts of the eigenfrequency solutions of the general dispertion relation for the m=1 mode (for which $\mathrm{Re}\,\nu$ is simply minus the pattern speed). The modes are well separated in the above limiting cases for which $\beta = \beta_{max}$ or β_{cusp}. Because the inner edge of the annulus is rotating faster than the outer edge, the inner modes have higher pattern speeds. As the annulus shrinks, however, the faster outer mode catches up with the slower inner mode and, voilá, the Papaloizou and Pringle instability sets in - the two modes join together to form a complex conjugate pair which corotate together with the equilibrium flow at some radius. As $\beta \to 0$ and the annulus becomes infinitely slender, the complex pair of modes join again to become the zeroth order corotating mode which is marginally stable as there is no shear left to drive the instability. On the other hand, the faster inner mode and the slower outer mode rotate with equal and opposite pattern speeds around the slender annulus. These are the pair of two-dimensional J=1 slender annulus f-modes (section V.1 - note that <u>all</u> these modes exist also in tori).

---

[1] The inner modes are marginally stable. If they were given nonlinear, finite amplitudes they would presumably go unstable and produce the cusp overflow.

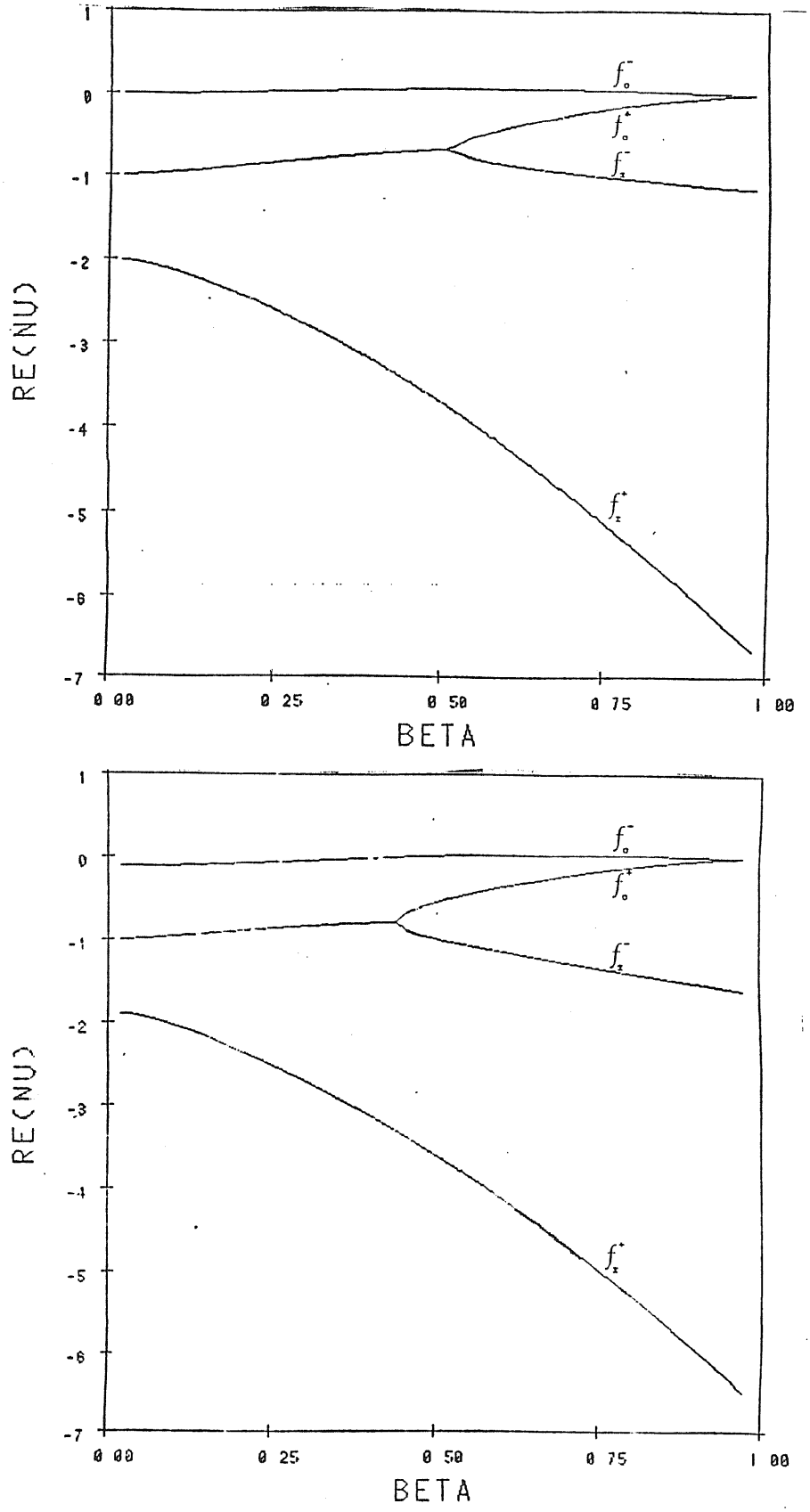

Figure 5-1. The real parts of the m=1 eigenfrequencies for the $\nabla\ell = 0$ incompressible annulus with $\mathcal{R}_6 = 0$ (upper) and $\mathcal{R}_6 = 0.1$ (lower). Relativity is unimportant here and the annuli extend to infinity at $\beta = \beta_{max}$.

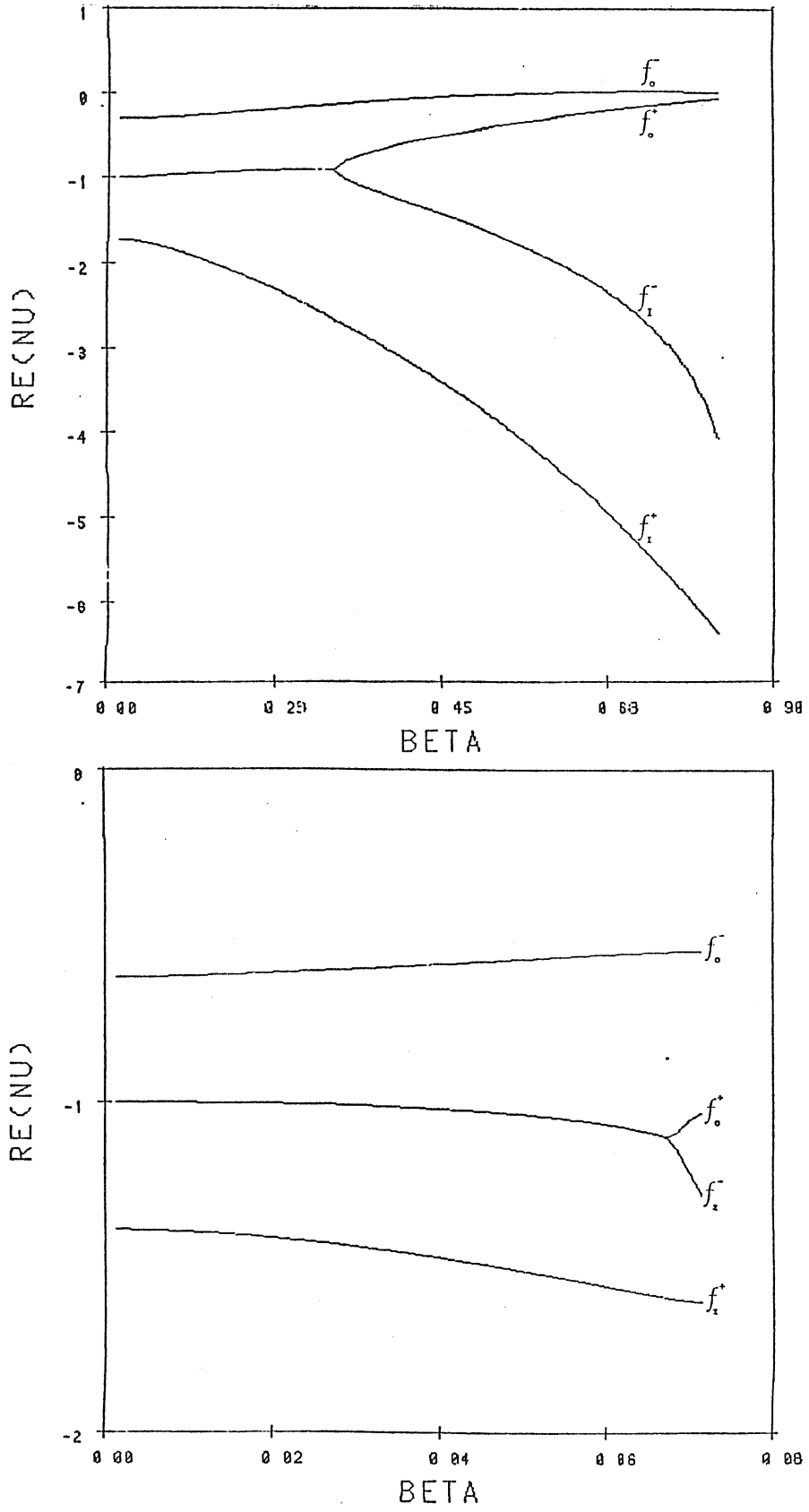

Figure 5-2. The real parts of the m=1 eigenfrequencies for the $\nabla \ell = 0$ incompressible annulus with $\mathcal{R}_c = 0.2$ (upper) and $\mathcal{R}_c = 0.3$ (lower). Relativity is important here and the annuli have cusps at $\beta = \beta_{cusp}$.

Expansion of the dispersion relation about the slender annulus limit leads to the growth rate

$$|\mathrm{Im}\,\nu| = m\beta\left[\frac{(1-\mathcal{R}_c)^2(3-\mathcal{R}_c)}{(1-3\mathcal{R}_c)}\right]^{\frac{1}{2}} + \sigma(\beta^2) \qquad (5.23)$$

which is identical to the slender torus expression (4.56) when $n=-\frac{1}{2}$. Figure 5-3 shows the growth rate as a function of m and $Q=\beta m$ for the Newtonian $\mathcal{R}_c=0$ case. As the slender annulus expands, the higher m modes grow fastest and dominate the instability. This is probably due to the fact that these modes are more efficient in transporting angular momentum. However, the high m modes also stabilize faster with β so that the thickest annuli which are unstable are subject only to the m=1 mode. This is easy to understand because the penetration depth for surface gravity waves decreases with increasing m (cf equation 5.17) and so the inner and outer modes quickly become independent for high m.

The most striking feature of figure 5-3 is that the growth rate is almost purely a function of Q. Indeed the critical value of Q above which a given mode is stable lies in the range

$$0.5164 = Q_{crit}(m=1) \leqslant Q \leqslant Q_{crit}(m=\infty) = 0.5218 \qquad (5.24)$$

In addition the value of Q which gives the maximum growth rate and the maximum growth rate itself satisfy

$$0.292 = Q_{max}(m=1) \leqslant Q \leqslant Q_{max}(m=\infty) = 0.312 \qquad (5.25)$$

$$0.268 = |\mathrm{Im}\,\nu|_{max}(m=1) \leqslant |\mathrm{Im}\,\nu|_{max} \leqslant |\mathrm{Im}\,\nu|_{max}(m=\infty) = 0.308 \qquad (5.26)$$

This behaviour extends to the $\mathcal{R}_c \neq 0$ case as well. Figure (5-4) illustrates the critical values of β, above which a given mode of wave-number m is stable, as a function of $\mathcal{R}_c$. The dashed curve shows $Q_{crit}(m=\infty)$ which closely follows the $\beta_{crit}(m=1)=Q_{crit}(m=1)$ curve. A <u>physical</u> explanation of this effect is still not known.

That the results of this section apply to more general configurations may be seen from the work of GGN and Glatzel (1986), already discussed at length in chapter II. The two dimensional surface wave instability does

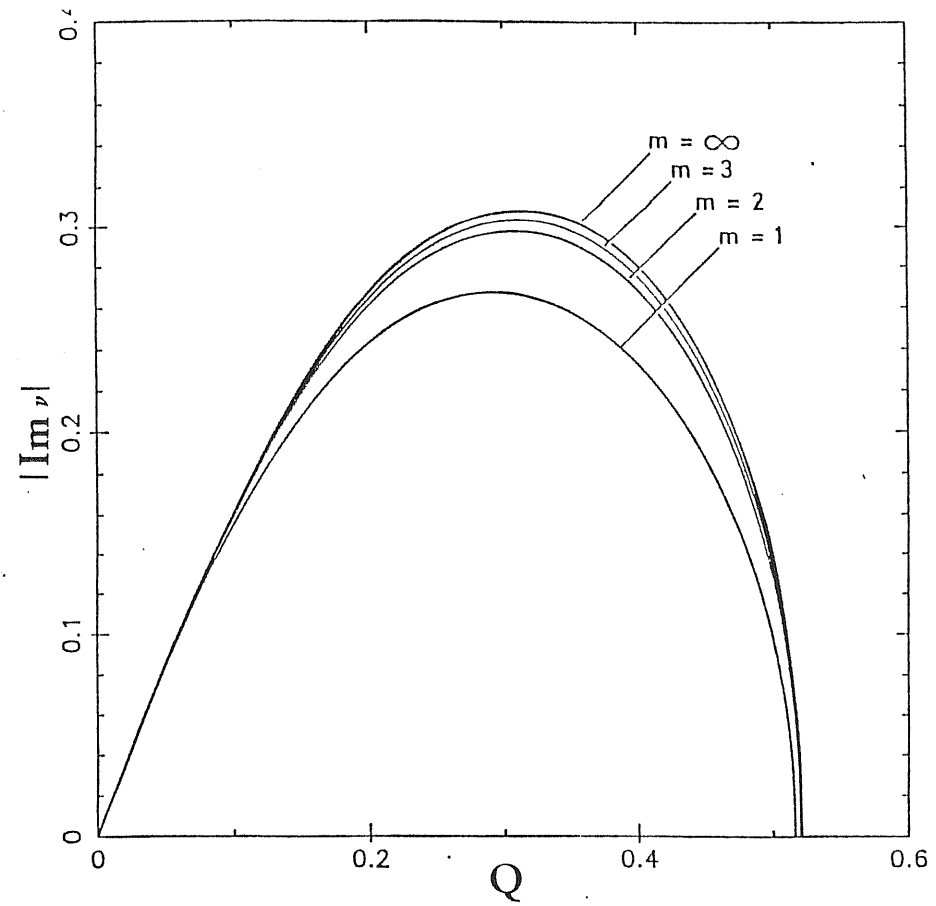

Figure 5-3. The growth rate for the Newtonian, $\nabla \cdot \ell = 0$ incompressible annulus.

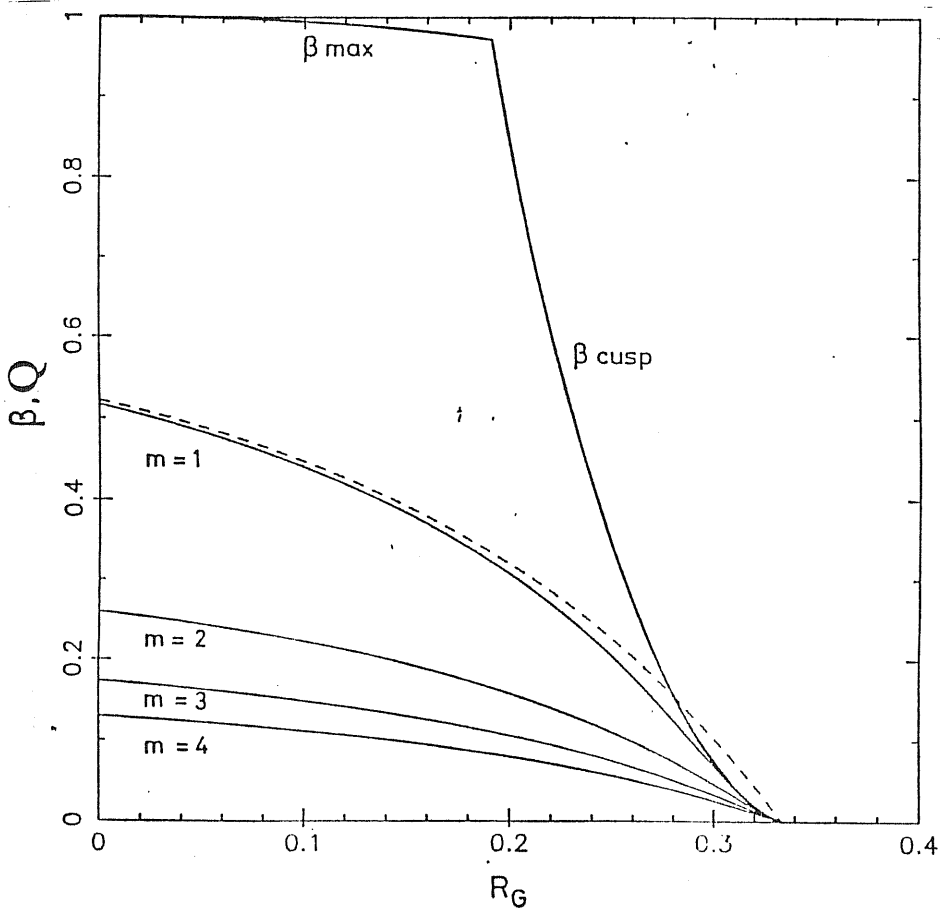

Figure 5-4. The critical values of β above which a given mode is stable. The dashed curve represents Q_{crit} (m=∞). For comparison the values of β_{max} and β_{cusp} are also shown.

exist in tori, and it is this mode which is stabilized by the critical angular momentum gradient discovered by PPII and discussed in section IV.4 . The main qualitative difference produced by conpressibility is the addition of further modes of instability which exist above Q_{crit} .

The results of GGN and Glatzel were obtained for Newtonian configurations. The question as to how far the cusp stabilization acts in compressible tori will be addressed in the next section.

V.4 Slender, $\nabla\ell = 0$ Tori with Cusps

All the slender torus analysis in the previous chapter is a priori invalid for a slender cusped torus precisely because it is asymptotic for small β , whereas a cusp necessarily occurs at a finite nonzero β . Indeed, the cusp stabilization in the case of the incompressible annulus cannot be seen from the asymptotic formula (5.23) for the growth rate, simply because an asymptotic expansion would not converge at a marginal stability point. All that one could derive from equation (5.23), and can derive from its compressible cousin (4.56), is that as $\mathcal{R}_0 \to 1/3$ and $\beta \to \beta_{cusp}$ $(\mathcal{R}_0 = 1/3) = 0$, the instability vanishes - but this is simply because that is the infinitely slender torus limit.

Consider a sequence of cusped $\nabla\ell = 0$ tori with varying $\mathcal{R}_0$. Equation (4.8) then gives the Lane-Emden function to be

$$f = 1 - \frac{2}{\beta_{cusp}^2}\left[\frac{1}{1-\mathcal{R}_0} - \frac{1}{(r^2+z^2)^{1/2} - \mathcal{R}_0} + \frac{1-r^2}{2(1-\mathcal{R}_0)^2}\right] \qquad (5.27)$$

As $\mathcal{R}_0 \to 1/3$ these tori become infinitely slender cusped rings located at the marginally stable orbit. Defining the parameter

$$\epsilon \equiv \frac{1}{3} - \mathcal{R}_0 \geq 0 \qquad (5.28)$$

Then equations (5.12), (5.13) and (5.27) may be expanded around the limit $\epsilon = 0$ to give

$$\frac{\beta_{cusp}^2}{2} = \frac{243}{4}\epsilon^3 + O(\epsilon^4) \qquad (5.29)$$

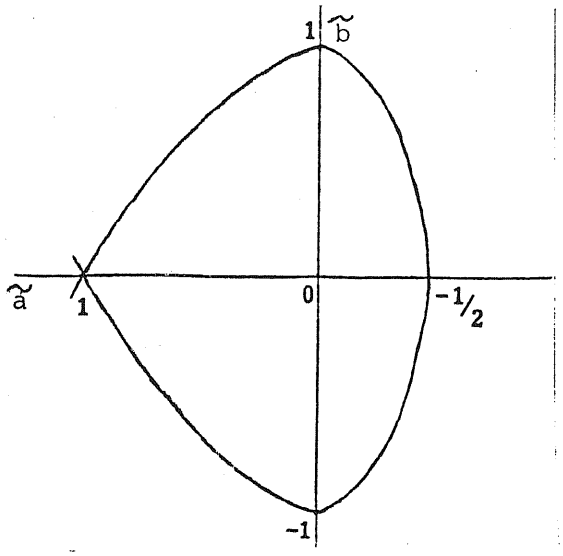

Figure 5-5. The cusped slender torus

$$r_{cusp} = 1 - 6\varepsilon + \mathcal{O}(\varepsilon^2) \tag{5.30}$$

$$f = 1 - \tilde{b}^2 - 3\tilde{a}^2 + 2\tilde{a}^3 + \mathcal{O}(\varepsilon) \tag{5.31}$$

where $\tilde{a}$ and $\tilde{b}$ are new collapsing radial and vertical coordinates defined by

$$\tilde{a} = \frac{1 - r}{1 - r_c} \qquad \tilde{b} = \frac{z}{h_o} \tag{5.32}$$

and where h_o is the height of the torus surface above the pressure maximum

$$h_o = \left\{ \left[\left(\frac{1}{1 - \mathcal{R}_c} - \frac{\mathcal{B}_{cusp}^2}{2} \right)^{-1} + \mathcal{R}_c \right]^2 - 1 \right\}^{\frac{1}{2}} = 54\varepsilon^3 + \mathcal{O}(\varepsilon^4) \tag{5.33}$$

The shape of the slender cusped torus is illustrated in figure 5-5. Its inner cusp and outer radius are at $\tilde{a}$=1 and -½ respectively.

W and $\mathcal{V}$ may be expanded as

$$W = W^{(0)} + \varepsilon W^{(1)} + \varepsilon^2 W^{(2)} + \mathcal{O}(\varepsilon^3)$$

$$\mathcal{V} = \mathcal{V}^{(0)} + \varepsilon \mathcal{V}^{(1)} + \varepsilon^2 \mathcal{V}^{(2)} + \mathcal{O}(\varepsilon^3) \tag{5.34}$$

and the perturbation methods of the previous chapter may be employed here. The calculation is rather tedious and is presented in Appendix C. There again exists a zeroth order corotating mode for which $\mathcal{V}^{(1)}$ satisfies

$$\int_{-\frac{1}{2}}^{1} (1 - \tilde{a})^{2n-1} (1 + 2\tilde{a})^{n-\frac{1}{2}} (\mathcal{V}^{(1)} + 12m\tilde{a})^2 d\tilde{a} = 0 \tag{5.35}$$

and the eigenfunction is exactly independent of height for small ϵ. Hence GGN's transformation (5.3) is valid in this case as well.

For $-\frac{1}{2} \leq n \leq 0$ the integral (5.35) diverges near $\tilde{a}=1$ unless $\nu^{(1)} = -12m$. This is just the value required for the mode to corotate on the cusp, in agreement with the incompressible annulus of the previous section. Figure 5-6 illustrates a numerical solution of equation (5.35) for $n > 0$. Compressible tori, even with cusps, are unstable.

This result should have been expected, as compressible fluids can support wave motion near their inner boundary even if a cusp is present. The incompressible torus cannot, as the unstable eigenfunction is independent of height and so the cusp plays the same stabilizing role as in the incompressible annulus.

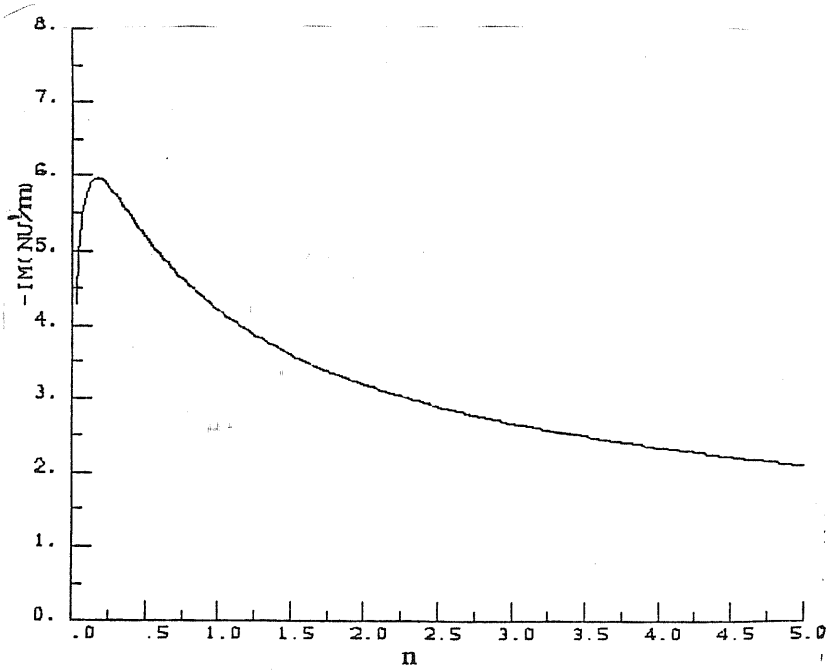

Figure 5-6. The imaginary part of $\nu^{(1)}$ as a function of polytropic index n for the $\Omega\ell = \Omega_s = 0$ cusped torus.

V.5 Pseudo-Newtonian, $\Omega\ell = 0$ Annuli

Primarily for the purpose of investigating accreting tori (see chapter VI), we have extended Glatzel's (1986) numerical integrations to pseudo-Newtonian annuli. Figure 5-7 illustrates some of the results for $n_2=3$ configurations, and these clearly bear a close resemblance to Glatzel's results for Newtonian annuli. Particularly important for the following chapter is the infinite, marginally bound annulus. Its unstable growth rate may be found by extra-

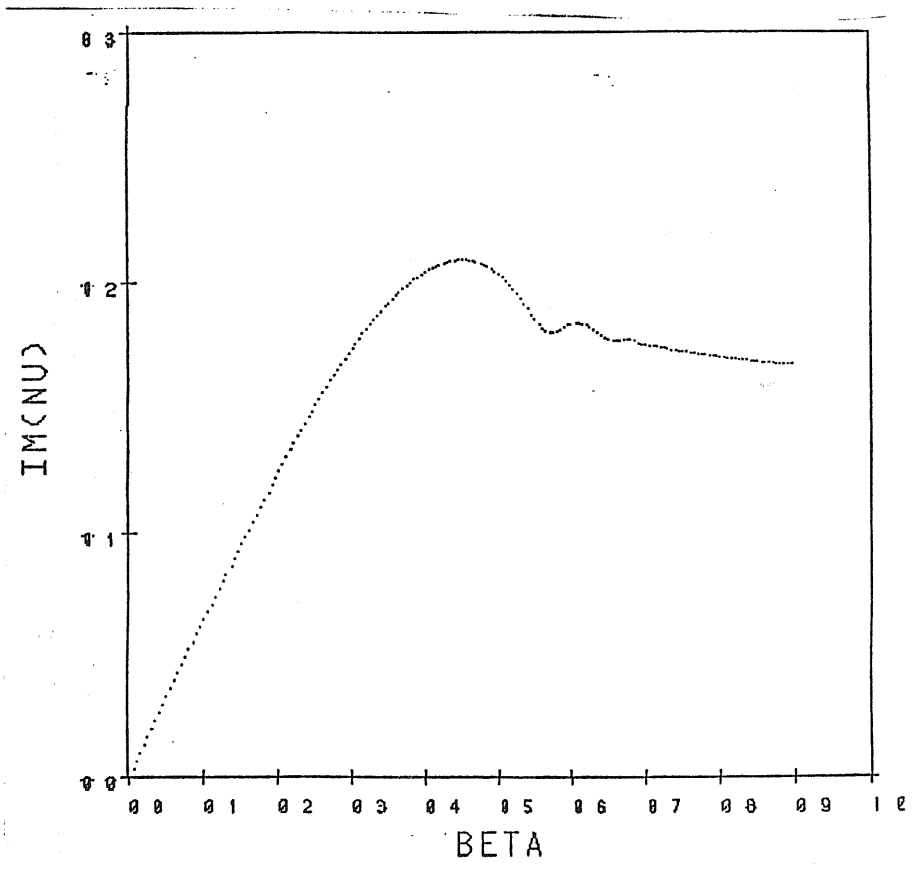

(a) $\mathcal{R}_e$=0

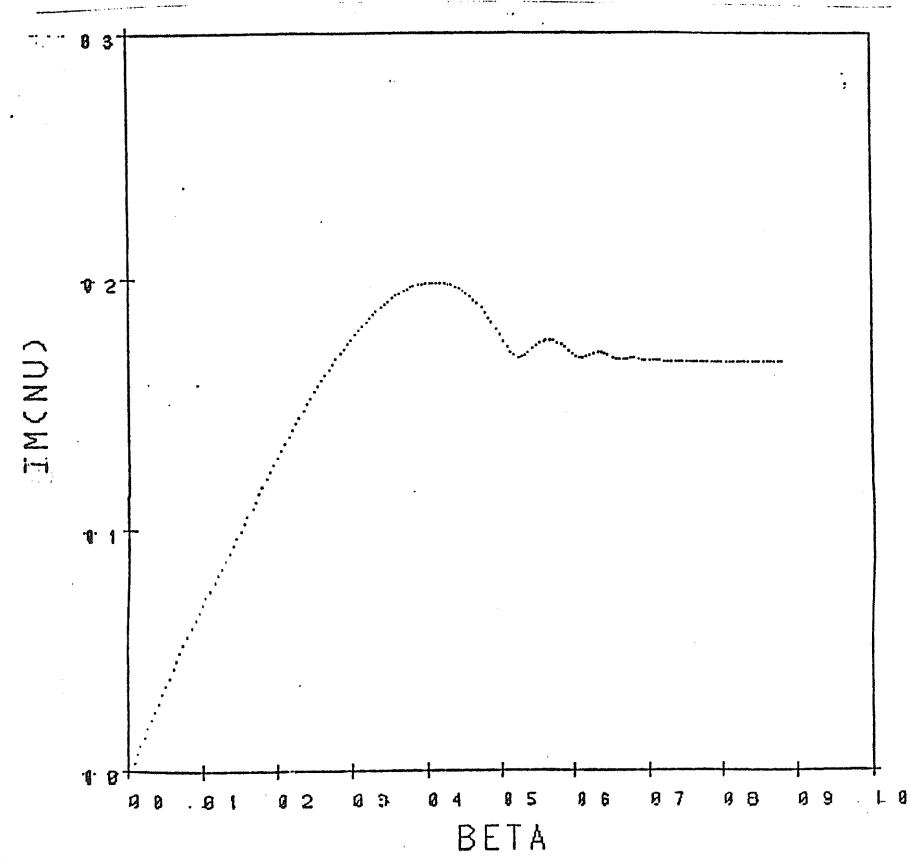

(b) $\mathcal{R}_e$=0.1

Figure 5-7. The growth rate of the m=1 mode in $\underline{\Omega}$=0 pseudo-Newtonian annuli with n_2=3 and various values of $\mathcal{R}_e$. The asterix in case (d) marks the value calculated for a cusped torus from equation (5.35) with n_3=2.5.

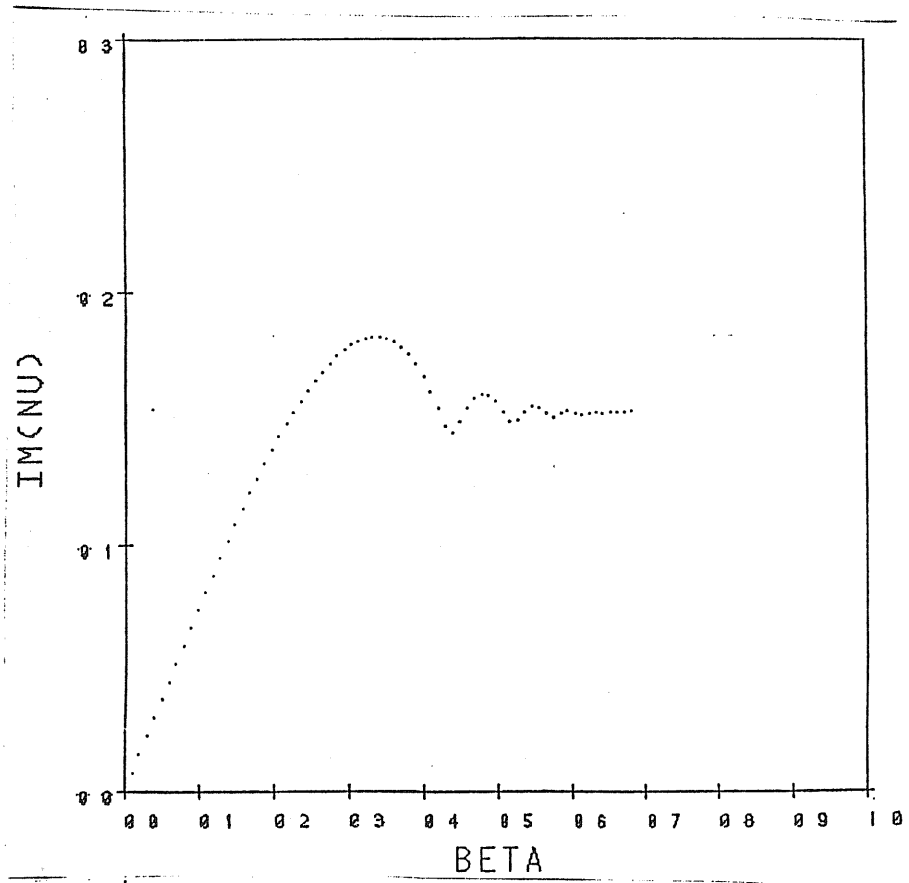

(c) $\mathcal{R}_c$=0.190983

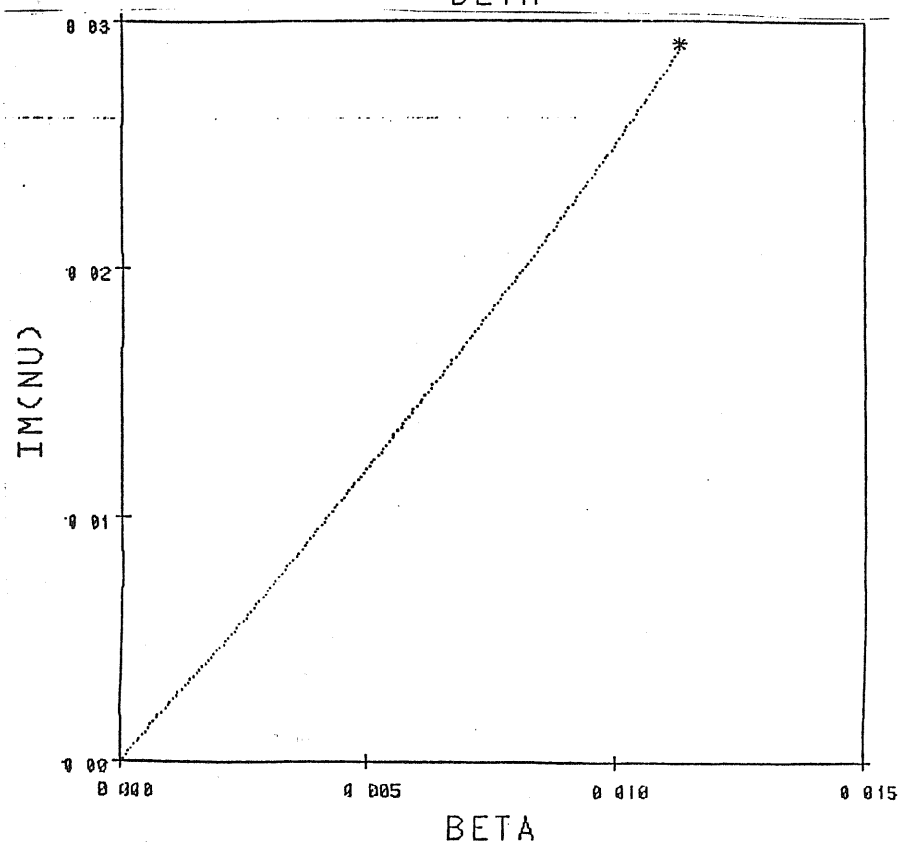

(d) $\mathcal{R}_c$=0.3

Figure 5-7. (cont.)

polating the curve in figure 5-7(c) to $\beta = \beta_{max} = \beta_{ensp}$. It is through this configuration that our investigation of accretion will take place.

VI. ACCRETING FLOWS

All the analysis presented so far in this thesis and all published work in the field has been confined to fluids in pure azimuthal flow. However, the fact that for thick tori the unstable eigenfunctions are concentrated near the inner boundary and the general surface nature of the most unstable mode indicate that cusp overflow could strongly influence the instability. Unfortunately, this is even more difficult to treat than the nonaccreting tori, as no analytic solutions for the possible stationary structures of an accreting torus exist. Indeed, a glance at the results of Hawley and Smarr's (1985) numerical simulations give an idea of the horrendous possibilities.[1]

Given these difficulties, it seems reasonable to consider a simplified model for a preliminary investigation before going on to more realistic but complicated flows. In the spirit of the previous chapter, we consider two-dimensional accretion, because in this way a continuous sequence of models can be constructed starting from pure rotation, which is unstable, and going to pure radial infall, which is stable. The location of the marginally stable transition point is still unknown, however, and a numerical investigation is under way.

VI.1 Stationary Structure of 2D Accretion Flows

In cylindrical polar coordinates, the equations of motion for a two dimensional axisymmetric flow in an external gravitational potential Φ are

$$\frac{d}{d\varpi}\left(\rho \varpi v_\varpi\right) = 0 \tag{6.1}$$

$$v_\varpi \frac{dv_\varpi}{d\varpi} - \frac{l^2}{\varpi^3} = -\frac{1}{\rho}\frac{dp}{d\varpi} - \frac{d\Phi}{d\varpi} \tag{6.2}$$

$$v_\varpi \frac{dl}{d\varpi} = 0 \tag{6.3}$$

---

[1] Unfortunately, it has not been possible to review this important work here due to lack of time, but readers interested in thick accretion flows are strongly recommended to read it. The work of Eggum, Coroniti and Katz (1985) is also of interest in this respect.

$$v_\varpi \frac{ds}{d\varpi} = 0 \tag{6.4}$$

If the inflow velocity v_ϖ is nonzero, equations (6.3) and (6.4) immediately imply that the specific angular momentum and specific entropy are constant and so the flow is potential. This is an obvious result, as individual fluid elements must preserve ℓ and s in an axisymmetric adiabatic flow. Because the case under consideration is two-dimensional, all streamlines are identical and so ℓ and s must be constant throughout. Specific angular momentum and entropy gradients were permitted in tori (and annuli) because the fluid lines were closed - here they are not. This discontinuous behaviour between the two types of flow is of course an artifact of the perfect fluid assumption. In real fluids the right hand sides of equations (6.3) and (6.4) would include dissipative terms which would generally give nonzero gradients in ℓ and s in addition to some radial infall.

Even in perfect fluids, however, one may obtain a smooth continuous transition between the two flow types by considering a marginally stable, $\nabla\ell = \nabla s = 0$ rotating annulus. As this is in any case the most vulnerable to Papaloizou and Pringle's instability, it is probably the most interesting model to investigate.

Because the flow is homentropic, a polytropic relation between pressure and density may be adopted:

$$p = K\rho^{\Gamma} = K\rho^{1+1/n} \tag{6.5}$$

Equations (6.1) and (6.2) may then be integrated to give

$$2\pi\rho\varpi v_\varpi = -\dot{M} \tag{6.6}$$

$$\tfrac{1}{2}v_\varpi^2 + \frac{\ell^2}{2\varpi^2} + nv_s^2 + \Phi = E \tag{6.7}$$

where v_s is the sound speed, $\dot{M}$ is the constant mass flux (assumed positive for inflow) and E is proportional to the square of the sound speed at infinity, assuming the flow starts off with zero infall velocity.

Equations (6.6) and (6.7) are essentially the equations for Newtonian spherical accretion (Bondi 1952) modified by the geometry and the presence of the angular momentum term. The latter is a crucial difference, however, as centrifugal forces always dominate Newtonian gravity at small radii and stop the accretion. General relativity is therefore essential here and for simplicity the pseudo-Newtonian potential (1.9) will be adopted.

It is convenient to introduce a relativistic scaling whereby velocities are measured in units of c and lengths in units of R :

$$r \equiv \frac{\varpi}{R_c} \qquad v \equiv \frac{v_\varpi}{c} \qquad a \equiv \frac{v_s}{c} \qquad \lambda \equiv \frac{l}{R_c c} \tag{6.8}$$

Then equations (6.6) and (6.7) may be written

$$r a^{2n} v = -\dot{m} \tag{6.9}$$

$$\tfrac{1}{2}v^2 + \frac{\lambda^2}{2r^2} + n a^2 - \frac{1}{2(r-1)} = \mathcal{E} \tag{6.10}$$

where $\dot{m}$ and $\mathcal{E}$ are non-negative constants.

Equations (6.9) and (6.10) are nonlinear algebraic equations which may be solved numerically for the stationary radial velocity and sound speed as functions of the radius. Apart from one modification they have been derived and their solutions investigated by Abramowicz and Zurek (1981, hereafter AZ) and Lu (1985). The single difference is that these authors had an r^2 in the mass equation instead of an r because they were interested in quasi-radial, conical inflow. Such a three-dimensional flow is, strictly speaking, inconsistent, but nevertheless it may be convenient to study it to gauge the importance of three-dimensional convergence effects. We therefore rewrite equation (6.9) as

$$r^N a^{2n} v = -\dot{m} \tag{6.11}$$

where N=1 for two-dimensional flow and N=2 for conical flow. We now rederive and elaborate on the essential results of the previous authors for the pur-

poses of the current investigation.

As $r \to \infty$ the infall velocity goes to zero while the sound speed is finite, and so the flow is subsonic in the outer regions. On the other hand as one approaches the event horizon the infall velocity blows up[2] and the flow is supersonic. The global flow is therefore transonic and imposition of regularity at the critical sonic point gives the accretion rate as a function of $\mathcal{E}$ and λ.

Differentiating equations (6.10) and (6.11) and solving for the derivatives,

$$\frac{da^2}{dr} = \frac{a^2}{nr(a^2-v^2)}\left[\frac{\lambda^2}{r^2} - \frac{r}{2(r-1)^2} + Nv^2\right] \tag{6.12}$$

$$\frac{dv}{dr} = \frac{-v}{r(a^2-v^2)}\left[\frac{\lambda^2}{r^2} - \frac{r}{2(r-1)^2} + Na^2\right] \tag{6.13}$$

Therefore the flow can only be regular at the sonic point $r=r_s$ if the sound speed there satisfies

$$a_s^2 = \frac{1}{Nr_s^2}\left[\lambda_{Kep}^2(r_s) - \lambda^2\right] \tag{6.14}$$

where λ_{Kep} is the Keplerian specific angular momentum at the sonic point:

$$\lambda_{Kep}^2(r_s) \equiv \frac{r_s^3}{2(r_s-1)^2} \tag{6.15}$$

For a disk overflowing its cusp, equation (6.14) implies that the sonic point will always lie <u>inside</u> the cusp ($\lambda < \lambda_{Kep}$.

Using equation (6.14) to eliminate a^2 at the sonic point,

$$\dot{m} = r_s^N\left[\frac{1}{Nr_s^2}\left(\lambda_{Kep}^2(r_s) - \lambda^2\right)\right]^{n+1/2} \tag{6.16}$$

$$\mathcal{E} = \frac{(n+1/2)r_s}{2N(r_s-1)^2} - \frac{\lambda^2(2n+1-N)}{2Nr_s^2} - \frac{1}{2(r_s-1)} \tag{6.17}$$

---

[2] This is an artifact of the pseudo-Newtonian model, which is <u>not</u> a good model for the inner supersonic flow regime. However Lu (1985) has investigated the problem for both cases and found only small quantitative differences between the location of the critical points and the resulting mass accretion rates in the two cases. As we are only interested in the subsonic part of the flow, we believe the pseudo-Newtonian potential to be adequate.

Given any pair of values for λ and $\mathcal{E}$, equations (6.16) and (6.17) may be solved to find the sonic radius and the accretion rate.

Figure (6.1) shows the location of the sonic point as a function of λ and $\mathcal{E}$ for the case n=3 and N=1. This is very similar to figure 1(a) of AZ, who pointed out the interesting fact that for $\mathcal{E}<\mathcal{E}_{crit}=0.09$ the sonic radius is apparently not unique. However, Lu (1985) has shown that it is in fact unique apart from discrete values of λ and $\mathcal{E}$ where it can jump. His result was obtained in an elegant manner by examining the global topology of the solutions with multiple critical points. It may also be quickly seen using an analysis similar to that of Novikov and Thorne's (1973)[3] treatment of Bondi accretion.

In the (v,a) plane, equations (6.10) and (6.11) define an ellipse and a hyperbola, respectively, for every value of r, as illustrated in figure (6-2). As the radius changes, these two curves may intersect in zero, one or two points. If for any pair of values of λ and $\mathcal{E}$ there exists a radius where the curves do not intersect, then no physical solution is possible for this pair. Differentiating equations (6.10) and (6.11) with respect to a at fixed radius implies that the curves intersect at only one point, and are therefore tangent, if and only if that point is a sonic point. If the curves intersect in two points, one always represents a supersonic solution and the other a subsonic solution.

The values of a at points where the hyperbola and ellipse cross the line $v^2=a^2$ are

$$a_c = \left(\frac{\dot{m}}{r^N}\right)^{1/(2n+1)} \tag{6.18}$$

$$a_b = \left[\frac{1}{(n+1/2)}\left(\mathcal{E} + \frac{1}{2(r-1)} - \frac{\lambda^2}{2r^2}\right)\right]^{1/2} \tag{6.19}$$

respectively. A necessary and sufficient condition for a solution to be physical is $a_c \leq a_b$ everywhere, i.e.

---

[3] I thank Roberto Turolla for bringing this treatment to my attention.

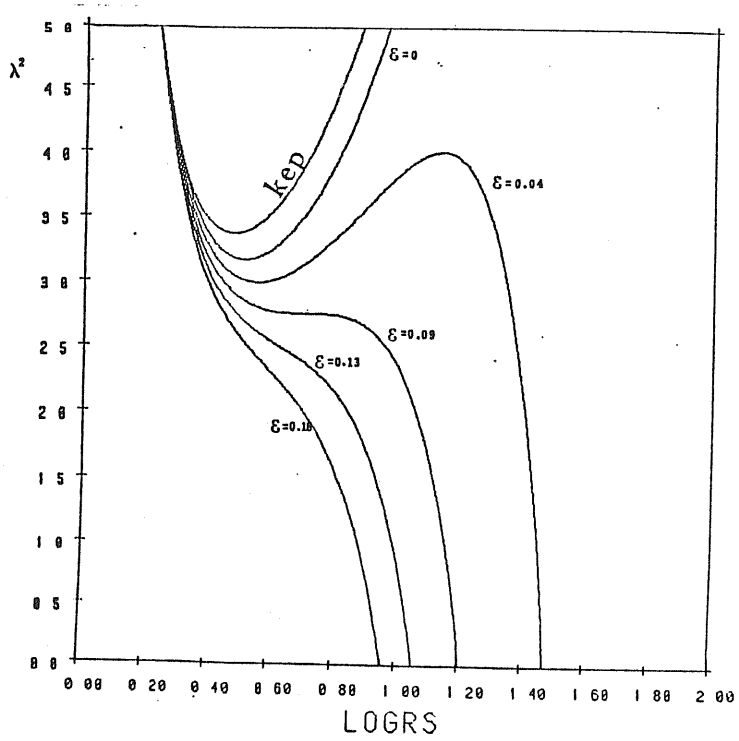

Figure 6-1. The location of the critical sonic point as a function of λ and $\mathcal{E}$ for a two dimensional flow with polytropic index n=3. The region above the top $\lambda^2 = \lambda^2_{kep}(r_s)$ curve is unphysical for accreting flows as the sound speed becomes negative by equation (6.14).

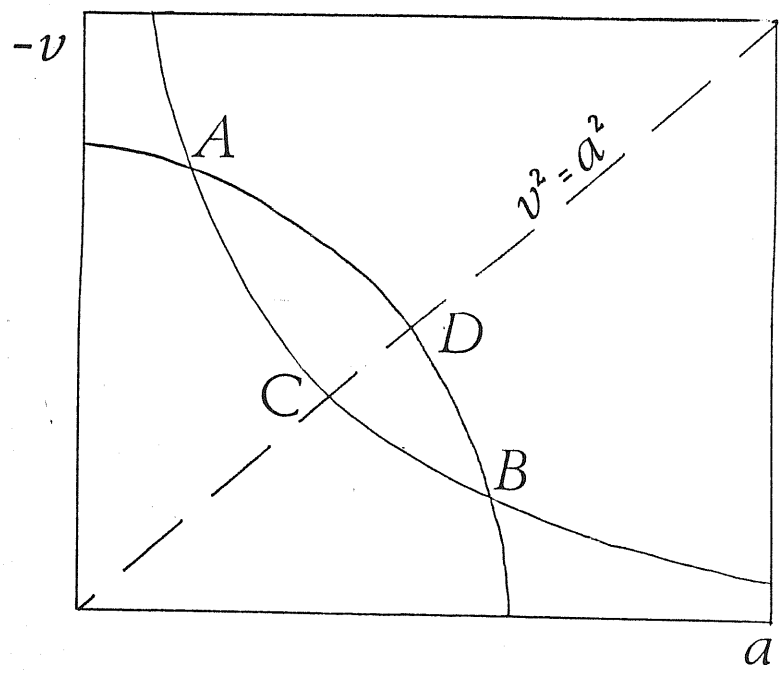

Figure 6-2. The curves defined by equations (6.10) and (6.11) in the (v,a) plane. The points of intersection give the actual solutions - A is supersonic and B is subsonic.

$$\lambda^2 \leq 2r^2\left[\mathcal{E} + \frac{1}{2(r-1)} - (n+\tfrac{1}{2})\left(\frac{\mathcal{M}}{r^N}\right)^{2/(2n+1)}\right] \quad \forall r \qquad (6.20)$$

Equality occurs at sonic points, and hence a given model will start to become unphysical if it admits more than one sonic point for the same values of λ^2, $\mathcal{M}$ and $\mathcal{E}$. Figure 6-3 is a replot of figure 6-1 with condition (6.20) added.

Consider starting from the lower right hand corner and increase λ^2 while keeping $\mathcal{E}$ fixed. The sonic point slowly moves inwards until the consistency curve is reached. At this point the solution <u>just</u> satisfies equation (6.20), and there is another sonic point at an inner radius for the same values of $\mathcal{E}$ and λ^2. If λ^2 increases still further the sonic point must jump inwards.

This interesting behaviour is not actually relevant for the current investigation. More important is the consistency curve itself which separates the parameter space into physical and unphysical regions. Also important are the intersections of the $\mathcal{E}$ = constant curves with the Keplerian curve. At these points equation (6.14) implies that the sound speed must be zero, and hence v must be zero everywhere. The Keplerian curve therefore represents a disk in pure azimuthal flow. The "sonic" point in this case is simply the inner, zero pressure edge of the flow. This edge is a cusp precisely because $\lambda = \lambda_{kep}$ there.

Positive values of $\mathcal{E}$ on the Keplerian curve imply that the disk has nonzero sound speed at infinity and must therefore have external pressure support. This corresponds to a $\beta = \beta_{cusp} > \beta_{max}$ configuration in the notation of the previous chapter. Negative values of $\mathcal{E}$ imply negative values of the sound speed squared at infinity, that is the disk does not in fact extend to infinity but has a zero pressure boundary at a finite radius. These are the $\beta = \beta_{cusp} < \beta_{max}$ models of the previous chapter and they cannot smoothly transform into accreting models unless matter is supplied at the outer radius.

The intersection of the $\mathcal{E}$ =0 curve with the Keplerian curve is the crucial point for this investigation. It represents an annulus with an outer, zero pressure boundary at infinity and an inner cusped edge at $r_s = 2$ (or $\varpi = 2R_s$), i.e. the marginally bound orbit. This is the $\beta = \beta_{max} = \beta_{cusp}$ configuration of

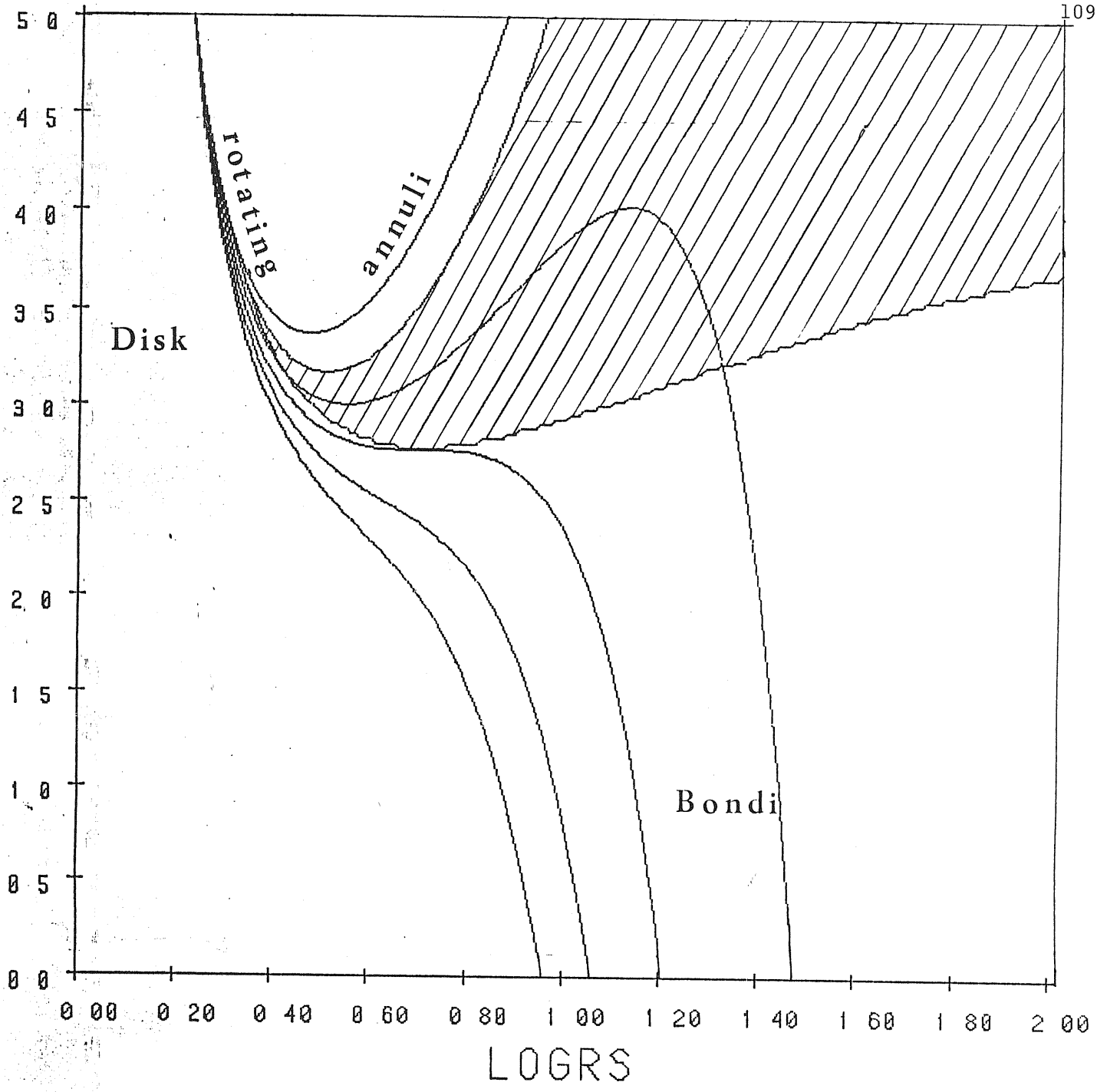

Figure 6-3. Only the unshaded portion of the diagram contains physical solutions. The upper left hand area where the angular momentum is high and the sonic point is close to the hole is termed the "disk-like" accretion region. The lower portion of the diagram, where the angular momentum is small represents "Bondi-like" accretion. The $\ell = \ell_{Kep}$ non-accreting annuli of the previous chapter all lie on the Keplerian curve. For clarity, the region above the $\mathcal{E}$ =0 curve has been left unshaded.

the previous chapter, and it is through this model that one may investigate the effects of accretion in a continuous manner on the Papaloizou and Pringle instability.

VI.2 The Perturbation Equations

Almost all the general stability theory for rotating flows reviewed in chapter III is inapplicable for accretion. Moncrief (1980) has however written a classic paper on the stability of accreting potential flows (in both general relativity and Newtonian theory) and one may use some of his results for the problem here.

Because the stationary flow is potential, Kelvin's circulation theorem implies that if the initial perturbations in vorticity and specific entropy are zero, then the perturbed flow will also be potential. Moreover, Moncrief showed that even if one started with nonzero entropy and vorticity perturbations over a region of finite extent, then these perturbations would simply be advected into the hole and the flow would thereafter be potential. The Newtonian version of this result follows immediately from the entropy and vorticity equations written in the following covariant form

$$\left(\frac{\partial}{\partial t} + \pounds_{\underline{v}}\right) s = 0 \tag{6.21}$$

$$\left(\frac{\partial}{\partial t} + \pounds_{\underline{v}}\right) \omega_{ij} = \frac{1}{\rho^2}\left(\frac{\partial p}{\partial s}\right)_\rho \left(\nabla_j \rho \nabla_i s - \nabla_i \rho \nabla_j s\right) \tag{6.22}$$

where

$$\omega_{ij} \equiv \nabla_j v_i - \nabla_i v_j \tag{6.23}$$

is the vorticity tensor and $\pounds_{\underline{v}}$ is the Lie derivative along the stationary flow lines. Because the stationary state is potential, the perturbed forms of these equations are

$$\left(\frac{\partial}{\partial t} + \pounds_{\underline{v}}\right) \delta s = 0 \tag{6.24}$$

$$\left(\frac{\partial}{\partial t} + \pounds_{\underline{v}}\right) \delta\omega_{ij} = \frac{1}{\rho^2}\left(\frac{\partial p}{\partial s}\right)_\rho \left[\nabla_j \rho \nabla_i \delta s - \nabla_i \rho \nabla_j \delta s\right] \tag{6.25}$$

Equation (6.24) implies that the entropy perturbations will simply be advected

with the stationary flow velocity into the hole. Hence if they were initially nonzero over a finite volume, they will simply disappear after a finite period of time. Equation (6.25) then implies that the vorticity perturbations would do the same.

One may still question whether this is good enough, as it says nothing about the case where δs and $\delta\omega_i$ are nonzero throughout the flow, nor even what would happen if an instability was somehow started and the flow went into the nonlinear regime before it could return to being potential. However, it is good enough for the present purpose which is to investigate the effects of accretion on the Papaloizou and Pringle instability. For a $\nabla\eta = \nabla s = 0$ torus, this instability is caused solely by potential perturbations.

The only two equations of relevance then are the time-dependent Bernoulli equation and the continuity equation. Following the scaling of the previous section, they may be written

$$\frac{\partial\psi}{\partial t} + \frac{1}{2}\left(\frac{\partial\psi}{\partial r}\right)^2 + \frac{1}{2r^2}\left(\frac{\partial\psi}{\partial\phi}\right)^2 + na^2 - \frac{1}{2(r-1)} = 0 \qquad (6.26)$$

$$\frac{\partial a^{2n}}{\partial t} + \frac{1}{r^N}\frac{\partial}{\partial r}\left(r^N a^{2n}\frac{\partial\psi}{\partial r}\right) + \frac{1}{r^2}\frac{\partial}{\partial\phi}\left(a^{2n}\frac{\partial\psi}{\partial\phi}\right) = 0 \qquad (6.27)$$

where ψ is the velocity potential. In the continuity equation the density has been replaced with the sound speed using the polytropic equation (6.5). In addition, the dimensional index N has been added to include the cases of conical (N=2) and Cylindrical (N=1) flows. Finally the standard procedure of using the gauge freedom of ψ to absorb the Bernoulli constant has been adopted (see e.g. Landau and Lifshitz 1959).

Linearizing these equations about the stationary state,

$$\frac{\partial\delta\psi}{\partial t} + v\frac{\partial\delta\psi}{\partial r} + \frac{\lambda}{r^2}\frac{\partial\delta\psi}{\partial\phi} + n\delta a^2 = 0 \qquad (6.28)$$

$$n\frac{\partial\delta a^2}{\partial t} + \frac{Nv}{r}\delta a^2 + \frac{Na^2}{r}\frac{\partial\delta\psi}{\partial r} + nv\frac{\partial\delta a^2}{\partial r} + n\frac{da^2}{dr}\frac{\partial\delta\psi}{\partial r} + \delta a^2\frac{dv}{dr} + a^2\frac{\partial^2\delta\psi}{\partial r^2} + \frac{n\lambda}{r^2}\frac{\partial\delta a^2}{\partial\phi} + \frac{a^2}{r^2}\frac{\partial^2\delta\psi}{\partial\phi^2} = 0 \qquad (6.29)$$

Eliminating δa^2, one obtains a single perturbation equation for $\delta\psi$,

$$-\left(\frac{\partial}{\partial t}+v\frac{\partial}{\partial r}+\frac{\lambda}{r^2}\frac{\partial}{\partial\phi}\right)^2\delta\psi-\frac{1}{n}\left(\frac{Nv}{r}+\frac{dv}{dr}\right)\left(\frac{\partial}{\partial t}+v\frac{\partial}{\partial r}+\frac{\lambda}{r^2}\frac{\partial}{\partial\phi}\right)\delta\psi$$
$$+a^2\left(\frac{N}{r}\frac{\partial\delta\psi}{\partial r}+\frac{\partial^2\delta\psi}{\partial r^2}\right)+n\frac{da^2}{dr}\frac{\partial\delta\psi}{\partial r}+\frac{a^2}{r^2}\frac{\partial^2\delta\psi}{\partial\phi^2}=0. \qquad (6.30)$$

In the non-accreting case v=0 this reduces to the perturbation equation for the $\nabla\ell=\nabla s=0$ annulus.

VI.3 Remarks

Moncrief showed that spherical accretion with no angular momentum is absolutely stable outside the sonic point, and this proof can be trivially extended to the $\lambda=0$, purely radial conical or cylindrical flow. It is also known, of course, that purely rotating $\nabla\ell=0$ annuli are marginally stable to axisymmetric perturbations by the Høiland criterion. Accreting flows may therefore be stable to axisymmetric perturbations and for completeness this hypothesis should be checked before going on to the non-axisymmetric case. In fact for the two-dimensional flows considered here it is possible to extend Moncrief's proof for this purpose, and this is done in Appendix D.

An attempt has been made to extend this result to three dimensional flows but without success. The reason is that Moncrief's stability proof fails when one allows equilibrium and perturbed velocity fields which are tangent to the sound horizon. The two-dimensional approach of this section may therefore be throwing away some important dynamics of three-dimensional accreting flows, but again for the purposes of studying Papaloizou and Pringle's instability it should be adequate.

Returning to nonaxisymmetric modes we Fourier analyze the perturbations in the usual way to obtain

$$-\left(\frac{\partial}{\partial t}+v\frac{\partial}{\partial r}+\frac{im\lambda}{r^2}\right)^2\delta\psi-\frac{1}{n}\left(\frac{Nv}{r}+\frac{dv}{dr}\right)\left(\frac{\partial}{\partial t}+v\frac{\partial}{\partial r}+\frac{im\lambda}{r^2}\right)\delta\psi$$
$$+a^2\left(\frac{N}{r}\frac{\partial\delta\psi}{\partial r}+\frac{\partial^2\delta\psi}{\partial r^2}\right)+n\frac{da^2}{dr}\frac{\partial\delta\psi}{\partial r}-\frac{m^2a^2}{r^2}\delta\psi=0. \qquad (6.31)$$

If we also restrict consideration to normal modes this equation becomes

$$a^2(a^2-v^2)\frac{d^2\delta\psi}{dr^2} + \left[-2i\bar{\nu}va^2 + \frac{Na^4}{r} - a^2v\frac{dv}{dr} + na^2\frac{da^2}{dr} + v^2\frac{da^2}{dr}\right]\frac{d\delta\psi}{dr} + \left[a^2\bar{\nu}^2 + i\bar{\nu}v\frac{da^2}{dr} + \frac{2imva^2}{r^3} - \frac{m^2a^4}{r^2}\right]\delta\psi = 0 \tag{6.32}$$

where $\bar{\nu}$ is the eigenfrequency scaled with R_ϵ/c and

$$\bar{\nu} \equiv \nu + \frac{m\lambda}{r^2} \quad . \tag{6.33}$$

In deriving equation (6.32) use has been made of the equilibrium continuity equation (6.9).

Though perfectly conventional, this last step is possibly dangerous as there is no completeness theorem for the normal modes of an accreting flow such as there was for a rotating flow (cf equation 3.22). It is hoped that a normal mode treatment is nevertheless sufficient for the present analysis, though it may turn out to be useful to solve the full time-dependent equations.

Equation (6.32) has a regular singular point at the sonic radius and an irregular singular point at infinity. Adopting a regularity condition at the sonic point and a radiating boundary condition at infinity completely defines the eigenvalue problem. This is now in the process of being solved numerically, and it is hoped that interesting results will be forthcoming shortly.

VII. CONCLUSIONS

Thick accretion disks offered a very attractive model for the central engines of active galactic nuclei and many theorists have been reluctant to see them die. This explains most of the current interest in understanding Papaloizou and Pringle's instability. Those who still hold thick disks close to their hearts, and those who strongly oppose them, should bear in mind the following points and unsolved questions:

(1) No compressible model yet studied (apart, perhaps, from Glatzel's infinite annuli with small but nonzero specific angular momentum gradients) has been proven to be absolutely stable. This holds for a wide variety of tori with or without gradients of specific entropy and specific angular momentum. However, there are indications (Frank, private communication) that infinitely thick tori may be absolutely stable.[1]

(2) Absolute stability isn't of course required for tori to be self-consistent. A torus would be effectively stable if the growth time was as large or larger than other timescales expected to be important, in particular the viscous timescale (this means that the general conclusions of PPI and II concerning the existence of instabilities but without knowing their growth times are of small practical interest). If one believes the phenomenological limits on α, however, the viscous timescale is atleast $10^3 - 10^4$ times the dynamical timescale in radiation tori so that for all practical purposes absolute stability is required. This is not true for ion tori, which can suffer, indeed require, high viscosities.

(3) Viscosity will be more important for some modes than others. In particular the very high m modes which PPI and II argue to be so generic and which are probably difficult to find and treat numerically may be subject to high damping and therefore be of little practical importance.

(4) The nonlinear calculations of Zurek and Benz indicate that the "surface-interaction" mode really produces global, violent changes in the

---

[1] cf Hacyan's (1982) original result in equation (2.1). There may yet be a vindication of this early work!

torus. Other modes, however, act slowly and indeed on the timescale of the code's own inherent molecular viscosity. Could it be that these other modes do not produce violent changes but simply turbulence, and if so, is the effective viscosity thereby produced high enough to rule out radiation tori?

(5) The fact that the use of a pseudo-Newtonian potential does not change anything substantial means that full general relativity is very unlikely to produce any qualitative difference except perhaps in extreme and uninteresting circumstances (is a slender torus rotating in the ergosphere of a maximal Kerr black hole stable?).

(6) All of the investigations have been limited to perfect fluid tori because the major portion of a thick disk as conceived in current theory is supposed to be in almost pure azimuthal flow. However, stationary thick disks have a transonic stream at their inner edges whose dynamical consequences for the global stability of the disk are still unknown, but can and are being investigated using the simplified treatment of chapter VI. Another question one might ask is whether thick disks could have global meridional circulation flows and what effect these could have on the instability. More conventionally, could an outflowing jet have any influence? These latter two questions, put to me respectively by Antonuccio and Rees (private communications) are probably too difficult to address at the present time.

The most favourable stand one could take (from the point of view of wanting thick disks) is that most of the calculations have been done for rather slender configurations and really thick, practically constant specific angular momentum configurations may still be stable for timescales approaching the viscous timescale, thus permitting narrow funnels with which to collimate jets. Accretion through the cusp is likely to aid stability even further. As the torus evolves in the manner described in section I.4, it shrinks and dynamical instabilities could then become important, either by producing violent structural changes or by increasing α via turbulence. Both cases could be extremely interesting from the point of view of short time variability in quasars.

Although one might entertain these speculations, I would be reluctant to make such assertions on the basis of our present knowledge. However, it is not yet clear that thick disks are ruled out, and more work along the lines suggested must be done to answer this most fundamental question.

APPENDIX A. GENERAL LIMITS ON THE EIGENFREQUENCY FOR A $\nabla\!\!\!/ = \nabla\!\!\!/_{s=0}$ TORUS

The perturbation equation for this case is equation (4.18):

$$\frac{1}{\varpi}\frac{\partial}{\partial\varpi}\left(\varpi\rho\frac{\partial W}{\partial\varpi}\right)+\frac{\partial}{\partial z}\left(\rho\frac{\partial W}{\partial z}\right)-\frac{m^2\rho W}{\varpi^2}+\frac{\bar{\sigma}^2\rho^2 W}{\gamma p}=0 \tag{A.1}$$

and, for compressible tori, the boundary condition (4.19) may be replaced with the constraint that W be regular. Multiplying equation (A.1) by W* and integrating over the torus cross-section,

$$\int\rho\left[\left|\frac{\partial W}{\partial\varpi}\right|^2+\left|\frac{\partial W}{\partial z}\right|^2+\frac{m^2}{\varpi^2}|W|^2\right]\varpi\,d\varpi\,dz=\int|W|^2\frac{\bar{\sigma}^2\rho^2}{\gamma p}\varpi\,d\varpi\,dz \tag{A.2}$$

where the first two terms arise from integration by parts.

The imaginary part of this equation is

$$2\,\mathrm{Im}(\sigma)\int\frac{|W|^2(\mathrm{Re}(\sigma)+m\Omega)\rho^2}{\gamma p}\varpi\,d\varpi\,dz=0 \tag{A.3}$$

so that if $\mathrm{Im}(\sigma)\neq 0$, the perturbation must corotate with the flow somewhere. This equation implies

$$\int\frac{|W|^2 2(\mathrm{Re}(\sigma))m\Omega\rho^2}{\gamma p}\varpi\,d\varpi\,dz=-2\int\frac{|W|^2(\mathrm{Re}(\sigma))^2\rho^2}{\gamma p}\varpi\,d\varpi\,dz \tag{A.4}$$

The real part of equation (A.2) is

$$\int\rho\left[\left|\frac{\partial W}{\partial\varpi}\right|^2+\left|\frac{\partial W}{\partial z}\right|^2+\frac{m^2}{\varpi^2}|W|^2\right]\varpi\,d\varpi\,dz=\int\frac{\rho^2|W|^2}{\gamma p}\left[m^2\Omega^2+\mathrm{Re}(\sigma)^2+2m\Omega\,\mathrm{Re}(\sigma)-\mathrm{Im}(\sigma)^2\right]\varpi\,d\varpi\,dz \tag{A.5}$$

or, using equation (A.4),

$$\int \rho \left[\left| \frac{\partial W}{\partial \omega} \right|^2 + \left| \frac{\partial W}{\partial \theta} \right|^2 + \frac{m^2 |W|^2}{\omega^2} \right] \omega \, d\omega \, d\theta \, dz$$

$$= \int \frac{\rho^2 |W|^2}{\gamma p} \left[m^2 \Omega^2 - (\mathrm{Re}(\sigma))^2 - (\mathrm{Im}(\sigma))^2 \right] \omega \, d\omega \, d\theta \, dz \qquad \text{(A.6)}$$

Therefore because the left hand side is postitive,

$$|\sigma|^2 \leq \frac{m^2 \int \frac{\rho^2 \Omega^2}{\gamma p} |W|^2 \omega \, d\omega \, d\theta \, dz}{\int \frac{\rho^2 |W|^2}{\gamma p} \omega \, d\omega \, d\theta \, dz} \qquad \text{(A.7)}$$

and so the mean value theorem implies

$$|\sigma|^2 \leq m^2 \Omega_{max}^2 \qquad \text{(A.8)}$$

APPENDIX B. THE INCOMPRESSIBLE $\Omega\ell = \Omega_s = 0$ SLENDER TORUS

It is straightforward to modify the analysis of sections IV.2 and IV.3 to treat the incompressible n=0 torus. In this case the perturbation equations (4.18) and (4.19) become

$$\nabla^2 W = 0 \tag{B.1}$$

and

$$\bar{\sigma}^2 W + \underline{g}_{\text{eff}} \cdot \underline{\nabla} W = 0 \tag{B.2}$$

which, as noted in chapter V, are the equations for surface gravity waves on the torus.

We restrict consideration to the Newtonian case. The slender torus limit of these equations is then

$$\left[\eta^2 \frac{\partial^2 W^{(0)}}{\partial \eta^2} + \frac{\partial^2 W^{(0)}}{\partial \theta^2} + \eta \frac{\partial W^{(0)}}{\partial \eta}\right] = 0 \tag{B.3}$$

$$\left[(\nu^{(2)} + m)^2 W^{(0)} - \eta \frac{\partial W^{(0)}}{\partial \eta}\right]_{\eta=1} = 0 \tag{B.4}$$

The general solution of (B.3) which is regular at $\eta = 0$ and periodic in θ is

$$W^{(0)} = \eta^k \begin{cases} \cos k\theta \\ \sin k\theta \end{cases} \tag{B.5}$$

where k is a non-negative integer. The boundary condition (B.4) then implies

$$(\nu^{(2)} + m)^2 = k \tag{B.6}$$

As expected, these are the Kelvin or f-modes of the compressible slender torus. Note that for high k these modes represent short wavelength oscillations propagating near the surface $\eta = 1$, confirming their physical status as surface gravity waves.

The fundamental k=0 corotating mode is still present and it gives rise to the instability as the torus thickens. The first order equations for

this mode are

$$\eta^2 \frac{\partial^2 W^{(1)}}{\partial \eta^2} + \frac{\partial^2 W^{(1)}}{\partial \theta^2} + \eta \frac{\partial W^{(1)}}{\partial \eta} = 0 \tag{B.7}$$

$$\left. \frac{\partial W^{(1)}}{\partial \eta} \right|_{\eta=1} = 0 \tag{B.8}$$

implying that $W^{(1)}$ is a constant and so the corotating eigenfunction is unchanged to first order.

The second order equations are

$$\eta^2 \frac{\partial^2 W^{(2)}}{\partial \eta^2} + \frac{\partial^2 W^{(2)}}{\partial \theta^2} + \eta \frac{\partial W^{(2)}}{\partial \eta} - m^2 \eta^2 W^{(0)} = 0 \tag{B.9}$$

$$\left[\bar{v}^{(1)2} W^{(0)} - \eta \frac{\partial W^{(2)}}{\partial \eta} \right]_{\eta=1} = 0 \tag{B.10}$$

It is straightforward to verify by direct substitution that the $n \rightarrow 0$ limit of equations (4.49) and (4.50) are the solutions to equations (B.9) and (B.10).

APPENDIX C. THE EIGENVALUE CONDITION FOR THE SLENDER $\nabla\ell = \nabla s=0$ CUSPED TORUS

The perturbation equation (4.18) and the boundary condition (4.19) may be written in $(\tilde{a},\tilde{b})$ coordinates as (see section V.4 for notation)

$$\frac{f}{(1-r_{cusp})^2}\frac{\partial^2 W}{\partial \tilde{a}^2} - \frac{1}{(1-r_{cusp})}\left[\frac{f}{(1-\tilde{a}-\tilde{a}r_{cusp})} - \frac{n}{1-r_{cusp}}\frac{\partial f}{\partial \tilde{a}}\right]\frac{\partial W}{\partial \tilde{a}}$$
$$+ \frac{f}{h_0^2}\frac{\partial^2 W}{\partial \tilde{b}^2} + \frac{n}{h_0^2}\frac{\partial f}{\partial \tilde{b}}\frac{\partial W}{\partial \tilde{b}} + \left[\frac{2n\bar{\nu}^2}{\beta_{cusp}^2(1-R_0)^2} - \frac{m^2 f}{(1-\tilde{a}-\tilde{a}r_{cusp})^2}\right]W = 0 \quad (C.1)$$

$$\left[\frac{2f^n\bar{\nu}^2}{\beta_{cusp}^2(1-R_0)^2}W + f^n\left(\frac{1}{(1-r_{cusp})^2}\frac{\partial W}{\partial \tilde{a}}\frac{\partial f}{\partial \tilde{a}} + \frac{1}{h_0^2}\frac{\partial W}{\partial \tilde{b}}\frac{\partial f}{\partial \tilde{b}}\right)\right]_{f=0} = 0 \quad (C.2)$$

To zeroth order in ε,

$$(1-\tilde{b}^2-3\tilde{a}^2+2\tilde{a}^3)\frac{\partial^2 W^{(0)}}{\partial \tilde{b}^2} - 2n\tilde{b}\frac{\partial W^{(0)}}{\partial \tilde{b}} + 2n\bar{\nu}^{(0)2}W^{(0)} = 0 \quad (C.3)$$

$$\left[2f^{(0)n}\bar{\nu}^{(0)2}W^{(0)} + f^{(0)n}\frac{\partial W^{(0)}}{\partial \tilde{b}}\frac{\partial f^{(0)}}{\partial \tilde{b}}\right]_{f^{(0)}=0} = 0 \quad (C.4)$$

Changing the independent variable to

$$u \equiv \frac{\tilde{b}}{(1-3\tilde{a}^2+2\tilde{a}^3)^{1/2}} \quad (C.5)$$

equation (C.3) becomes Gegenbauer's equation:

$$(1-u^2)\frac{\partial^2 W^{(0)}}{\partial u^2} - 2nu\frac{\partial W^{(0)}}{\partial u} + 2n\bar{\nu}^{(0)2}W^{(0)} = 0 \quad (C.6)$$

The boundary condition (C.4) as usual rules out any singular solutions so that $W^{(0)}$ is given by Gegenbauer polynomials

$$W^{(0)}(\tilde{a},\tilde{b}) = g_k(\tilde{a})\,C_k^{n-1/2}(u) \quad (C.7)$$

$$\bar{\nu}^{(0)2} = \frac{k}{2n}(k+2n-1) \quad (C.8)$$

where g_k is an undetermined function of $\tilde{a}$ and k is a non-negative integer.

In particular the zeroth order corotating solution is

$$W^{(0)} = g_0(\tilde{a}) \tag{C.9}$$

For this mode the first order equation is

$$\frac{f^{(0)}}{36}\frac{d^2 g_0}{d\tilde{a}^2} + \frac{n}{36}\frac{dg_0}{d\tilde{a}}\frac{\partial f^{(0)}}{\partial \tilde{a}} + \frac{f^{(0)}}{54}\frac{\partial^2 W^{(1)}}{\partial \tilde{b}^2} + \frac{n}{54}\frac{\partial f^{(0)}}{\partial \tilde{b}}\frac{\partial W^{(1)}}{\partial \tilde{b}} = 0 \tag{C.10}$$

$W^{(1)}$ may be eliminated from this equation by expanding it in the complete set of Gegenbauer polynomials

$$W^{(1)} = \sum_{k=0}^{\infty} q_k(\tilde{a}) C_k^{n-1/2}(u) \tag{C.11}$$

and integrating the equation over $\tilde{b}$ for fixed $\tilde{a}$ (similar to the treatment of section 4.4). Then

$$\frac{d}{d\tilde{a}}\left[(1-3\tilde{a}^2+2\tilde{a}^3)^{n+1/2}\frac{dg_0}{d\tilde{a}}\right] = 0 \tag{C.12}$$

The two linearly independent solutions to this equation are

$$g_0 = \text{constant}$$

$$g_0 = \int \left[1-3\tilde{a}^2+2\tilde{a}^3\right]^{-n+1/2} d\tilde{a} \tag{C.13}$$

The second solution is singular and must be rejected as it violates the boundary condition at $a=-\frac{1}{2}$. Equations (C.10) and (C.11) then together imply $q_k = 0$ for all nonzero k, and so $W^{(1)}$ is an arbitrary function of $\tilde{a}$:

$$W^{(1)} = g_0(\tilde{a}) \tag{C.14}$$

The second order equation for this mode is

$$\frac{f^{(0)}}{36}\frac{d^2 g_0}{d\tilde{a}^2} + \frac{n}{36}\frac{dg_0}{d\tilde{a}}\frac{\partial f^{(0)}}{\partial \tilde{a}} + \frac{1}{54}\left[f^{(0)}\frac{\partial^2 W^{(2)}}{\partial \tilde{b}^2} + n\frac{\partial f^{(0)}}{\partial \tilde{b}}\frac{\partial W^{(2)}}{\partial \tilde{b}}\right] + W^{(0)}\left[\frac{n(\gamma''+12m\tilde{a})^2}{24}\right] = 0 \tag{C.15}$$

Expanding $W^{(2)}$ in Gegenbauer polynomials and integrating as before,

$$\frac{d}{d\tilde{a}}\left[(1-3\tilde{a}^2+2\tilde{a}^3)^{n+\frac{1}{2}}\frac{dq_0}{d\tilde{a}}\right] + \frac{4W^{n}(n+\frac{1}{2})}{3}(v''+12m\tilde{a})^2(1-3\tilde{a}^2+2\tilde{a}^3)^{n-\frac{1}{2}} = 0 \quad \text{(C.16)}$$

On integrating this equation over $\tilde{a}$, the first term vanishes due to the boundary condition

$$\left[(1-3\tilde{a}^2+2\tilde{a}^3)^{n-\frac{1}{2}}(1+2\tilde{a})^{\frac{1}{2}}\frac{dq_0}{d\tilde{a}}\right]_{\tilde{a}=-\frac{1}{2},1} \quad \text{(C.17)}$$

and hence v'' may be determined from

$$\int_{-\frac{1}{2}}^{1}(1-\tilde{a})^{2n-1}(1+2\tilde{a})^{n-\frac{1}{2}}(v''+12m\tilde{a})^2 d\tilde{a} = 0 \quad \text{(C.18)}$$

APPENDIX D. AXISYMMETRIC STABILITY OF 2D ACCRETING FLOWS

Moncrief (1980) pointed out that equation (6.30) may be derived by extremizing the functional

$$\mathcal{I} = \frac{1}{2}\int dr\,dt\,d\phi\, r^{N}\left\{(a^2)^{n-1}\left(\delta\varphi_{,t} + v\,\delta\varphi_{,r} + \frac{\lambda}{r^2}\delta\varphi_{,\phi}\right)^2 - a^{2n}\delta\varphi_{,r}^2 - \frac{a^{2n}}{r^2}\delta\varphi_{,\phi}^2\right\} \tag{D.1}$$

where, for the sake of brevity, the comma notation for derivatives (e.g. $\delta\varphi_{,t} \equiv \frac{\partial\,\delta\varphi}{\partial t}$) has been adopted. The Lagrangian density for this functional is

$$\mathcal{L} = \frac{1}{2}r^{N}\left\{(a^2)^{n-1}\left(\delta\varphi_{,t} + v\,\delta\varphi_{,r} + \frac{\lambda}{r^2}\delta\varphi_{,\phi}\right)^2 - a^{2n}\delta\varphi_{,r}^2 - \frac{a^{2n}}{r^2}\delta\varphi_{,\phi}^2\right\} \tag{D.2}$$

Because the stationary flow is time independent and axisymmetric $\mathcal{L}$ has no explicit dependence on ϕ or t, and so there exist two conservation laws:

$$\frac{\partial}{\partial t}\left(\frac{\partial\mathcal{L}}{\partial\,\delta\varphi_{,t}}\delta\varphi_{,t} - \mathcal{L}\right) + \frac{\partial}{\partial r}\left(\frac{\partial\mathcal{L}}{\partial\,\delta\varphi_{,r}}\delta\varphi_{,t}\right) + \frac{\partial}{\partial\varphi}\left(\frac{\partial\mathcal{L}}{\partial\,\delta\varphi_{,\phi}}\delta\varphi_{,t}\right) = 0 \tag{D.3}$$

$$\frac{\partial}{\partial t}\left(\frac{\partial\mathcal{L}}{\partial\,\delta\varphi_{,t}}\delta\varphi_{,\phi}\right) + \frac{\partial}{\partial r}\left(\frac{\partial\mathcal{L}}{\partial\,\delta\varphi_{,r}}\delta\varphi_{,\phi}\right) + \frac{\partial}{\partial\varphi}\left(\frac{\partial\mathcal{L}}{\partial\,\delta\varphi_{,\phi}}\delta\varphi_{,\phi} - \mathcal{L}\right) = 0 \tag{D.4}$$

Not surprisingly, these equations correspond to conservation laws of energy and angular momentum. The energy and angular momentum density are

$$\mathcal{E} = \frac{1}{2}(a^2)^{n-1}\delta\varphi_{,t}^2 - \frac{1}{2}(a^2)^{n-1}\left(v\,\delta\varphi_{,r} + \frac{\lambda}{r^2}\delta\varphi_{,\phi}\right)^2 + \frac{1}{2}a^{2n}\delta\varphi_{,r}^2 + \frac{1}{2}\frac{a^{2n}}{r^2}\delta\varphi_{,\phi}^2 \tag{D.5}$$

$$\mathcal{J} = (a^2)^{n-1}\delta\varphi_{,\phi}\left(\delta\varphi_{,t} + v\,\delta\varphi_{,r} + \frac{\lambda}{r^2}\delta\varphi_{,\phi}\right) \tag{D.6}$$

and the total perturbation energy and angular momentum outside the sonic point are

$$E = \int_0^{2\pi}\int_{r_s}^{\infty}\mathcal{E}\,r^{N}\,dr\,d\phi \tag{D.7}$$

$$J = \int_0^{2\pi}\int_{r_s}^{\infty} j\, r^N\, dr\, d\phi \tag{D.8}$$

On integrating the conservation equations (D.3) and (D.4) over the entire volume outside the sonic point, one obtains the rate of change of these quantities with time,

$$\frac{dE}{dt} = \int_0^{2\pi} d\phi \left[r^N (a^2)^{n-1} v\, \delta\rho_{,t} \left(\delta\rho_{,t} + v\,\delta\rho_{,r} + \frac{\lambda}{r^2}\delta\rho_{,\phi} \right) - r^N a^{2n}\, \delta\rho_{,t}\, \delta\rho_{,r} \right]\Bigg|_{r_s}^{\infty} \tag{D.9}$$

$$\frac{dJ}{dt} = \int_0^{2\pi} d\phi \left[r^N (a^2)^{n-1} v\, \delta\rho_{,\phi} \left(\delta\rho_{,t} + v\,\delta\rho_{,r} + \frac{\lambda}{r^2}\delta\rho_{,\phi} \right) - r^N a^{2n}\, \delta\rho_{,t}\, \delta\rho_{,r} \right]\Bigg|_{r_s}^{\infty} \tag{D.10}$$

For axisymmetric perturbations, all the derivatives of $\delta\rho$ must be independent of ϕ, implying that $\delta\rho$ must be of the form

$$\delta\rho(t, r, \phi) = \delta\rho_1(t, r) + C\phi \tag{D.11}$$

where C is a constant. Nonzero C means a perturbation in the specific angular momentum which is <u>everywhere</u> constant. We view this as an unphysical perturbation, as it does not decay to zero at infinity. Moreover, equations (D.5) and (D.7) imply that the perturbation energy would blow up if $C \neq 0$. By "axisymmetric" we therefore restrict consideration to $\delta\rho = 0$. Then equations (D.5), (D.7) and (D.9) imply

$$E = \frac{1}{2}\int_0^{2\pi}\int_{r_s}^{\infty} r^N \frac{1}{2}(a^2)^{n-1} \left\{ \delta\rho_{,t}^2 + (a^2 - v^2)\,\delta\rho_{,r}^2 \right\} dr\, d\phi \tag{D.12}$$

and

$$\frac{dE}{dt} = \int_0^{2\pi} d\phi \left\{ r^N (a^2)^{n-1} \left[v\,\delta\rho_{,t}^2 + (v^2 - a^2)\,\delta\rho_{,r}\,\delta\rho_{,t} \right] \right\}\Bigg|_0^{\infty} \tag{D.13}$$

E is clearly non-negative as $a^2 > v^2$ in the subsonic region. Assuming $\delta\rho$ decays to zero fast enough at infinity to ensure that E is finite,

$$\delta\varphi_{,t} \sim r^{-\frac{(N+1+\delta)}{2}} \qquad \delta\varphi_{,r} \sim r^{-\frac{(N+1+\delta)}{2}} \tag{D.14}$$

where $\delta > 0$, then the surface integral at infinity vanishes in equation (D.13). In addition, the second term vanishes at the sound horizon and therefore because $v < 0$,

$$E > 0 \quad \text{and} \quad \frac{dE}{dt} < 0. \tag{D.15}$$

Hence E, viewed as a norm of the perturbations, must decay with time and the flow is stable.

APPENDIX E. MISCELLANEOUS SYMBOLS USED IN THE TEXT

a sound speed scaled with c (Ch. VI only)

c speed of light

$C(\varpi)$ ratio of actual flux to Eddington flux

D $\bar{\sigma}^2 - \kappa^2$

$\mathcal{E}$ scaled Bernoulli constant = na_∞^2

f Lane Emden function

$\underline{g}_{eff}$ effective gravitational acceleration (rotation and gravity)

G gravitational constant

H half-thickness of disk

k Boltzmann constant

$\underline{k}$ wavevector

ℓ specific angular momentum

L luminosity

L_E Eddington luminosity

m azimuthal wavenumber ($\delta Q \sim \exp[im\phi]$)

m_p proton rest mass

M central mass (usually, in section I.4 it is the torus mass)

$\dot{M}$ mass accretion rate

$\dot{M}_E$ Eddington accretion rate

$\dot{m}$ (Ch. VI only) scaled accretion rate

n polytropic index (n_2=2D, n_3=3D)

N Brunt-Väisälä frequency

N (Ch. VI only) dimensional parameter (1 for 2D flow, 2 for conical flow)

p pressure

q specific angular momentum index, $\ell = \ell_{Kep}(\varpi/\varpi_0)^{2-q}$

Q $m\beta$

R_c $2GM/c^2$ = Schwarzschild radius

$\mathcal{R}$ R_c/ϖ_0

s specific entropy

t time

v_s sound speed

$\underline{v}$ velocity

w effective gravitational potential

W $\delta p/\delta\varpi$, $\delta p/\rho^{\kappa}\bar{\sigma}$ in section III.4(b)

z height above equatorial plane

α Shakura-Sunyaev viscosity parameter

β $\left[2(n+1)p_0\varpi_0/GM\rho_0\right]^{\frac{1}{2}}$ = thickness parameter

β_{max} β for which torus extends to infinity

β_{cusp} β for which torus inner edge is on cusp

γ $\frac{\rho}{p}\left(\frac{\delta p}{\delta\rho}\right)_s$ = adiabatic index

Γ $1+1/n$ = polytropic adiabatic index

δ Eulerian perturbation

Δ Lagrangian perturbation = $\delta + \underline{\xi}\cdot$

η $(1-f)^{\frac{1}{2}}$

Θ angular coordinate orthogonal to f (cf figure 2-1)

κ opacity (Ch. I only)

κ epicyclic frequency

λ $\ell/R_0 c$

ν σ/Ω_0

$\underline{\xi}$ Lagrangian displacement

π 3.14159...

ϖ distance from rotation axis

ϖ_0 radius of pressure maximum

ϖ_{cusp} cusp radius

ϖ_{in} disk inner radius

ϖ_{mb} marginally bound orbit

ϖ_{ms} marginally stable orbit

ϖ_{out} disk outer radius

ρ density

σ eigenfrequency ($\delta Q \sim \exp[i\sigma t]$)

$\bar{\sigma}$ $\sigma + m\Omega$ = Doppler-shifted frequency

τ optical depth

ϕ azimuthal angle

$\bar{\Phi}$ gravitational potential

$\bar{\Phi}_{rot}$ $-\int \Omega^2 \varpi d\varpi$ = "rotational" potential

ψ velocity potential

ω vorticity

Ω angular velocity

Ω_p $-\mathrm{Re}(\sigma)/m$ = pattern speed (azimuthal phase velocity of mode)

$\mathcal{L}$ Lie derivative

REFERENCES

Abramowicz, M.A. 1981. Nature, 294, 235.

Abramowicz, M.A., Calvani, M., and Nobili, L. 1980. Ap. J., 242, 772 (ACN).

Abramowicz, M.A., Curir, A., Schwarzenberg-Czerny, A., and Wilson, R.E. 1984a. Mon. Not. R. astr. Soc., 208, 279.

Abramowicz, M.A., Henderson, P.F., and Ghosh, P. 1983. Mon. Not. R. astr. Soc., 203, 323.

Abramowicz, M.A., Jaroszyński, M., and Sikora, M. 1978. Astron. Astrophys., 63, 221

Abramowicz, M.A., Livio, M., Piran, T., and Wiita, P.J. 1984b. Ap. J., 279, 367.

Abramowicz, M.A., and Zurek, W.H. 1982. Ap. J., 246, 314.

Abramowitz, M., and Stegun, I.A. 1972. Handbook of Mathematical Functions, Dover, New York.

Balbinski, E. 1984. Mon. Not. R. astr. Soc., 209, 145.

Balbinski, E. 1985. Astron. Astrophys., 149, 487.

Begelman, M.C. 1984. p. 411 in Proceedings of the 1984 Santa Cruz Summer Workshop in Astronomy Astrophysics "Astrophysics of Active Galaxies and Quasi-Stellar Objects", J.S. Miller, ed. (University Science Books).

Begelman, M.C., Blandford, R.D., and Rees, M.J. 1984. Rev. Mod. Phys., 56, 255.

Begelman, M.C., and Meier, D.L. 1982. Ap. J., 253, 873.

Blaes, O.M. 1985a. Mon. Not. R. astr. Soc., 212, 37P.

Blaes, O.M. 1985b. Mon. Not. R. astr. Soc., 216, 553.

Blaes, O.M., and Glatzel, W. 1986. Mon. Not. R. astr. Soc., in press.

Blandford, R.D. 1985. p. 281 in Active Galactic Nuclei, J.E. Dyson, ed. (Manchester University Press).

Blandford, R.D., Jaroszyński, M., and Kumar, S. 1985. Mon. Not. R. astr. Soc., 215, 667.

Bondi, H. 1952. Mon. Not. R. astr. Soc., 112, 195.

Calvani, M., and Nobili, L. 1981. Astrophys. Space Science, 79, 387.

Case, K.M. 1960. Phys. Fluids, 3, 143.

Chakrabarti, S.K. 1985. Ap. J., 288, 1.

Drazin, P.G., and Reid, W.H. 1981.Hydrodynamic Stability, Cambridge University Press.

Drury, L. O'C. 1985. Mon. Not. R. astr. Soc., 217, 821.

Dyson, J., and Schutz, B.F. 1979. Proc. R. Soc. Lond. A, 368, 389.

Eggum, G.E., Coroniti, F.V. and Katz, J.I. 1985. Ap. J. Letters, 298, L41.

Fishbone, L.G. 1977. Ap. J., 215, 323.

Fishbone, L.G., and Moncrief, V. 1976. Ap. J., 207, 962.

Frank, J. 1979. Mon. Not. R. astr. Soc., 187, 883.

Fricke, K.J., and Smith, R.C. 1971. Astron. Astrophys., 15, 329.

Friedman, J.L., and Schutz, B.F. 1978a. Ap. J., 221, 937.

Friedman, J.L., and Schutz, B.F. 1978b. Ap. J., 222, 281.

Glatzel, W. 1986. Mon. Not. R. astr. Soc., submitted.

Goldreich, P., Goodman, J., and Narayan, R. 1986. Mon. Not. R. astr. Soc., submitted. (GGN)

Goldreich, P., and Lynden-Bell, D. 1965. Mon. Not. R. astr. Soc., 130, 126.

Goldreich, P., and Narayan, R. 1985. Mon. Not. R. astr. Soc., 213, 7P.

Grinfeld, M.A. 1984. Geophys. Astrophys. Fluid Dyn., 28, 31.

Hacyan, S. 1982. Ap. J., 262, 322.

Hawley, J.F., and Smarr, L.L. 1985. University of Illinois preprint.

Jaroszyński, M. 1985. preprint.

Jaroszyński, M., Abramowicz, M.A., and Paczyński, B. 1980. Acta Astron., 30, 1.

Kojima, Y. 1986. Progress of Theoretical Physics, 75, 251.

Kozłowski, M., Jaroszyński, M., and Abramowicz, M.A. 1978. Astron. Astrophys., 63, 209.

Landau, L.D., and Lifshitz, E.M. 1959. Fluid Mechanics, Pergamon Press, London.

Lightman, A.P. 1974. Ap. J., 194, 429.

Lightman, A.P., and Eardley, D.M. 1974. Ap. J. Letters, 187, L1.

Lin, C.C., Yuan, C., and Shu, F.H. 1969. Ap. J. , 155, 721.

Lu, J. 1985. PhD thesis, International School for Advanced Studies, Trieste.

Lynden-Bell, D. 1978. Phys. Scripta, 17, 185.

Lynden-Bell, D., and Ostriker, J.P. 1967. Mon. Not. R. astr. Soc., 136, 293.

Lynden-Bell, D., and Pringle, J.E. 1974. Mon. Not. R. astr. Soc., 168, 603.

Margon, B. 1984. Ann. Rev. Astron. Astrophys., 22, 507.

Mark, J.W-K. 1976. Ap. J., 205, 363.

Meier, D.L. 1979. Ap. J., 233, 664.

Meier, D.L. 1982a. Ap. J., 256, 681.

Meier, D.L. 1982b. Ap. J., 256, 693.

Meier, D.L. 1982c. Ap. J., 256, 706.

Moncrief, V. 1980. Ap. J., 235, 1038.

Nobili, L., Calvani, M., and Turolla, R. 1985. Mon. Not. R. astr. Soc., 214, 161.

Novikov, I., and Thorne, K.S. 1973. p; 343 in Black Holes, B. DeWitt and C. DeWitt, eds., Gordon and Breach, New York.

Paczyński, B. 1980. Acta Astron., 30, 347.

Paczyński, B. 1982. Astronomische Gesellschaft Mitteilungen, 57, 27.

Paczyński, B., and Abramowicz, M.A. 1982. Ap. J., 253, 897.

Paczyński, B., and Wiita, P.J. 1980. Astron. Astrophys., 88, 23. (PW)

Papaloizou, J.C.B., and Pringle, J.E. 1982. Mon. Not. R. astr. Soc., 200, 49.

Papaloizou, J.C.B., and Pringle, J.E. 1984. Mon. Not. R. astr. Soc., 208, 721. (PPI)

Papaloizou, J.C.B., and Pringle, J.E. 1985. Mon. Not. R. astr. Soc., 213, 799. (PPII)

Piran, T. 1978. Ap. J., 221, 652.

Pringle, J.E. 1981. Ann. Rev. Astron. Astrophys., 19, 137.

Pringle, J.E., and Rees, M.J. 1972. Astron. Astrophys., 21, 1.

Pringle, J.E., Rees, M.J., and Pacholczyk, A.G. 1973. Astron. Astrophys., 29, 179.

Rees, M.J. 1982. p. 166 of The Galactic Center, AIP Conference Proceedings No. 83, ed. Riegler, G.R., and Blandford, R.D.

Rees, M.J. 1984. Ann. Rev. Astron. Astrophys., 22, 471.

Rees, M.J., Begelman, M.C., Blandford, R.D. and Phinney, E.S. 1982. Nature, 295, 17.

Schutz, B.F. 1980. Mon. Not. R. astr. Soc., 190, 7.

Schutz, B.F., and Sorkin, R. 1977. Ann. Phys., 107, 1.

Seguin, F.J. 1975. Ap. J., 197, 745.

Shakura, N.I., and Sunyaev, R.A. 1973. Astron. Astrophys., 24, 337.

Shakura, N.I., and Sunyaev, R.A. 1976. Mon. Not. R. astr. Soc., 175, 613.

Smak, J. 1984. Pub. A. S. P., 96, 5.

Sung C.-H. 1974. Astron. Astrophys., 33, 99.

Taam, R.E., and Lin, D.N.C. 1984. Ap. J., 287, 761.

Tassoul, J.-L. 1978. Theory of Rotating Stars, Princetion University Press.

Toomre, A. 1977. Ann. Rev. Astron. Astrophys., 15, 437.

Wiita, P.J. 1982a. Ap. J., 256, 666.

Wiita, P.J. 1982b. Comments Astrophys., 9, 251.

Zurek, W.H. and Benz, W. 1986. Ap. J. in press.